©Copyright 2016
Ames C. Register

Characterization and Exploitation of Bidirectional Allosteric Coupling in Multi-Domain Tyrosine Kinases using Conformation-Selective ATP-Competitive Inhibitors

Ames C. Register

A dissertation
submitted in partial fulfillment of the
requirements for the degree of

Doctor of Philosophy

University of Washington

2016

Reading Committee:

Dustin J. Maly, Chair

Michael Gelb

Matthew Bush

Program authorized to offer degree:

Chemistry

University of Washington

Abstract

Characterization and Exploitation of Bidirectional Allosteric Coupling in Multi-Domain Tyrosine Kinases using Conformation-Selective ATP-Competitive Inhibitors

Ames C. Register

Chair of Supervisory Committee:
Professor Dustin J. Maly
Department of Chemistry

Protein kinases are a large family of enzymes that play integral roles in cell signaling networks and are thus critical for effecting appropriate cellular responses to environmental stimuli. Much of kinase biological function has been studied in terms of catalytic activity: phosphorylation of substrate proteins as part of signaling cascades. However, recent evidence has shown that kinases play many important non-catalytic functions such as DNA-binding, scaffolding, and participating in a variety of physiologically relevant protein-protein interactions. While critical, these roles have not been thoroughly explored, in large part due to limited availability of selective ATP-competitive inhibitors. Selectivity for a specific kinase is difficult to achieve due to high structural homology between the ATP-binding sites of the 518 human kinases.

Additionally, it has been shown over the past two decades that it is possible to stabilize structurally distinct ATP-binding site conformations using conformation-selective

inhibitors, termed Type I and Type II inhibitors, in many kinases. In several cases, inhibition of kinase ATP-binding sites with Type I or Type II inhibitors has been shown to divergently affect cell signaling events as a result of allosteric coupling between important structural features in the ATP-binding site and distal protein-protein interaction sites on the inhibited kinase. Thus, it is important not only to build selective ATP-competitive inhibitors but to understand how their binding affects global kinase conformation through allosteric coupling. This thesis describes my work characterizing allosteric networks in multi-domain tyrosine kinases (Src-Family Kinases (SFKs) and Abl) using conformation-selective inhibitors as well as developing a method for using conformation-selective inhibitors in cells to better understand how non-catalytic function of a kinase of interest determines its role in cell signaling networks.

TABLE OF CONTENTS

LIST OF ABBREVIATIONS

3D	Three-domain
Hck	Hematopoietic cell kinase
Abl	Ableson tyrosine kinase
ACN	Acetonitrile
Act	Activated
Ala	Alanine
APS	Abl-Peptide Substrate
AS	Analogue-Sensitive
ATP	Adenosine triphosphate
Arg	Arginine
BCR	Breakpoint Cluster Region
BME	β-Mercapto ethanol
BSA	Bovine Serum Albumin
CAM	S-carboxyamidomethylcysteine
CD	Catalytic Domain
CID	Collision-induced Dissociation
Co-IP	Co-Immuniprecipitation
Csk	C-terminal Src Kinase
CSKtide	Csk Peptide Substrate
Cys	Cysteine
Dap	L-2,3-diaminopropionic acid
DFG	Aspartate-phenylalanine-glycine
DMEM	Dubecco's Modified Eagle Medium
DMSO	Dimethyl Sulfoxide
DNABD	DNA-Binding Domain
Dox	Doxycycline
DR	Drug-resistant
DTT	Dithiothreitol
EDTA	Ethylenediaminetetraacetic acid
EGFR	Epidermal Growth Factor Receptor Kinase
EGTA	Ethylene glycol tetra acetic acid
FAK	Focal Adhesion Kinase
FBS	Fetal Bovine Serum
FABD	F-Actin Binding Domain
Glu	Glutamate
Gly	Glycine
GST	Glutathione S-Transferase
HEK293T	Human Embryonic Kidney 293T cells
HeLa	Henrietta Lacks cervical cancer cells
HEPES	4-(2-hydroxyethyl)-1-piperazineethanesulfonic acid
HPLC	High-Performance Liquid Chromatography
IC_{50}	Half-maximal inhibitory concentration
IP	Immunoprecipitation
IPTG	Isopropyl β-D-1-thiogalactopyranoside

K_d	Dissociation constant
K_i	Substrate-independet half-maximal inhibitory concentration
K_m	Michaelis constant
LB	Lauria Bertani Broth
Lck	Lymphocyte-specific kinase
Lys	Lysine
MBP	Myelin Basic Protein
Met	Methionine
Mod. RIPA	Modified Radioimmunoprecipitation buffer
Mps1/TTK1	Dual Specificity Kinase TTK
MS	Mass Spectrometry
m/z	Mass to charge ratio
NES	Nuclear Export Sequence
OD	Optical Density
OE	Over Expression
PAGE	Polyacrylamide Gel Electrophoresis
PBS	Phosphate Buffered Saline
PDB	Protein Data Bank
Phe	Phenylalanine
PPII	Poly-Proline Type II
SDS	Sodium dodecyl sulfide
Ser	Serine
SFK	Src-family kinase
SH2	Src-Homology 2
SH2diseng	SH2 disengaged
SH2eng	SH2 engaged
SH3	Src-Homology 3
SH3diseng	SH3 disengaged
SH3eng	SH3 engaged
SILAC	Stable Isotope Labeling with Amino acids in Cell culture
SPS	Src-Peptide Substrate
SYF (-/-) 3T3	Src/Yes/Fyn Knockout 3T3 cells
TBS	Tris buffered saline
TCEP	Tris (2-carboxyethyl) phosphine hydrochloride
TEAB	Triethyl ammonium bicarbonate
Thr	Threonine
Tris	Tris(hydroxymethyl)aminomethane
Trp	Tryptophan
WT	Wild-type

Units

°	Degree
C	Celsius

µ	Micro
Ci	Curie
g	Gram
hr	Hour
L	Liter
m	Milli
M	Molar
min	Min
mol	Mole
n	nano
p	pico
s	second

LIST OF FIGURES

Introduction:

Chapter 1:

Chapter 2:

Chapter 3:

LIST OF TABLES

Chapter 1:

Chapter 2:

Chapter 3:

ACKNOWLEDGEMENTS

This work would not have been possible without the support and expertise of many people. I would like to thank my advisor, Dustin Maly, for his help envisioning this project and practical advice during each step of its unfolding. Most importantly, thank you for helping me to become a more rigorous, thoughtful, and productive scientist. Much of this work, especially the last chapter, has been very collaborative and so I would like to thank everyone who contributed: Rama Subba Rao Vidadala and Linglan Fang made the majority of ATP-competitive inhibitors; Matthew Chang and Martin Golkowski helped with the SILAC MS experiments and their design; Emily Dieter took on SFK CD crystallization; Bridget Trevillian did confocal microscopy to track SFK localization; and Sujata Chokraborty contributed to SFK biochemical assays. For funding, thank you to the NIH and BPSD program for their support through the Molecular Biophysics Training Grant. Additionally, thank you to all members of the Maly lab, past and present, for making lab a fun and warm place to work, even when things were not going well; especially Stephen Leonard, Bridget Trevillian, Hannah Feldman, Carrie Gower, Ratika Krishnamurty, Sanjay Hari, and Emily Dieter.

Without the guidance of Marcus Carr and Cory Rillahan as graduate-student mentors I'm not sure I would even have gotten to this point—thank you. Thank you to Judith Klinman and James Paulson for taking me on as an undergraduate in your labs. Additionally, thank you to the faculty, staff, and students in the Berkeley Gender and Women's Studies department, for helping me develop the social conscience and critical-thinking skills that I am thankful for every day. Thanks also to Christine Esteben for mentoring me through high school and beyond.

My friends outside of lab have been a constant source of joy and encouragement. Thank you Tracy, Maddy, Ana, Madalee, Louise, Samantha, Rachel, Agathe, Tom, and Emmett. Sorry I am not always the best at keeping in touch. I hope you know how much I appreciate you.

Thank you Dad and Paul for your endless love and support. Thank you Mom for encouraging me to pursue my education and believing in me, even though things have not been easy lately. Thank you Carrie for loving me, supporting me, and spending time with me, even when I am cranky and weird. Thank you Franklin for your companionship and for purring on my lap (especially while I was writing this). Thank you Sparky for being sweet and entertaining. Thank you Joey for letting me live with you.

DEDICATION

To Franklin and anyone who reads this.

VITA

2007……El Camino High School, Valedictorian
Oceanside, CA

2011……B.S. Chemistry, UC Berkeley
Minor, Gender and Women's Studies
Berkeley, CA

2016……PhD Chemistry, University of Washington
Seattle, WA

PUBLICATIONS

Register, A.C., Chokraborty, S., and Maly, D.J. (TBA). Allosteric modulation of Src-family kinases with ATP-competitive inhibitors. *Methods Mol. Bio.* (Accepted).

Register, AC, Leonard, S.E., and Maly, D.J. (2014). SH2-catlaytic domain linker heterogeneity influences allosteric coupling across the SFK family. Biochemistry *53*, 6910-6923.

Leonard, S.E., Register, A.C., Krishnamurty, R., Brighty, G.J., and Maly, D.J. (2014). Divergent modulation of Src-family kinase regulatory interactions with ATP-competitive inhibitors. ACS Chem. Biol. *9*, 1894-1905.

Rillahan, C.D., Brown, S.J., Register, A.C., Rosen, H., and Paulson, J.C. (2011). High-throughput screening for inhibitors of sialyl- and fucosyltransferases. Angew. Chem. Int. Ed. Engl. *50*, 12534-12537.

Introduction

A cell must sense and respond to a multitude of environmental signals promoting diverse processes such as growth, response to stress/injury, movement, and division. Cells have evolved complex signaling networks consisting of enzymes, substrates, scaffolding proteins, and other factors that efficiently and accurately translate stimuli into phenotypic responses. A family of enzymes known as protein kinases are key actors in these cellular signaling networks.

Protein Kinases are a large family of more than 500 members in humans that transfer the gamma phosphate of ATP to serine, threonine, and tyrosine (Skamnaki, et al., 1999). Canonically, phosphorylation leads to activation of a kinase, promoting phosphorylation of downstream kinases and effectors (Adams, et al., 1995). Within a prototypical signaling network, a signal, such as a growth factor, leads to activation of a receptor kinase, which then phosphorylates downstream cytosolic kinases that further amplify the signal by phosphorylating additional substrates; resulting in a cascade that typically culminates in suppression or activation of gene expression (Seger and Krebs, 1995). In addition to substrate phosphorylation, kinases play many vital *non-catalytic* roles within signaling cascades such as scaffolding, DNA binding, and serving as substrates for phosphorylation events themselves (Kung and Jura, 2016; Rauch, et al., 2011). Though known to be important, these functions are difficult to study and thus less well understood.

Due to the fact that proper propagation of signals and therefore proper kinase function (catalytic and non-catalytic) is essential, signaling networks are tightly regulated.

It is therefore unsurprising that kinase misregulation is known to drive many forms of cancer, as well as inflammation and diabetes (Roberts and Der, 2007).

Given their prominent role in disease, kinases have been the focus of drug discovery efforts, but selective pharmacological targeting of individual kinases has proven to be difficult due to high structural homology between the 500+ members of the family (Anastassiadis, et al., 2012). Structural studies, primarily crystal structures of catalytic domains bound to ATP-competitive inhibitors, have provided a wealth of information about the structural features of kinase active sites and how specific residues contribute to catalytic activity (Nolen et al., 2004; Muller, et al., 2015). Kinase catalytic domains are composed of an N-lobe consisting of mostly β-strands and one α-helix (the αC helix) and a C-lobe consisting mainly of α-helices. The ATP-binding site is located between these two lobes. A flexible loop known as the activation loop resides at the edge of the ATP-binding site and usually contains phosphorylatable residues (Knighton, et al., 1991). Activation loop phosphorylation often results in a dramatic increase in kinase catalytic activity (Ohashi, et al., 2000). A conserved, catalytically important Asp-Phe-Gly (DFG) motif is located at the base of the activation loop (**Figure I-1**).

Figure I-1

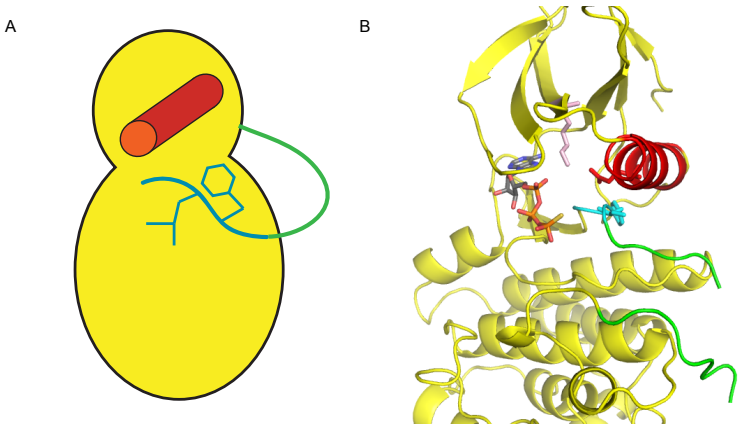

Figure I- 1: General structure of a protein kinase catalytic domain

A. Cartoon of a generic kinase catalytic domain with illustrated αC helix (red), DFG-motif (cyan), and activation loop (green). **B**. Crystal structure of the kinase LimK1 bound to ATP-γ-S (PDB: 5L6W), with the same coloring as in A. The catalytic lysine (pink), Glu310, and Phe of the DFG motif are shown as sticks. ATP-γ-S is colored by element.

Within the ATP-binding site, adenosine makes hydrogen bonding contacts with the hinge region that connects the N- and C-lobes. Lys298 (residue numbering from the kinase Src will be used throughout this document), known as the catalytic lysine, forms a salt bridge with the side chain of Glu310 on the αC helix, helping to mitigate negative charge build-up during phosphate transfer. Mutation of Lys298 (typically to Met or Arg) abolishes catalytic activity, and is frequently used in the literature to inactivate a kinase of interest (Honegger, et al., 1987). The Asp residue of the DFG motif points in towards the active site ("DFG-in") and serves to coordinate a magnesium ion, that further mitigates negative charge build-up during phosphate transfer. Together, these ATP-binding site structural features are hallmarks of a catalytically active kinase. Most ATP-competitive inhibitors, termed Type I inhibitors in the literature, stabilize the ATP-binding site in an active conformation, with all catalytically important residues oriented as described above (**Figure I-2A**). However, some ATP-competitive inhibitors (Type II inhibitors) stabilize the ATP-binding site in structurally distinct conformations relative to the active conformation (Roskoski, 2016).

There are two classes of Type II inhibitors that stabilize two *distinct* inactive conformations—αC helix-out and DFG-out (Palmieri and Rastelli, 2012). αC helix-out inhibitors make similar contacts with the hinge-region of the catalytic domain as Type I inhibitors, but contain large hydrophobic functionalities that occupy a pocket produced when the αC helix rotates out of the active conformation. The αC helix-out conformation

is characterized by a >12 Å translocation that disrupts the salt-bridge between Glu310 and the catalytic Lys. In contrast, DFG-out inhibitors contain functionalities that occupy a pocket produced when the Phe of the DFG motif flips 180°, such that the Phe side chain is oriented out of the ATP-binding site (Pargellis, et al., 2002). Additionally, inhibitors often contain an amide or urea that hydrogen bonds to the backbone of the flipped DFG-motif and Glu310 in the αC helix (**Figure I-2B**).

Figure I-2

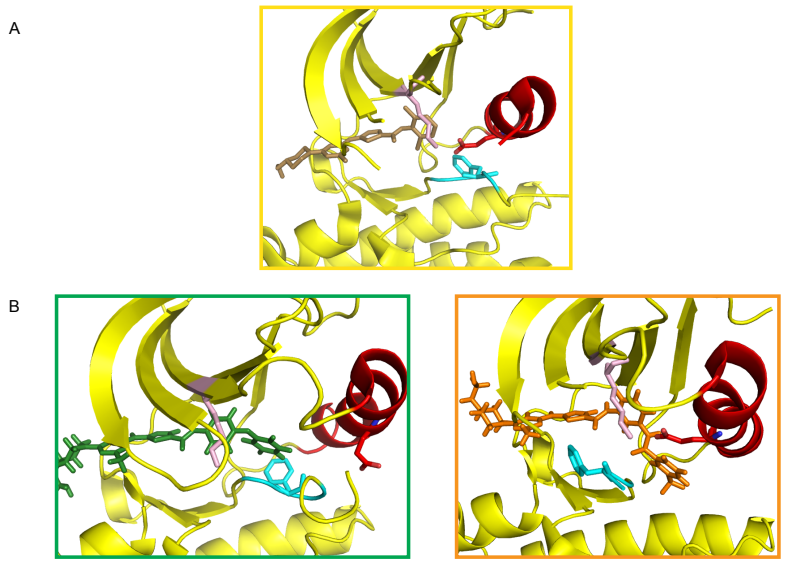

Figure I- 2: Conformation-selective inhibitors stabilize distinct ATP-binding site conformations

A. Crystal structure of the Src catalytic domain bound to the Type I/Active-stabilizing ATP-competitive inhibitor dasatinib (PDB: 3G5D). The ✔C helix is colored red, the DFG motif is colored cyan, and the catalytic Lys is colored pale pink, with Lys295, Glu310, and the DFG-motif residues shown as sticks. **B**. Crystal structures of Type II inhibitor-stabilized ATP-binding sites. Left: ATP-binding site of Src bound to an ✔C helix-out-stabilizing analogue of dasatinib (green sticks, PDB 4YBK) inhibitor-stabilized ATP-binding site conformation. Right: ATP-binding site of Src bound to a DFG-out stabilizing analogue of dasatinib (orange sticks, PDB: 4YBJ). Same color scheme as described in A.

Though it was first hypothesized that only a few kinases could adopt specific inactive conformations, further study has shown that kinases throughout the kinome can

adopt αC helix-out and DFG-out ATP-binding site conformations (Mol, et al., 2004; Shan, et al., 2013). Furthermore, movement of the αC helix acts as a switch between active/inactive catalytic domains in a variety of kinases including Src-family kinases (SFKs), Cyclin-dependent Kinases (CDKs), EGFR, and many others (Huang, et al., 2012). Most intriguingly, movement of the αC helix is known to be allosterically coupled to the availability of distal binding surfaces participating in protein-protein interactions (Krishnamurty, et al., 2012; Zeqiraj, et al., 2009) and the same is true of the DFG motif's conformation (Wang, et al, 2012; Leonard, et al. 2014; Hari, et al., 2014). *This has led to the hypothesis that kinase inactive conformations have evolved to mediate important non-catalytic functions*.

There are many examples in the literature of kinases playing important biological roles despite possessing catalytically inactivating mutations or inhibition by small molecules (Rauch, et al., 2011). Furthermore, there is evidence that the mode of inhibition (which ATP-binding site conformation is stabilized by a small molecule) has important but difficult to predict biological consequences. A recent illustrative example of this phenomenon involves the RAF kinases, which consist of three isoforms: ARAF, BRAF, and CRAF. ATP-competitive BRAF inhibitors developed with the intention of dampening RAS-RAF-MEK-ERK signaling paradoxically resulted in increased MEK and ERK activity in certain cell types despite BRAF inhibition (Hatzivassilou, et al., 2010). Further study revealed that this paradoxical activation is because of stabilization of both active and DFG-out inactive conformations—both αC helix-in—stabilizes heterodimers of BRAF and CRAF, leading to CRAF activation and enhancement of downstream signaling (Heidorn, et al., 2010; Hu, et al., 2013; Lavoie, et al., 2013; Cox and Der, 2010). Crystal structures

of RAF dimers showed that the αC helix rests at the dimer interface, and inhibitors that stabilize an αC helix-out conformation are less optimal for dimer formation, which results in destabilized dimeric RAF and as a lack of enhanced RAS-RAF-MEK-ERK signaling (Thevakumaran, et al., 2015; Zhang, et al. 2015).

Thus, stabilizing a DFG-out versus αC helix-out ATP-binding site conformation has divergent effects on signaling downstream of RAF, with important implications for cancer therapies targeting RAF with small molecules. Furthermore, this example and others illustrate that in order to fully understand cell signaling networks and how kinase-targeted drugs affect these networks, the relationship between kinase ATP-binding site conformation and non-catalytic function must be investigated. Conformation-selective inhibitors are invaluable tools for elucidating the molecular basis of how the αC helix and DFG motif are coupled to distal regions of a kinase of interest, and how this allostery contributes to a kinase's role in signaling cascades.

This thesis describes my efforts to develop and employ active-conformation, DFG-out, and αC helix-out stabilizing inhibitors as tools for understanding the molecular basis for coupling between the ATP-binding site and the regulatory domains of multi-domain tyrosine kinases, as well as how this coupling affects kinase function in cell signaling networks. **Chapter One** describes an investigation of the SFKs, using conformation-selective inhibitors and several mutant SFK constructs to demonstrate that sequence variation in the linker connecting the SH2 regulatory domain the catalytic domain results in differential allosteric coupling between αC helix conformation and SH3/SH2 regulatory domain engagement. **Chapter Two** applies a similar method of study to the multi-domain tyrosine kinase Abl—a close relative of SFKs. This work shows that the αC helix and

DFG-motif are similarly coupled to the regulatory domains of Abl as they are in SFKs, despite what has been hypothesized previously. Finally, **Chapter Three** describes a chemical-genetic strategy for sensitizing a kinase of interest to inhibition by covalent, conformation-selective inhibitors, by mutating a conserved, functionally silent Val residue to a Cys in the kinase N-lobe. As a proof-of-concept, SFK/Abl protein-protein interactions, subcellular localization, and phosphorylation state are divergently modulated via the ATP-binding site in cells using these conformation-selective inhibitors.

Chapter 1: SH2-Catalytic Domain Linker Heterogeneity Affects Allosteric Coupling Across the SFK Family*

I. Introduction:

Src-Family Kinases (SFKs) are a family of nine non-receptor tyrosine kinases (Src, Hck, Fyn, Lyn, Lck, Yes, Fgr, Blk, and Frk) that play a variety of important biological functions both through catalysis and inter-molecular protein-protein interactions (**Figure 1-1A**) (Thomas et al., 1997; Engen et al., 2008). Due largely to the potential roles that they play in human disease, SFKs have become popular subjects for study, with most biochemical and structural research focusing on Src and Hck (Engen et al., 2008; Kim et al., 2009; Sicheri and Kuriyan, 1997). All SFKs consist of an N-terminal unique domain, regulatory SH3 and SH2 domains, catalytic domain, and C-terminal tail (**Figure 1-1B**). Catalytic activity in SFKs is regulated by a combination of post-translational modification (phosphorylation) and intra-molecular protein-protein interactions (Engen et al., 2008; Sicheri and Kuriyan, 1997). In the autoinhibited form, SFKs adopt a closed global conformation stabilized by intra-molecular interactions between the SH3 domain and the SH2-catalytic domain linker (polyproline type two (PPII) helix) and between the SH2 domain and the C-terminal tail, which is enhanced by phosphorylation of Tyr527 on the C-terminal tail. In the active, open conformation, these intra-molecul†ar interactions are weakened and the regulatory domains are freed to interact with other binding partners in the cell. The active form is further stabilized by phosphorylation of the activation loop at

* This chapter is reproduced with permission from Register, A.C., Leonard, S.E., and Maly, D.J. (2014). SH2-catalytic domain linker heterogeneity affects allosteric coupling across the SFK family. Biochemistry *53*, 6910-6923. Copyright © 2014 American Chemical Society

Tyr416 (Xu et al., 1999; Moarefi et al., 1997; Sicheri et al., 1997; Boggon and Eck, 2004; Yadav and Miller, 2007; Trible et al., 2006).

Mutational studies and crystal structure analyses have shown that the SH2-catalytic domain linker region plays an important role in allosteric coupling between the ATP-binding site and the regulatory domains (Superti-Furga et al., 2000; Krishnamurty et al., 2012; Gonfloni et al., 1997). Crystal structures of autoinhibited Src and Hck constructs show that a conserved Trp260 contacts the catalytic domain, near the αC-helix and forms a pi-stacking/hydrophobic network with other aromatic residues contacting the SH3 domain, most notably Leu255 in Src (Trp255 in Hck) (**Figure 1-1B/C**) (Moarefi et al., 1997; Sicheri et al., 1997; Gonfloni et al., 1997; LaFevre-Bernt et al., 1998). Mutating Leu255 to valine activates Src without disrupting binding between the SH2-catalytic domain linker and the SH3 domain, indicating that these interactions are mediating allosteric coupling between the ATP-binding site and regulatory domains (LaFevre-Bernt et al., 1998). The conformation of helix αC is known to play a critical role in facilitating transitions between autoinhibited and active states (Superti-Furga et al., 1999). The proximity of the αC helix to Trp260 and its interaction with Leu255 indicates that it plays a role in transmitting changes in ATP-binding site conformation to the regulatory domains and vice versa. The allosteric relationship described above is *bi-directional*, in that ATP-binding site conformation also influences regulatory domain engagement (Yadav and Miller, 2007; Trible et al., 2006). In fact, our lab has shown that ATP-competitive ligands that stabilize Src and Hck in an inactive αC helix-out conformation strengthen intra-molecular SH3/SH2 domain engagement upon binding (Krishnamurty et al., 2012; Leonard et al., 2014). In contrast, inhibitors that stabilize helix αC in an active

conformation, weaken interactions between the SH2/SH3 domains and their respective intra-molecular ligands. While the basic allosteric regulatory network between the catalytic and regulatory domains of SFKs is well characterized, less is known about how SH2-catalytic domain linker heterogeneity affects the magnitude of this bi-directional relationship. For example, we have observed differences in the relative magnitude of allosteric coupling between Src and Hck (Krishnamurty et al., 2012; Leonard et al., 2014). Due to their overall structural homology, allosteric regulation in Src and Hck has been assumed to be the same in many studies. Differences in SH2 and SH3 domain availability for inter-molecular associations could have unexplored biological consequences and help explain non-redundant functions of individual SFKs. Thus, a more thorough exploration of the SFK family is needed to understand how SH2-catalytic domain linker variability affects regulatory domain accessibility and ATP-binding site conformation.

Figure 1-1

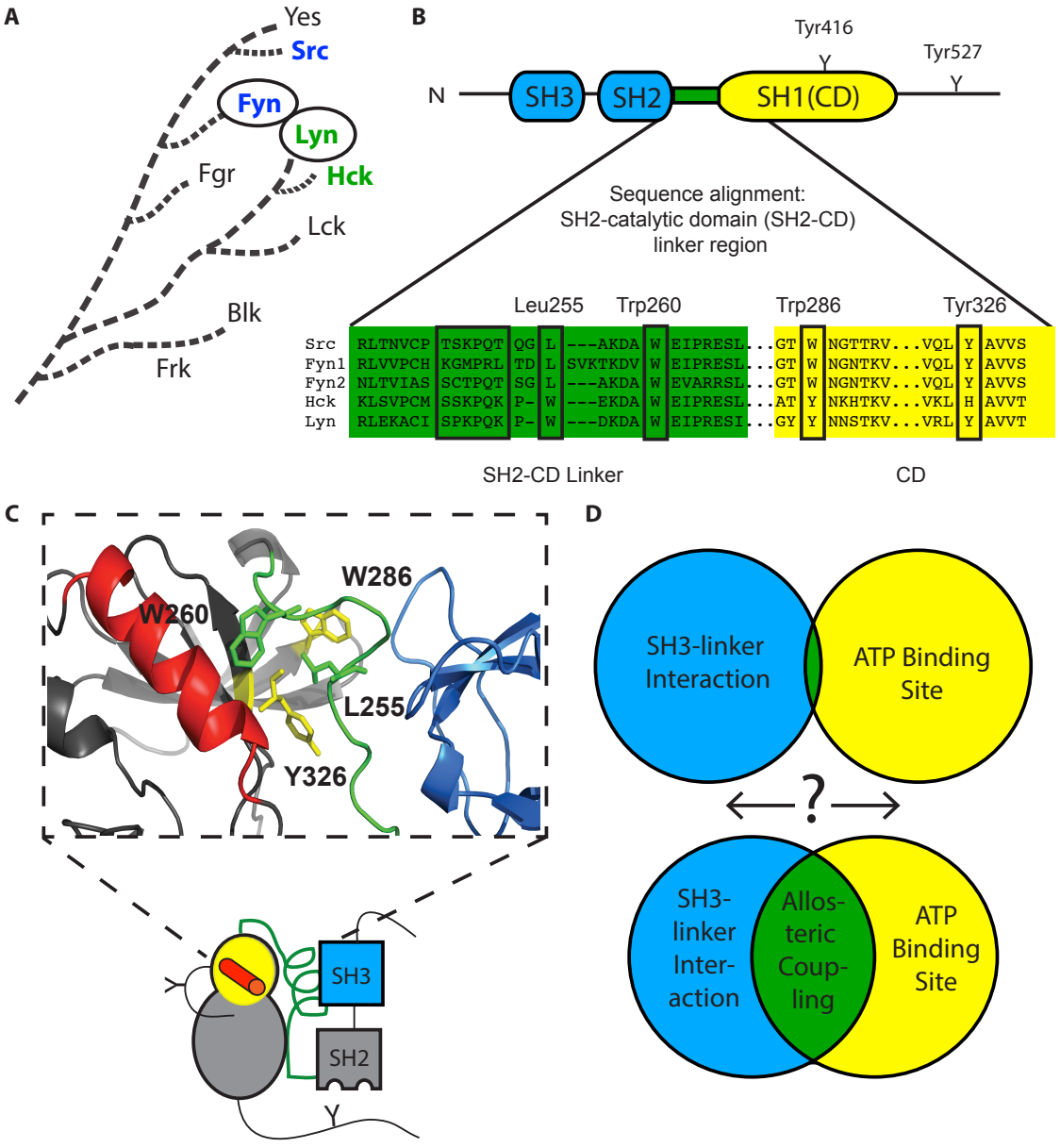

Figure 1-1: Allosteric relationships in the Src-Family Kinases (SFKs)

A. Dendrogram showing the evolutionary relationship of the Src-Family Kinases (SFKs). **B**. Conserved domain architecture of SFKs. SH3 and SH2 regulatory domains are connected to the catalytic domain (CD) by the SH2-catalytic domain linker and C-terminal tail. The SH3 domain binding epitope in the linkers of Src, Fyn1, Fyn2, Hck, and Lyn are boxed, and key residues thought to allosterically connect the αC helix (ATP-binding site) and the SH3 domain are boxed and labeled (Src numbering). Note that Fyn1 has a longer linker than Fyn2 and Src. **C**. A cartoon representation of the three-dimensional structure of an autoinhibited SFK. The crystal structure (PDB: 2SRC) shows a portion of the catalytic domain (yellow), αC helix (red), SH2-catalytic domain linker (green), and SH3 domain (blue), known to be important for mediating allosteric

connection of the ATP-binding site and regulatory domains. Key residues highlighted in B are shown as sticks. Of particular interest, is the proximity of helix αC to Trp260 and the hydrophobic contacts made by Leu255. **D**. Schematic illustrating the goal of this study: to probe the degree of bi-directional allosteric coupling between the ATP-binding site (helix αC) and the regulatory domains among SFK family members via the SH3-linker interaction.

SFK's possess very similar SH2 and SH3 domain binding epitopes and their catalytic domains have almost identical substrate specificities *in vitro*, but their sequences diverge at the SH2-catalytic domain linker (Williams et al., 1998; MacAuley and Cooper, 1988; Lim, 2003; Miller, 2003). Hck and Src are evolutionarily disparate—occupying different branches of the tyrosine kinase portion of the kinome dendrogram (**Figure 1-1A**) (Williams et al., 1998). SFK's have been characterized as "Src-like" or "Hck-like" with respect to their linker sequences—Src's linker is one residue longer than Hck's—and it has been proposed that variation in linker length/sequence may be a source of functional differences between these homologous family members (e.g. recruitment of different binding partners). In fact, global conformational differences, presumably due to SH2-catalytic domain linker heterogeneity, between the two SFK subfamilies have been exploited with bivalent peptide inhibitors that target the catalytic domain and the SH2 domain (Hah et al., 2006). A bivalent ligand that is more than 1000-fold selective for Src-like SFKs (Src, Fyn, Yes, and Fgr) over Hck-like SFKs (Hck, Lyn, Lck, and Blk) has been generated, indicating a detectable difference in the relative proximity and accessibility between the SH2 domains and catalytic domains in the two subgroups of SFKs. Furthermore, studies have shown that a chimeric SFK, made by swapping the SH3 domain of Src with that of Lck (Hck-like), displays impaired autoinhibition, while swapping the SH3 domains of Src and Fyn (both Src-like) results in a fully autoinhibited kinase (Kashishian et al., 1990; Erpel et al., 1995). These data suggest that the SH3 - SH2-catalytic domain linker interaction is tuned within each SFK subgroup and highlights the

ability of the SH2-catalytic domain linker to determine the degree of allosteric coupling between the SH3 domains and the ATP-binding sites of SFKs.

Given the SH2-catalytic domain linker's prominent role in SFK ATP-binding site – regulatory domain coupling and its relatively low sequence homology, we hypothesize that SH2-catalytic domain linker variability between SFKs produces differences in the magnitude of coupling between individual family members, even those belonging to the same subgroup. Such variation could have important cellular consequences and contribute to experimentally observed non-redundancy. To better understand how SH2-catalytic domain linker diversity leads to variability in SFK regulatory interactions, we explored the bi-directional relationship between the regulatory domains and catalytic domains of the SFKs Fyn (Src-like) and Lyn (Hck-like). We also performed the same analysis on two splice-variants of Fyn (Fyn1 and Fyn2), which contain divergent linkers within the context of nearly identical SH3, SH2, and catalytic domains (Resh, 1998). Using a panel of conformation-selective ATP-competitive inhibitors in combination with a panel of Fyn1, Fyn2, and Lyn regulatory state mutants, our study explores the degree of allosteric coupling between each regulatory domain and the ATP-binding site for each SFK (**Figure 1-1D**). Systematically profiling the effects of αC helix conformation on regulatory domain accessibility across the SFK family is necessary to explain how these highly homologous family members are able to perform non-redundant cellular functions, as well as provides insight into how allosteric regulation governs and adds complexity to the behavior of homologous multi-domain protein kinases. Our study consists of two components: 1) exploration of how SH2 and SH3 domain engagement affects ATP-binding site conformation via the SH2-catalytic domain linker and 2) characterization of

how αC helix conformation influences regulatory domain accessibility via the SH2-catalytic domain linker for Fyn1, Fyn2, and Lyn.

II. Results and Discussion:

A. Intra-molecular regulatory domain interactions differentially modulate the catalytic activities of Fyn1, Fyn2, and Lyn.

Autoinhibited and activated Src and Hck constructs have previously been generated by introducing mutations that enhance or weaken intra-molecular SH2 and SH3 regulatory domain interactions. To explore the effects of SH2 and SH3 domain engagement on catalytic activity within the context of Lyn, Fyn1, and Fyn2, analogous regulatory state mutants of each SFK were generated (**Figure 1-2A**). All SFKs discussed in this work are three domain (3D) constructs, meaning that they are full length except that they lack the unique domain. Activated Lyn and Fyn (SFK^{Act}) constructs were generated by activation loop auto-phosphorylation of Y527F mutants, which cannot undergo C-terminal tail autoinhibitory phosphorylation (Hirai et al., 1990; Osusky et al., 1995; Smart et al., 1981). Quantitative activation loop phosphorylation was confirmed *via* immunoblotting with antibodies that selectively recognize either phosphorylated or non-phosphorylated SFK activation loops (data not shown). Mutations that strengthen intra-molecular SH2 and SH3 regulatory domain interactions were used to create autoinhibited Lyn and Fyn constructs. Constructs with increased engagement between the C-terminal regulatory tail and the SH2 domain (SFK^{SH2eng}) were generated by changing the three residues following Tyr527 to a high affinity SH2 domain-binding epitope (Glu-Glu-Ile) (Wang et al., 2006; Porter et al., 2000). Constructs with increased engagement between the SH2-catalytic domain linker and the SH3 domain (SFK^{SH3eng}; **Table 1-1**) were generated by introducing two high affinity PXXP motifs (PPXPP) into the SH2-catalytic

domain linker (**Table 1-1**) (Lerner et al., 2005). This epitope has been shown to possess a similarly high affinity for the SH3 domains of SFKs (Lim, 2003; Nguyen et al., Delgarno et al., 1997; Douangamath et al., 2002; Kay et al., 2000; Meyer, 2001). Adding PXXP sequences to the linkers of Fyn1, Fyn2, and Lyn enhances intra-molecular SH3 domain engagement within the context of the native SFK linker, which has been shown in chimera studies to be tuned specifically for each SFK (Kashishian et al., 1990; Erpel et al., 1995).

Table 1-1

Table 1- 1: SH2-catalytic domain linker sequences of Fyn1, Fyn2, Lyn, and Hck

Prolines introduced by site directed mutagenesis to create a higher affinity SH3 binding epitope are shown in red. Mutations were chosen based on alignment to the HckSH3eng construct, which is biochemically well characterized. Each SFK^{SH3eng} construct contains a PPXPP motif. SH3 domains have been shown to generally bind PXXP motifs, and the pattern PPXPP, effectively results in two PXXP motifs within the context of the native SFK linker (shown in brackets).

Figure 1-2

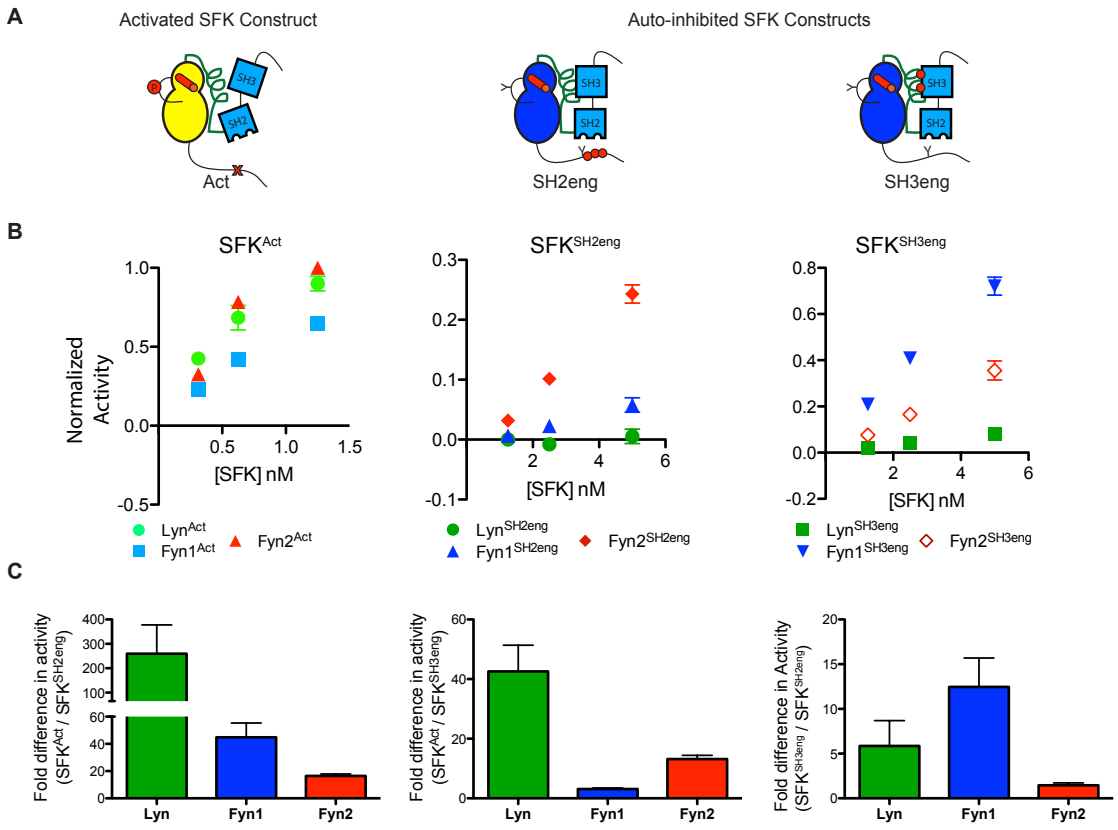

Figure 1-2: Intra-molecular regulatory domain interactions affect the catalytic activities of Lyn, Fyn1, and Fyn2

A. Cartoon representations of the SFK regulatory state mutants used in this study (SFK^{Act}, SFK^{SH2eng}, SFK^{SH3eng}). Disruptive mutations are illustrated as red X's while mutations that lead to greater intra-molecular engagement are illustrated as red dots. **B**. Activity of Lyn, Fyn1, and Fyn2 activated (left) and autoinhibited (SH2eng and SH3eng, middle and right) regulatory state mutants obtained by radioactive phosphate transfer assay and plotted as signal versus enzyme concentration (mean ± SEM, n=3). **C.** Fold difference in activity between SFK^{Act} and SFK^{SH2eng} (left). SFK^{Act} and SFK^{SH3eng} (middle), SFK^{SH2eng} and SFK^{SH3eng} and (right) (mean ± SEM, n=3).

The catalytic properties of all nine Lyn and Fyn constructs were tested in enzymatic assays. Interestingly, all nine constructs possess a similar K_m for ATP (**Table 1-2**). In addition, the overall activation state of each SFK had only a small effect on the K_m for peptide substrate. Next, the relative catalytic activity of each construct was tested at a concentration of ATP well below its K_m. As expected, the SFK^{Act} constructs are the most

active, with Lyn, Fyn1, and Fyn2 demonstrating very similar catalytic activities (**Figure 1-2B**). This shows that, in the absence of intra-molecular regulatory domain engagement, SFKs are functionally equivalent.

Table 1-2

SFK	K_m ATP (μM)	K_m SPS (μM)
Lyn^{Act}	42 ± 7	11 ± 2
Lyn^{SH2eng}	54 ± 5	60 ± 10
Lyn^{SH3eng}	100 ± 10	46 ± 8
$Fyn1^{Act}$	70 ± 10	4.7 ± 0.8
$Fyn1^{SH2eng}$	31 ± 9	8.5 ± 1.0
$Fyn1^{SH3eng}$	45 ± 6	160 ± 30
$Fyn2^{Act}$	50 ± 8	31 ± 7
$Fyn2^{SH2eng}$	90 ± 30	40 ± 10
$Fyn2^{SH3eng}$	40 ± 3	70 ± 20

Table 1- 2: K_is for ATP and Src peptide substrate (SPS) determined for each SFK regulatory state mutant (mean ± SEM, n=3)

Consistent with the introduced regulatory mutations strengthening autoinhibitory interactions, SFK^{SH3eng} and SFK^{SH2eng} constructs are less active than their SFK^{Act} counterparts (**Figure 1-2B**). However, in contrast to SFK^{Act} constructs, there is greater diversity in catalytic activity amongst autoinhibited constructs. For example, $Fyn1^{SH3eng}$ is notably more active than $Fyn2^{SH3eng}$ or Lyn^{SH3eng} (**Figure 1-2B**, right panel). This Fyn1 mutant exhibits an activity more than 10-fold greater than $Fyn1^{SH2eng}$—only about 3-fold less active than $Fyn1^{Act}$ (**Figure 1-2C**, right panel). However, $Fyn2^{SH2eng}$ is much more active than either $Fyn1^{SH2eng}$ or Lyn^{SH2eng} (**Figure 1-2B**, middle panel). To confirm that $Fyn1^{SH3eng}$'s relatively high catalytic activity compared to $Fyn2^{SH3eng}$ is not the result of

differences in occupancy between the introduced high affinity SH2-catalytic domain linker and the Fyn SH3 domain, a series of pull-down experiments to determine SH3 domain accessibility were performed (**Figure 1-3**). Fyn constructs of interest were incubated with resin displaying an SH3 domain-binding peptide. After washing, the bound kinase was eluted and quantified. The amount of SFK retained on the beads is a reflection of the relative accessibility of their SH3 domains to engage in inter-molecular binding interactions. Comparing the relative amounts of retained $Fyn1^{SH3eng}$ and $Fyn2^{SH3eng}$ provides a measure of how tightly each constructs' high affinity linker engages the Fyn SH3 domain. Both $Fyn1^{SH3eng}$ and $Fyn2^{SH3eng}$ possess relatively inaccessibly SH3 domains, presumably due to linker-SH3 domain engagement, relative to $Fyn1^{Y527F}$ (**Figure 1-3B**). Pull-downs using resin loaded with 5 times (5x) and 10 times (10x) more SH3 ligand were performed to test if intra-molecular engagement could be out-competed by higher amounts of immobilized SH3 domain ligand. The amount of $Fyn1^{SH3eng}$ and $Fyn2^{SH3eng}$ captured (and unbound) by each resin loading was almost identical, demonstrating that both Fyn1 and Fyn2 SH3eng constructs have similarly engaged SH3 domains (**Figure 1-3C** and **3D**). Thus, the ability of regulatory interactions to transmit autoinhibition to the ATP-binding site varies dramatically between Fyn1, Fyn2, and Lyn. The fact that Fyn1 and Fyn2 have identical SH3 and SH2 domains provides evidence that SH2-catalytic domain linker variability strongly contributes to the relative ability of an SH2 or SH3 domain to autoinhibit the kinase domain. The functional consequences of SH2-catalytic domain linker variability—modulating the degree of allosteric coupling between intra-molecular regulatory domain engagement and the ATP-binding site—may point to a source of non-redundancy between SFK family members in cells.

Figure 1-3

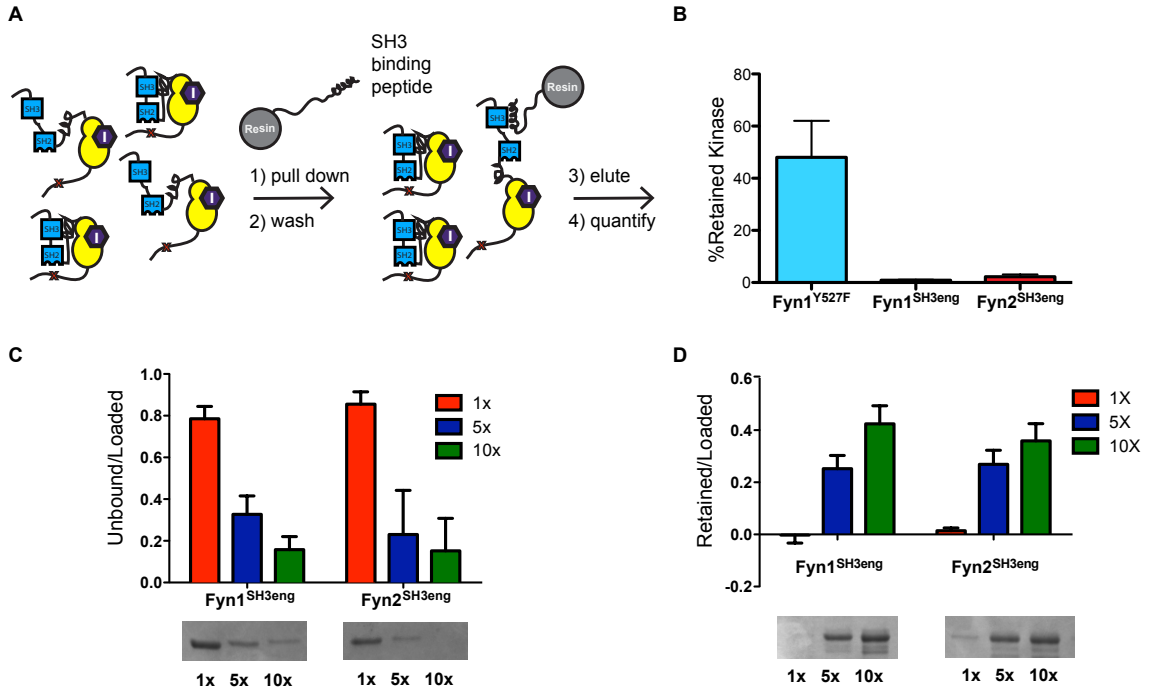

Figure 1-3: The linkers of Fyn1 and Fyn2 SH3engaged constructs have similar affinities for the Fyn SH3 domain

A. Schematic of the SH3 pull-down assay. SFK constructs are exposed to beads displaying an SH3 domain-binding peptide. After washing, retained kinase is eluted, subjected to SDS-PAGE and quantified by Western Blot or Coomassie staining. **B**. Pull-down comparing the percent SFK retained on SH3 binding resin. $Fyn1^{Y527F}$ possesses a relatively accessible SH3 domain compared to $Fyn1^{SH3eng}$ and $Fyn2^{SH3eng}$, which are similarly inaccessible (mean ± SEM, n=3). C. SDS-PAGE quantification of unbound $Fyn1^{SH3eng}$ and $Fyn2^{SH3eng}$ after incubation with 1.5mM (1x), 7.5mM (5x), and 15mM (10x) SH3 peptide resin (mean ± SEM, n=3). D. SDS-PAGE quantification of $Fyn1^{SH3eng}$ and $Fyn2^{SH3eng}$ eluted from resin after incubation with 1x, 5x, and 10x loading resin (mean ± stdev, n=2)

B. Conformation-selective, ATP-competitive inhibitors allow for dissection of the role of the αC helix in allosteric coupling

The data in **Figure 1-2** do not provide information about the overall conformation of the ATP-binding site for each SFK regulatory state mutant. In order to thoroughly explore how domain engagement influences SFK ATP-binding sites, a method to sense ATP-binding site conformation is required. To provide more information about this

parameter, the sensitivities of activated and autoinhibited Lyn, Fyn1, and Fyn2 constructs to conformation-selective ATP-competitive inhibitors were determined. A representative panel of ATP-competitive ligands that are known or predicted to stabilize *distinct* SFK ATP-binding site conformations was employed (**Figure 1-4A**). By determining affinities of these ligands for various regulatory state SFK mutants, the influence of intra-molecular interactions on ATP-binding site conformation can be determined. All inhibitors tested are pyrazolopyrimidine-based compounds with variable substituents at the C3 position. **1** (PP2) contains a 4-chlorophenyl group at the C3 position, and has previously been found to have a minimal activation state preference for Src and Hck, making it a useful control for these studies (Krishnamurty et al., 2012). **2-4** display small aryl moieties containing hydrogen bond donors/acceptors from their C3 positions, and have been found to be selective for activated Src and Hck constructs over their autoinhibited forms (Krishnamurty et al., 2012; Levinson et al., 2008). These inhibitors are predicted to stabilize an active ATP-binding site conformation by forming electrostatic interactions with catalytic residues that are aligned for catalysis. In contrast, **5-7** contain extended hydrophobic substituents at the C3 position, which have been shown to stabilize the ATP-binding sites of SFKs in an inactive conformation that involves rotation of the αC helix out of a catalytically competent alignment—the αC helix-out inactive conformation. Inhibitors of this class have been found to have a higher affinity for autoinhibited Src and Hck constructs than their activated counterparts. Unlike **2**-**4**, **5**-**7** are not compatible with the αC helix being in an active conformation (see **Figure 1-4B**). Profiling active compatible (αC helix-in) and active incompatible (αC helix-out) ligands against Lyn and Fyn

regulatory state mutants provides insight into how the allosteric relationship between αC helix conformation and regulatory domains for Fyn/Lyn compares to Src/Hck.

Figure 1-4

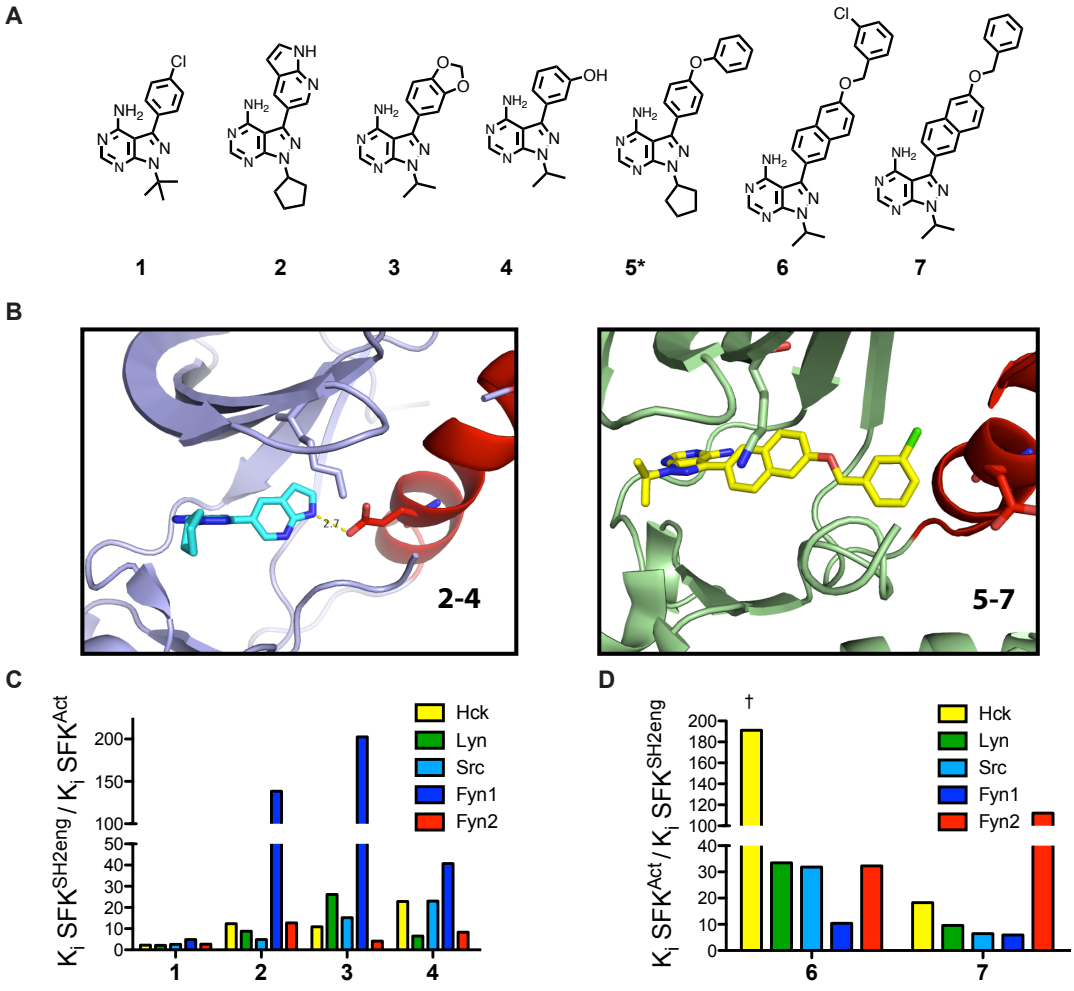

Figure 1-4: Binding preferences of conformation selective inhibitors reveal differences in allosteric coupling between Lyn, Fyn1, and Fyn2

A. Conformation-selective inhibitor panel: **2**-**4** favor the ATP-binding site of active (αC helix-in) SFKs, while **5**-**7** stabilize the αC helix-out, inactive ATP-binding site conformation. These ligands allow systematic analysis of ATP-binding site conformation in response to domain engagement. **B**. Ligands that stabilize active and αC helix-out conformations make different contacts with the ATP-binding sites of SFKs. Left panel: Src bound to **2** with the ATP-binding site in an active conformation (PDB: 3EN4). An electrostatic interaction between the inhibitor and E310 in the αC helix is shown. Right panel: Src bound to **6** with the ATP-binding site in the αC helix-out inactive conformation (PDB: 4DGG). Helix αC is rotated out of the active site, disrupting the interaction between K295 and E310. **C**. Quantitative comparison of the fold differences in K_i values between activated SFKs (SFK^{Act}) and their respective autoinhibited constructs (SFK^{SH2eng}) for **1**-**4**.

Previously reported data for Src and Hck are plotted for reference (Leonard et al., 2014).† The absolute fold difference in K_i value could not be determined because inhibitor affinity is less than the enzyme concentration used in the assay **D**. Quantitative comparison of the differences in K_i values between activated SFKs (SFK^{Act}) and their respective autoinhibited constructs (SFK^{SH2eng}) for **6** and **7**. Previously reported data for Src and Hck plotted for reference. Ligand **5**, which is marked with an asterisk, is too potent for K_i determination. All values are the average of assays performed in triplicate; the SEM for each value is less than 20% of the average K_i value).

Comparing affinities of active and αC helix-out stabilizing ligands for autoinhibited (SFK^{SH2eng}) and activated (SFK^{Act}) constructs allows investigation of how intra-molecular regulatory domain engagement influences ATP-binding site conformation for a particular SFK. More specifically, the fold difference in K_i values for a given ligand between SFK^{Act} and SFK^{SH2eng} constructs provides information about the equilibrium between active (αC helix-in) and inactive (αC helix-out) conformations of an SFK's ATP-binding site. SFK^{Act} and SFK^{SH2eng} constructs were selected because they represent the extremes of regulatory domain allosteric control over catalytic activity for both Fyn and Lyn—fully active and fully autoinhibited. K_i values for the entire panel of active stabilizing and αC helix-out preferring ligands were obtained for Lyn^{Act}, $Fyn1^{Act}$, $Fyn2^{Act}$, Lyn^{SH2eng}, $Fyn1^{SH2eng}$, and $Fyn2^{SH2eng}$ using standard activity assays (see **Table 1-3** for values). The results of the assays performed are summarized in **Figure 1-4C** and **4D**, which plots the ratio of inhibitor affinity for the SFK^{Act} construct over inhibitor affinity for the SFK^{SH2eng} construct, or vice versa. K_i values for these ligands against Src and Hck were also included as a reference (Leonard et al., 2014). As expected, compound **1** displays a minimal activation-state binding preference for Lyn, Fyn1, and Fyn2 (**Figure 1-4C**). Consistent with previous observations for Src and Hck, αC helix-out ligands **6** and **7** bind with higher affinity to SFK^{SH2eng} constructs, than to activated SFKs (**Figure 1-4D**). Active ATP-binding site-stabilizing ligands **2-4** show the opposite preference (**Figure 1-4C**). Despite the overall similar trend in conformation-selective inhibitor selectivity for Hck, Src,

Lyn, Fyn1, and Fyn2 regulatory state mutants, there are some significant differences in the magnitudes of these preferences amongst the SFKs. Most notably, Fyn1 possesses the most distinct conformation-selective inhibitor profile. $Fyn1^{SH2eng}$ shows the lowest selectivity for ligands **6** and **7** relative to its activated construct ($Fyn1^{Act}$). Furthermore, **2**-**4** demonstrate a much larger fold difference in affinity for $Fyn1^{Act}$ versus $Fyn1^{SH2eng}$, relative to the other SFKs. As both ligand classes (**2**-**4** and **6**-**7**) most likely make favorable contacts with different conformations of the αC helix, this structural element appears to be unique in Fyn1. The difference in fold preference is especially striking when compared to Fyn2, which possesses the exact same SH3 and SH2 domains as Fyn1 and 97% identical catalytic domains (only 8 residues different in the N-terminal lobe). The fact that Fyn2 behaves more like Hck, Src, and Lyn than Fyn1 in the presence of conformation-selective inhibitors suggests that the SH2-catalytic domain linker, which is unique for Fyn1, plays a major role in the conformation of the αC helix.

Table 1-3

Ligand	Lyn^{Act}	Lyn^{SH2eng}	$Fyn1^{Act}$	$Fyn1^{SH2eng}$	$Fyn2^{Act}$	$Fyn2^{SH2eng}$
1	56	120	19	93	45	120
2	9.1	240	1.8	260	4.6	59
3	160	1450	25	5200	180	740
4	210	1380	15	620	21	180
5	66	<45	6.9	<29	-----	-----
6	3800	110	3700	360	7100	220
7	790	82	710	120	2700	24

Table 1- 3: K_i values (nM) for data shown in Figure 1-4

All SEMs are within 20% of the reported average.

*C. Regulatory domain engagement, but not activation loop phosphorylation, is the major determinant of SFK sensitivity to ligands **2**-**4***

SFK catalytic activity is predominantly governed by two factors: activation loop phosphorylation (activating) and regulatory domain engagement (autoinhibiting). We were interested in seeing if we could use our panel of inhibitors and regulatory state mutants to determine which factor—activation loop phosphorylation or regulatory domain engagement—governs the changes in ATP-binding site conformation driving the extreme difference in affinity observed between $Fyn1^{Act}$ and $Fyn1^{SH2eng}$ for ligands **2**-**4**. To do this, K_i values for ligands **2**-**4** were determined for each SFK^{Y527F} construct and compared to SFK^{Act}—to probe activation loop phosphorylation, or SFK^{SH2eng}—to probe SH2 domain engagement (**Figure 1-5** and **Table 1-4**). The Y527F construct was chosen as a basis for comparison because it is neither activation loop phosphorylated nor engineered to favor regulatory domain engagement. This analysis shows that SH2 domain engagement determines the affinity of ligands **2**-**4** for the ATP-binding sites of all SFKs tested, because a larger difference in affinity is observed between SFK^{SH2eng} and SFK^{Y527F}, than between SFK^{Y527F} and SFK^{Act}. This is particularly true for Fyn1, providing evidence that the ATP-binding site conformation equilibrium for $Fyn1^{Y527F}$ favors the active, αC helix-in conformation to a greater extent than all other SFK^{Y527F} constructs tested, even in the absence of activation loop phosphorylation.

Figure 1-5

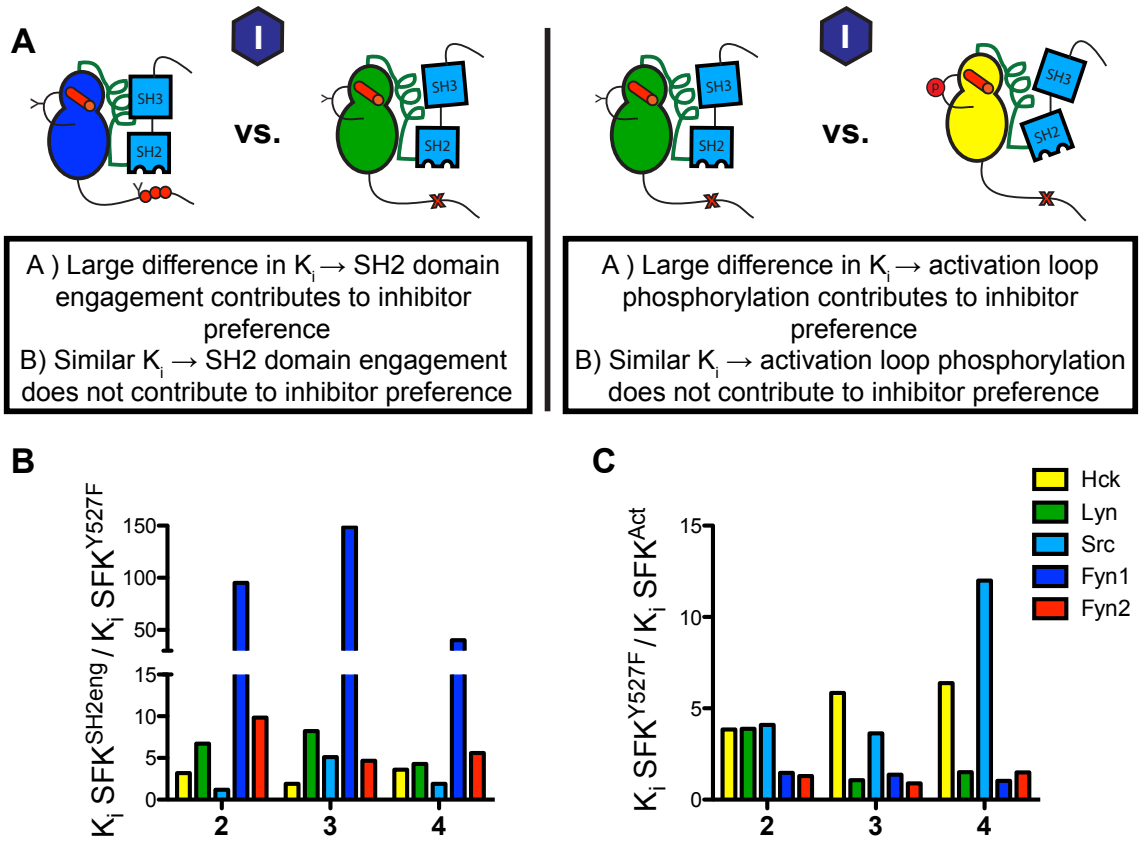

Figure 1-5: Effects of activation loop phosphorylation and regulatory domain engagement on the ATP-binding sites of SFKs

A. Schematic of the analysis that was performed. K_i values for SFK^{SH2eng} and SFK^{Act} are compared to SFK^{Y527F} in order to determine whether activation loop phosphorylation or SH2 domain engagement influences the affinity of **2**-**4**. **B**. Quantitative comparison of the differences in K_i values between SFK^{SH2eng} versus SFK^{Y527F} for ligands **2**-**4**. All values are the average of assays performed in triplicate; the SEM for each value is less than 20% of the average K_i value. **C**. Quantitative comparison of the fold difference in K_i values for SFK^{Y527F} versus SFK^{Act}. All values are the average of assays performed in triplicate; the SEM for each value is less than 20% of the average K_i value.

Table 1-4

Ligand	Lyn^{Act}	Lyn^{Y527F}	Lyn^{SH2eng}	$Fyn1^{Act}$	$Fyn1^{Y527F}$	$Fyn1^{SH2eng}$	$Fyn2^{Act}$	$Fyn2^{Y527F}$	$Fyn2^{SH2eng}$
2	9.1	35	240	1.8	<3	260	4.6	6.0	59
3	160	180	1450	25	35	5200	180	160	740
4	210	320	1380	15	15	620	21	31	180

Table 1- 4: K_i values (nM) for data shown in Figure 1-5

All SEMs are within 20% of the reported average.

D. ATP-binding site profiling of SFK^{SH3eng} and SFK^{SH2eng} regulatory state mutants confirms de-coupling of SH3 domain engagement from αC helix conformation in Fyn1

Due to the disparate activities of the autoinhibited SH2eng and SH3eng Fyn1 constructs (**Figure 1-2B**), we investigated whether this difference in activity is manifested in the observed affinities for inhibitors **2**-**4** for Fyn1^{SH3eng} versus Fyn1^{SH2eng} using a similar strategy as described in Figure 5 (**Figure 1-6A**). SH3 domain binding is predicted to align a network of residues in the SH2-catalytic domain linker that stabilizes the αC helix in an inactive conformation (**Figure 1-1C**). Therefore, it is odd that enhancing the affinity of Fyn1's SH2-catalytic domain linker for its SH3 domain would not autoinhibit the enzyme to an extent similar to that observed for Lyn and Fyn2 (**Figure 3**). Based on the relatively large differences in catalytic activities between the Fyn1^{SH3eng} and Fyn1^{SH2eng} constructs, we predicted that Fyn1^{SH3eng} would possess a more active ATP-binding site conformation. To test this, the K_i values of ligands that prefer an active conformation (**2**-**4**) were determined for Fyn1^{SH3eng} and Fyn1^{SH2eng} (**Table 1-5**). As predicted, ligands that prefer an active ATP-binding site conformation possess a higher affinity for Fyn1^{SH3eng} than Fyn1^{SH2eng} (**Figure 1-6B**). In contrast the SH3eng and SH2eng constructs of Lyn and Fyn2 possess similar affinities (SH3eng/SH2eng ~ 1-10) for these ligands. The fact that ligands **2**-**4** do not show as great of a preference for Fyn2^{SH3eng} over Fyn2^{SH2eng} is strong evidence that the de-coupling of Fyn1's SH3 domain from the αC helix is SH2-catalytic domain linker dependent. Unlike most SFKs, in which SH3 domain engagement results in autoinhibition directly, Fyn1's SH2-catalytic domain linker requires SH2 domain engagement to allosterically couple SH3 domain binding to the αC helix.

Figure 1-6

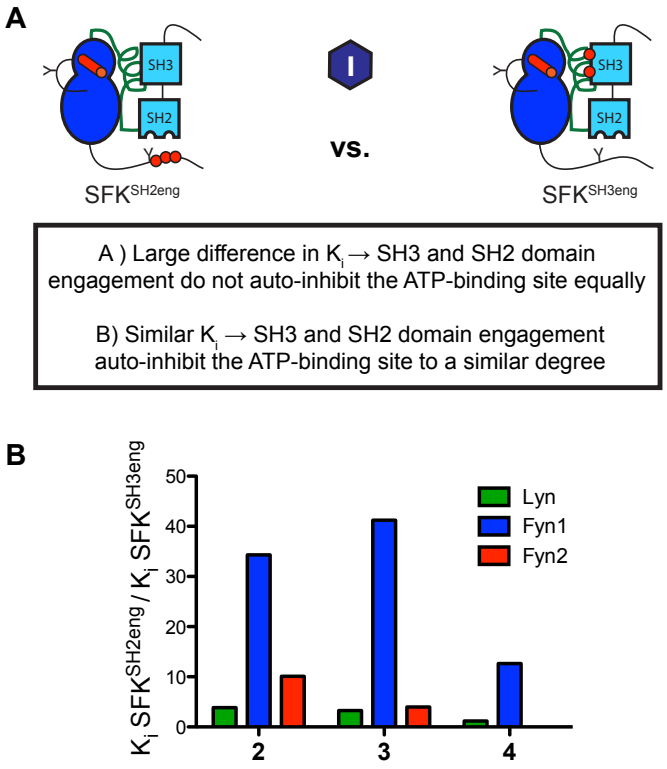

Figure 1-6: Intra-molecular engagement of Fyn1's SH3 domain minimally influences the conformation of its αC helix

A. Schematic of the analysis that was performed in C. K_i's for SFK^{SH2eng} and SFK^{SH3eng} were measured and compared for each SFK. Differences in affinity between SFK^{SH2eng} and SFK^{SH3eng} indicate differential effects of SH3 and SH2 binding on the ATP-binding site. **B**. Quantitative comparison of the fold difference in K_i values for SFK^{SH2eng} and SFK^{SH3eng}, illustrating the effects of SH2 domain or SH3 domain binding on ATP-binding site conformation. Compounds **2**, **3**, and **4** greatly prefer $Fyn1^{SH3eng}$ over $Fyn1^{SH2eng}$ showing that despite enhanced SH3 domain engagement Fyn1 maintains an active, αC helix-in binding site.

Table 1-5

Ligand	Lyn^{SH3eng}	Lyn^{SH2eng}	$Fyn1^{SH3eng}$	$Fyn1^{SH2eng}$	$Fyn2^{SH3eng}$	$Fyn2^{SH2eng}$
2	440	240	7.5	260	5.8	59
3	350	1450	120	5200	190	740
4	1160	1380	49	620	----	180

Table 1- 5: K_i values (nM) for data shown in Figure 1-6

All SEMs are within 20% of the reported average.

E. αC helix conformation is less coupled to SH3 domain intra-molecular engagement in Fyn1 than in Fyn2, Lyn, Src, and Hck.

Given the surprising differences that were observed in how regulatory domain engagement affects ATP-binding site conformation in Fyn1 and Fyn2, we next investigated how αC helix conformation affects intra-molecular regulatory domain engagement using our panel of conformation-selective ligands. SH3 domain accessibility was measured using the pull-down assay described in Figure 3. Each SFK of interest was incubated with a saturating amount of a conformation-selective inhibitor before exposure to SH3 domain-binding peptide resin. Comparing the relative amounts of retained Lyn, Fyn1, and Fyn2 when bound to active or αC helix-out stabilizing ligands, provides a measure of how αC helix conformation influences SH3 domain accessibility within the context of each SFK. Ligand **8**, which stabilizes an inactive activation loop conformation (DFG-out) but an active αC helix conformation (αC helix-in), was also tested in order to investigate the contribution of the activation loop to regulatory domain accessibility. Ligands that stabilize the DFG-out inactive conformation form a hydrogen bond with Glu310 in the αC helix—similar to αC helix-in, active ligands **2**-**4**—and are thus predicted to prefer the ATP-binding sites of activated over autoinhibited SFK constructs (**Figure 1-7A**). Consistent with this hypothesis, stabilizing the DFG-out conformation of Src and Hck results in increased SH3 domain accessibility.[18] SH3 pull-downs were performed with Lyn^{Y527F}, $Fyn1^{Y527F,}$ and $Fyn2^{Y527F}$ in the presence of a saturating concentration of **1, 2, 5, 6**, or **8** (**Figure 1-7B**). For each of these experiments, ligand **1**, which has a minimal preference for SFK activation state, was used as a reference compound.

Figure 1-7

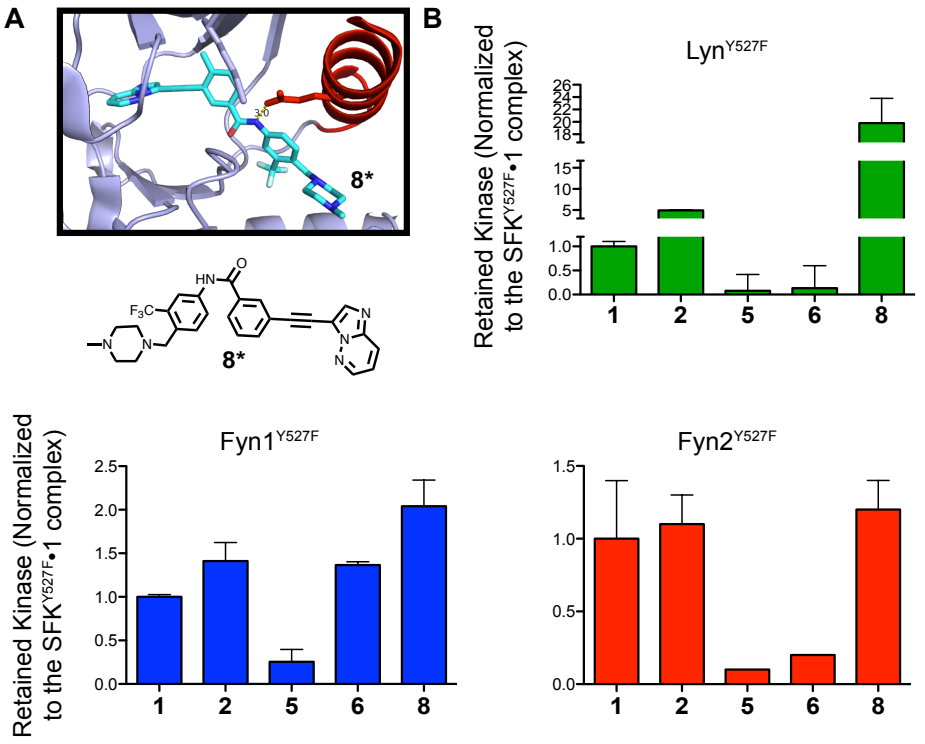

Figure 1-7: Conformation-selective inhibitors differentially modulate the SH3 domain accessibilities of Lyn, Fyn1, and Fyn2

A. Molecular structure of ligand **8** as well as a crystal structure of **8** bound to the ATP-binding site of Abl (PDB: 3OXZ). **8** stabilizes the DFG-out inactive conformation and is predicted to stabilize helix αC in an active conformation by forming an electrostatic interaction with Glu310. **B**. Quantification of the SH3 pull-down experiment performed with Lyn^{Y527F}, $Fyn1^{Y527F}$, and $Fyn2^{Y527F}$ in the presence of saturating **1**, **2**, **4**, **5**, or **8** (mean ± SEM, n=3). All data normalized to the SFK^{Y527F}·**1** complex (**1** does not show a strong preference for SFK^{Act} over SFK^{SH2eng}).

Consistent with their predicted effects and previous results observed for Hck, more Lyn^{Y527F} kinase was retained by the SH3 peptide ligand resin in the presence of **2** compared to **1** (~5-fold increase), while much less bound the resin in the presence of **5** and **6** (~10-fold decrease, **Figure 1-7B**). Strikingly, a ~20-fold increase in retained kinase was observed in the presence of compound **8**. This agrees with recently reported results for Src and Hck, and is consistent with the observation that DFG-out ligands stabilize the αC helix in an active conformation. The same pull-down experiment was used to probe

Fyn1 SH3 domain accessibility. Interestingly, while the trends in SH3 domain accessibility are the same for each Fyn1^{Y527F} inhibitor complex, the relative differences in SH3 domain accessibility are much smaller compared to Fyn1^{Y527F}·**1** (**Figure 1-7B**)**.** Compound **5** reduced SH3 domain accessibility several fold, but the reduction is not as dramatic as that observed for Lyn^{Y527F}, and compound **6** failed to change SH3 domain accessibility to any detectable extent. Similarly, **2** and **8** do not significantly increase Fyn1's SH3 domain accessibility. Next, pull-down assays were repeated using Fyn2^{Y527F} in order to probe whether Fyn1's anomalous SH2-catalytic domain linker is responsible for de-coupling the αC helix from SH3 domain accessibility. The fact that Fyn2 displays a greater reduction of SH3 domain accessibility when bound to either **5** or **6** (comparable to the reduced levels observed with Src), suggests that this is indeed the case. However, unlike Lyn and Hck, Fyn2^{Y527F} does not show a dramatic increase in SH3 domain accessibility in the presence of inhibitors **2** and **8**. Thus, while the SH3 domain of Fyn2 shows stronger allosteric coupling to its ATP-binding site than Fyn1, this SFK behaves more like Src than Hck or Lyn. This similarity in behavior correlates with differences in the SH2-catalytic domain linker (**Figure 1-1B**).

Inhibitor binding-mediated changes in SH3 domain accessibility were also explored using the SFK^{SH2eng} construct (**Figure 1-8A**). Both Lyn^{SH2eng}·**1** and Fyn1^{SH2eng}·**1** display a relatively inaccessible SH3 domain compared with SFK^{Y527F}·**1**, consistent with enhanced SH2–C-terminal tail intra-molecular engagement promoting SH3 domain-SH2-catalytic domain linker interaction in both kinases. When bound to ligand **2**, the SH3 domain accessibility of Fyn1^{SH2eng} and Lyn^{SH2eng} returns to a level on par with Fyn1^{Y527F}·**1** and Lyn^{Y527F}·**1**, respectively (**Figure 1-8B**). These data show that adopting an active ATP-

binding site conformation is able to overcome engineered regulatory domain engagement. It also indicates that although Fyn1 displays reduced coupling between the SH3 domain and the ATP-binding site, enhancing the interaction between the SH2 domain and C-terminal tail is able to engage the SH3 domain and stabilize an αC helix-out inactive ATP-binding site. These effects can be reversed by stabilizing an αC helix-in, active ATP-binding site with a ligand.

Figure 1-8

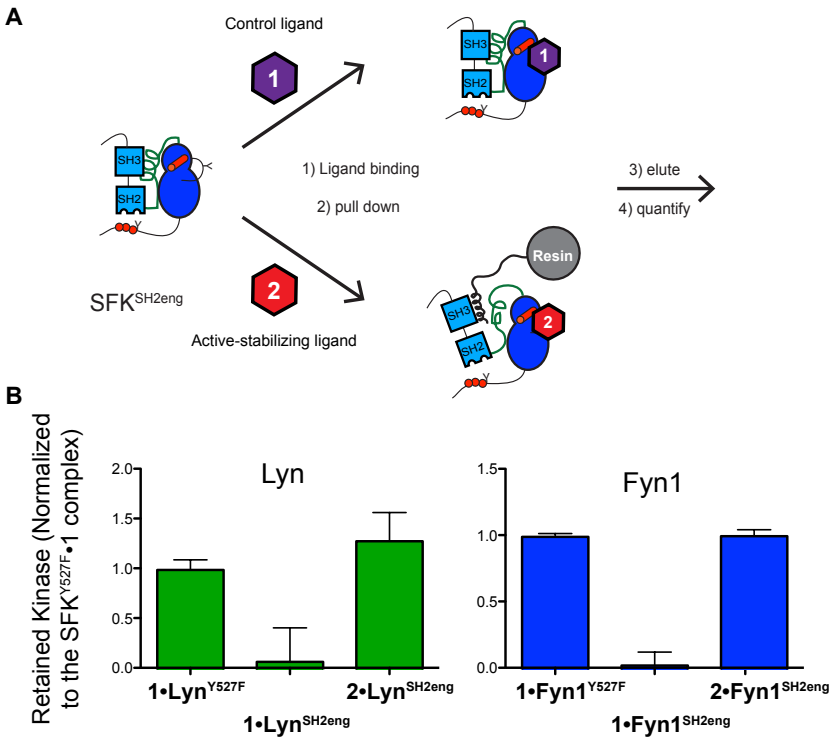

Figure 1-8: Stabilizing an active ATP-binding site conformation overcomes regulatory interactions in Lyn and Fyn1

A. SH3 pull-downs were performed using SFK^{SH2eng} constructs. SFK^{SH2eng} were incubated with control ligand **1** or active-preferring ligand **2** and the amount of kinase retained on the resin compared. **B**. Quantification of SFK^{SH2eng} SH3 pull-down experiment (mean ± SEM, n=3). All data normalized to the SFK^{Y527F}·**1** complex.

The ability of ATP-binding site conformation to allosterically influence SH2 domain accessibility was also probed for Fyn1, Fyn2, and Lyn 3D constructs in pull-downs utilizing

resin displaying an SH2 binding peptide (**Figure 1-9**). The observed trends mirror the results from the SH3 pull-down experiments but overall differences in SH2 regulatory domain accessibility are smaller. However, these results suggest that ATP-binding site conformation allosterically modulates SH2 domain accessibility to differing degrees between SFK family members.

Figure 1-9

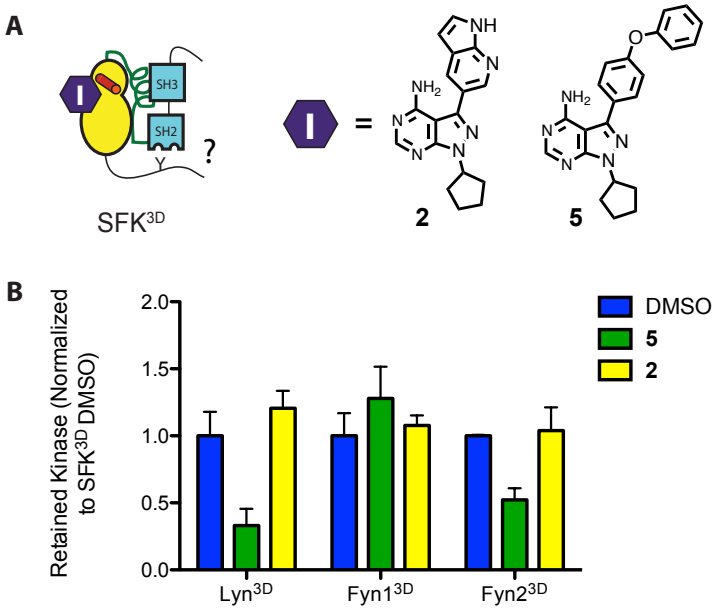

Figure 1-9: Conformation-selective inhibitors differentially modulate Lyn and Fyn SH2 domain accessibility

A. SH2 pull-downs were performed to assess the accessibility of SFK^{3D} constructs SH2 domains when bound to active-stabilizing ligand **2** and αC helix-out, inactive-stabilizing ligand **5**. **B**. Quantification of SFK^{3D} SH2 pull-down experiment (mean ± stdev, n=2). All data normalized to SFK^{3D}·DMSO.

F. Comparison of Fyn1 and Fyn2 SH2 domain accessibility demonstrates biologically relevant consequences of SH2-catalytic domain linker mediated coupling among SFKs

Fyn1 and Fyn2's SH2-catalytic domain linker variability results in surprising differences in degree of allosteric coupling between the SH2 and SH3 domains and the ATP-binding site, but what are the biological consequences of more versus less coupling

for a particular SFK? Csk is the primary kinase responsible for autoinhibition of SFKs in most cells (Okada et al., 1991; Superti-Furga et al., 1993). It phosphorylates Tyr527 on the C-terminal tail of all SFK family members, resulting in enhanced intra-molecular engagement of the SH2 domain and autoinhibition. The biochemical studies described so far suggest that Fyn1's reduced ATP-binding site - regulatory domain coupling results in greater overall regulatory domain accessibility regardless of ATP-binding site conformation compared to Fyn2. Thus, one would predict that Fyn1's C-terminal tail would be more vulnerable to phosphorylation by Csk than Fyn2's. Csk has been shown crystallographically to interact only with the C-terminus of Src (Levinson et al., 2008). Fyn1 and Fyn2 possess identical C-termini, thus comparing the rate of phosphorylation is directly probing how SH2-catalytic domain linker variation between the two isoforms affects post-translational modification (**Figure 1-10A**).

Figure 1-10

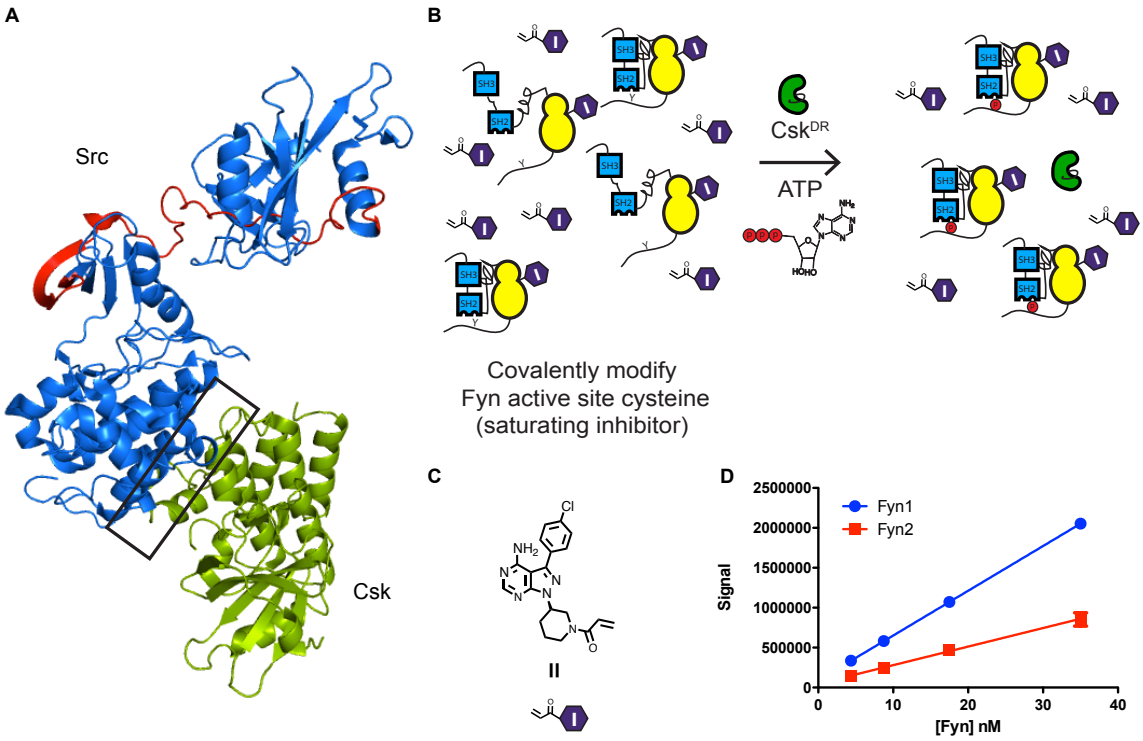

Figure 1-10: The SH2-catalytic domain linker affects availability of the C-terminal tail to post-translational modification by Csk

A. A crystal structure of regulatory domain-disengaged Src (blue, PDB: 1Y57) super imposed onto a co-crystal structure of the Src catalytic domain-Csk complex (green, PDB: 3D7T). The interface between Csk and Src is boxed, while the variable region between Fyn1 and Fyn2 is colored red. Regions shown in blue are identical between Fyn1 and Fyn 2. **B**. Scheme for measuring pTyr527 phosphorylation of inhibitor-bound Fyn1 and Fyn2 complexes by Csk. **C**. Structure of a Michael acceptor analogue of ligand **1**. **D**. Graph displaying results of pTyr527 experiment. Radioactive phosphate signal is plotted versus Fyn concentration in nM (mean ± SEM, n=3).

To prevent the complication of competing C-terminal tail auto-phosphorylation obscuring the activity of Csk, inhibitor-bound complexes of Fyn1 and Fyn2 were used. Due to high sequence homology, the ATP-competitive ligands used in this study inhibit Csk in addition to SFKs, making it necessary to devise a scheme in which Fyn is completely inhibitor bound but pTyrY527 by Csk is uninhibited. To this end, Ser350 and Ser347 in the active sites of Fyn1 and Fyn2, respectively, were mutated to Cys, and a Michael acceptor analogue of **1** was used to covalently modify the Fyn active sites (**Figure 1-10C**). The pharmacophore of ligand **1** was selected due to its lack of activation state preference. As expected, the electrophile-modified version of **1** is a much more potent inhibitor of Fyn1 and Fyn2 active site Cys constructs than their wild type counterparts (**Table 1-6**). Furthermore, it is possible to inhibit >98% of $Fyn1^{S350C}$ and Fyn^{2S347C} without inhibiting a drug resistant Csk construct (Csk^{DR}) (**Table 6**). A Csk substrate peptide previously reported was used to verify the catalytic activity of Csk^{DR} (Sondhi et al., 1998).

Varying concentrations of inhibitor-bound $Fyn1^{S350C}$ and $Fyn2^{S347C}$ were incubated with Csk^{DR} and γ-^{32}P-ATP and the amount of pTyr527 was monitored over time (**Figure 1-10B**). Plotting radioactive signal versus Fyn concentration reveals that $Fyn1^{S350C}$ is a better substrate for Csk than $Fyn2^{S347C}$ (**Figure 1-10D**). Activity assays in Figure 2 revealed that Fyn1 is more autoinhibited than Fyn2 when intra-molecular engagement of

the SH2 domain is enhanced. Therefore, these results predict that Fyn1 is more autoinhibited *in vivo* despite possessing an ATP-binding site that favors an active conformation more so than all SFKs examined due to αC helix decoupling. This conclusion is supported by cell biology experiments: in HEK293 cells, Fyn1 displays more pTyr527 and less pTyr416 than Fyn2. As a result, the SH3 domain of Fyn1 is *less* available for inter-molecular interactions than the SH3 domain of Fyn2 (Brignatz et al., 2009).

Table 1-6

Kinase Construct	Percent Inhibition at 50μM pharmacophore **1**
Csk^{DR}	13 ± 12
$Fyn1^{S350C}$	99 ± 1
$Fyn2^{S347C}$	103 ± 4

Table 1- 6: Activity assays of pharmacophore 1 and Csk^{DR}, $Fyn1^{S350C}$, and $Fyn2^{S347C}$

Activity assays utilizing the peptide substrates of $Fyn1^{S350C}$/$Fyn2^{S347C}$ and Csk^{DR} show that Csk^{DR} is uninhibited at the concentration of pharmacophore **1** used in the pTyr5277 assay (50 μM). In contrast, $Fyn1^{S350C}$ and $Fyn2^{S347C}$ are completely inhibited at this same concentration.

III. Conclusion:

In this study, we have investigated how SH2-catalytic domain linker heterogeneity between SFKs influences bi-directional coupling between the αC helix and regulatory domains. Using a panel of ATP-competitive inhibitors that stabilize the αC helix in two distinct conformations, we have probed a) the conformation of the αC helix when intra-molecular engagement of the SH2 and SH3 domains is enhanced or weakened and b) how αC helix conformation affects SH2 and SH3 domain availability for inter-molecular

interactions for Fyn and Lyn. Given the high sequence homology of SFK SH2, SH3, and catalytic domains, we like many others in the field, focused on the relatively non-homologous SH2-catalytic domain linker as a source of non-redundant biological functions between SFKs. Based on previous work with Src and Hck, we further hypothesized that the SFK SH2-catalytic domain linkers uniquely govern the magnitude of allosteric coupling between the regulatory domains and the ATP-binding site, thus influencing the availability of the regulatory domains for inter-molecular interactions. This comprehensive biochemical study is an important first step towards understanding how homologous protein kinases play non-redundant cellular roles.

Analysis of Fyn1 and Fyn2 serves as a direct probe into the influence of the SH2-catalytic domain linker on coupling between the SH3 and SH2 domains and the ATP-binding site. Fyn1's longer dissimilar linker, characterized by a 3-residue insertion, is primarily responsible for reduced allosteric coupling between the αC helix and the SH3 domain compared to Fyn2 and all other SFKs investigated. Intriguingly, engagement of Fyn1's SH2 domain autoinhibits the kinase to a greater extent than Fyn2 as demonstrated by decreased catalytic activity and diminished affinity for inhibitors that stabilize an active ATP-binding site. Rigorous analysis of the ATP-binding sites of Fyn1, Fyn2, Lyn, Src, and Hck with conformation-selective inhibitors suggests that, in the absence of post-translational modification and SH2 domain engagement, the ATP-binding site of Fyn1 favors an active conformation. In contrast, Fyn2 and other SFKs exhibit an ATP-binding site conformation somewhere between active and autoinhibited.

It has been proposed that allosteric regulation in SFKs follows a "snap-lock" mechanism, which postulates that SH3 and SH2 domains are coupled by the short linker

segment connecting the two domains. The SH3-SH2 domain linker has been shown to be important for catalytic domain regulation by mutagenesis and molecular dynamics simulations (Young et al., 2001). Tightly coupled SH3 and SH2 domains produce a kinase in which engagement of either the SH2 or SH3 domain recruits the other domain, while less coupled SH3 and SH2 domains results in decreased synchronization between domains. NMR studies have shown that the SH3-SH2 domains of Fyn—identical between isoforms 1 and 2—are tightly coupled compared to the SFK Lck, which has a flexible SH3-SH2 linker (Hoffman et al., 2005). However, despite having identical SH3-SH2 linkers, Fyn1 shows an anomalous mechanism of autoinhibition in which SH3 domain engagement does not induce SH2 domain engagement nor complete autoinhibition of the catalytic domain, as is generally the case for Fyn2, as well as Src, Lyn, and Hck. Yet Fyn1 SH2 domain engagement is extremely effective at autoinhibiting the catalytic domain through a mechanism that is not entirely clear. It is possible that SH2 domain engagement stabilizes the SH2-catalytic domain linker in a conformation that allows for allosteric control over the catalytic domain through SH3 binding. SH2-catalytic domain linker variability can thus influence coupling of SH3 and SH2 domain engagement beyond the contribution of the SH3-SH2 linker. This result illustrates the importance of studying multi-domain SFKs as opposed to individual domains.

SH2-catalytic domain linker heterogeneity has important consequences for SFK regulation and function in cells. This is illustrated by investigation of Fyn1 and Fyn2 C-terminal tail availability for phosphorylation by Csk. All *in vitro* evidence suggests that Fyn1 would be more active in cells—it is characterized by more SH3 domain accessibility regardless of αC helix conformation and favors an active ATP-binding site conformation

compared to Fyn2 and other SFKs. However, experiments in HEK293 cells report that Fyn1 is less activation loop phosphorylated and possesses an SH3 domain that is less available for inter-molecular interactions compared to Fyn2 (Brignatz et al., 2009). We have shown that, due to its more accessible SH2 domain, Fyn1 is a better substrate for Csk phosphorylation and thus is more autoinhibited in cells when Csk is active. This implies that, because of Fyn1's strong autoinhibition by SH2 domain engagement brought about by its unique SH2-catalytic domain linker, Fyn1's cellular function is determined by the competing activities of Csk and phosphatases to a greater extent than Fyn2 and other SFKs. This finding draws attention to the surprising consequences of SH2-catalytic domain linker differences in the complex environment of the cell. Beyond providing insight into allosteric regulation within the SFKs, these studies suggest how individual SFKs are able to play non-redundant roles in cellular processes despite high sequence homology and co-expression. For example, in Mast cell and B cell signaling, Fyn and Lyn have been demonstrated to play opposing and/or non-redundant functions (Palacios and Weiss, 2004; Okutaro et al., 1997; Parravicini et al., 2002; Xu et al., 2012; Falanga et al., 2012). The structural source of this non-redundancy is currently unknown, but our results indicate that it may be due to SH2-catalytic domain linker heterogeneity between the two kinases. The biological repercussions of varied coupling between SFK SH3 and SH2 domains are an interesting avenue for future exploration.

IV. Materials and Methods:

A. SFK regulatory state mutant design and protein expression.

Quikchange mutagenesis was used to introduce all point mutations. SFK^{Y527F} constructs: Lyn Y508F, Fyn1 Y531F, and Fyn2 Y528F. SFK^{SH2eng} constructs: Lyn

Q509E/Q510E/Q511I, Fyn1 Q532E/P533E/G534I, Fyn2 Q529E/P530I/G531I. SFK^{SH3eng} constructs: Lyn K233P/K236P, Fyn1 M251P/L254P/T255P, Fyn2 T251P/T254P/S255P. Fyn active-site cysteine constructs: Fyn1 S350C and Fyn2 S347C. The Src-family kinases Fyn1 (residues 82–537), Fyn2 (residues 82-534), and Lyn (residues 64–512) were expressed with YopH and GroEL and purified as previously described for Src and Hck (Krishnamurty et al., 2012; Seeliger et al., 2005). All constructs possess an N-terminal his-tag to facilitate purification and TEV protease cleavage site. All constructs were obtained in 95% or greater purity. Csk^{DR} plasmid was transformed into BL21 (DE3) competent cells and purified by GST resin.

B. Preparation of activation loop-phosphorylated SFK (pTyr416 SFK) (Krishnamurty et al., 2012; Leonard et al., 2014).

SFK was auto-phosphorylated at Tyr416 by incubating SFK (250 nM) with ATP (1 mM) and BSA (1 mg/mL) in activation buffer (50 mM HEPES, pH = 7.5, 10 mM $MgCl_2$, 2.5 mM EGTA, 100 mM NaCl). The reaction was incubated at 25^{o}C for 1.5 hr. Quantitative phosphorylation was monitored with antibodies that specifically recognize activation loop-phosphorylated Src (1:2000 P-Src Family (Tyr416 DM9G4) Cell Signaling) and non-pTyr416 (1:2,000 non-pY416 (7G9) Cell Signaling) (data not shown).

C. Substrate K_m determination.

Peptide substrate K_m determination. Activity of SFK regulatory state mutants in the presence of varying concentrations of Src-peptide substrate (Ac-EIYGEFKKK-OH) were determined (3-fold dilutions starting at an initial concentration of 900 μM, 7 data points) in assay buffer containing 75 mM HEPES, pH = 7.5, 15 mM $MgCl_2$, 3.75 mM EGTA, 1mM Na_3VO_4, 150 mM NaCl, 0.2 mg/mL BSA, γ32P ATP (0.2 μCi/well) at room temperature and ambient pressure. The concentrations of SFK constructs were as follows: 0.7 nM

Lyn^{Act}, 0.3 nM $Fyn1^{Act}$, 2. 5nM $Fyn2^{Act}$, 10 nM Lyn^{SH2eng}, 10 nM $Fyn1^{SH2eng}$, and 3 nM $Fyn2^{SH2eng}$. The final volume of each assay well was 30 µL. The enzymatic reaction was run at room temperature for 2 hrs and then terminated by spotting 4.6 µL of the reaction mixture onto a phosphocellulose membrane. Membranes were washed with 0.5% phosphoric acid (3x, 10 minutes each wash), dried, and the radioactivity was determined by phosphorimaging with a GE Typhoon FLA 9000 phosphor scanner. The scanned membranes were quantified with ImageQuant. Data was analyzed using Prism Graphpad software and K_m values were determined using Michaelis-Menten analysis.

ATP K_m determination. Activity of SFK regulatory state mutants in the presence of varying concentrations of ATP were determined (3-fold dilutions starting at 500 µM, 7 data points). Assay conditions are the same as described above with 100 µM SPS added to the assay buffer solution. The concentration of γ32P ATP was increased to 0.8 µCi/well, while the overall ATP concentration was varied using non-radioactive ATP. The concentrations of SFK constructs were as follows: 0.7 nM Lyn^{Act}, 0.3 nM $Fyn1^{Act}$, 2.5 nM $Fyn2^{Act}$, 10 nM Lyn^{SH2eng}, 10 nM $Fyn1^{SH2eng}$, 3 nM $Fyn2^{SH2eng}$, 5 nM Lyn^{SH3eng}, 1.2 nM $Fyn1^{SH3eng}$, and 2.2 nM $Fyn2^{SH3eng}$. The scanned membranes were quantified with ImageQuant. Data was analyzed using Prism Graphpad software and K_m values were determined using Michaelis-Menten analysis.

D. Enzymatic activity determination.

Titrations of SFK regulatory state mutants (2-fold serial dilutions starting and 20nM, 7 data points) were assayed in buffer containing 75 mM HEPES, pH = 7.5, 15 mM $MgCl_2$, 3.75 mM EGTA, 1mM Na_3VO_4, 150 mM NaCl, 0.2 mg/mL BSA, γ32P ATP (0.2 µCi/well), and 100 µM SPS. The final volume of each assay well was 30 µL. The enzymatic reaction

was run at room temperature for 2 hrs and then terminated by spotting 4.6 µL of the reaction mixture onto a phosphocellulose membrane. Membranes were washed with 0.5% phosphoric acid (3x, 10 minutes each wash), dried, and the radioactivity was determined by phosphorimaging with a GE Typhoon FLA 9000 phosphor scanner. The scanned membranes were quantified with ImageQuant and converted to percent activity. Data was analyzed using Prism Graphpad (mean ± SEM, n = 3).

E. Activity assays for inhibitor K_i determination (Krishnamurty et al., 2012; Leonard et al., 2014).

Inhibitors (initial concentration = 10 µM, 3-fold serial dilutions, 10 data points) were assayed in triplicate against all SFK constructs. Assay conditions were the same as described for enzymatic activity assays. Concentrations of SFK constructs are as described above in SPS K_m determination. Assays of Csk^{DR} (25nM) were performed using 100 µM CSKtide (KKKEEIYFFFG-NH_2). Blot radioactivity was determined by phosphorimaging with a GE Typhoon FLA 9000 phosphor scanner. The scanned membranes were quantified with ImageQuant and converted to percent inhibition. Data was analyzed using Prism Graphpad software and K_i values were determined using non-linear regression analysis.

F. Pull-down assays to determine regulatory domain accessibility (Krishnamurty et al., 2012; Leonard et al., 2014).

Formation of the kinase–inhibitor complex. The kinase of interest (100 nM) and mammalian lysate (0.2 mg/ml) were diluted in immobilization buffer (50 mM Tris, 100 mM NaCl and 1 mM DTT, pH 7.5). A saturating amount of the inhibitor of interest (5 µM or 10 µM) was added to this kinase dilution. The mixture was allowed to incubate for 30 min before loading on the resin.

SH3 Pull-down. Forty microliters of a 50% slurry of SNAP-Capture Pull-Down Resin (NEB) was placed in a microcentrifuge tube. The resin was washed (twice, ten-bed volumes) with immobilization buffer. A SNAP tag–polyproline peptide fusion (VSLARRPLPPLP) (10 μM) was loaded onto the resin at a final volume of 100 μl in buffer. The resin was rotated at room temperature for 90 min. After polyproline peptide immobilization, the resin was washed (twice, ten-bed volumes), and 100 μl of the kinase–inhibitor complex was loaded. The resin was allowed to shake at room temperature for 1 hr. After incubation with the kinase–inhibitor complex, the flow through was collected, and the resin was washed (three times, ten-bed volumes). To elute the retained kinase, 100 μl of 1× SDS loading buffer was added, and the beads were boiled at 90 °C for 10 min. All samples were separated by SDS-PAGE and visualized by western blotting using a His6-specific antibody (at a 1:5,000 dilution (abm, HIS.H8)). The scanned blots were quantified with LI-COR Odyssey software to determine the percentage of kinase retained on the resin on the basis of the loaded and eluted fractions (mean ± SEM, n = 3).

SH2 Pull-down. Pull-downs were performed as described previously using resin displaying an SH2 binding peptide (EPQpYEEIPIYL) (Leonard et al., 2014). *G.Phosphorylation of Tyr527 assay.*

Titrations of Fyn1^{S350C} and Fyn2^{S347C} starting at 35nM (2-fold serial dilutions, 4 data points) were incubated with 50 μM pharmacophore **1** with 0.25 mg/mL BSA, 1mM Na_3VO_4, and 0.5 mM DTT in activation buffer pH 7.5. Following 4 hr incubation at room temperature, 25 nM Csk^{DR} was added and phosphorylation was initiated by the addition of γ32P ATP (0.2 μCi/well). The final volume of each assay well was 30 μL. The enzymatic

reaction was run at room temperature for 1 hr and then terminated by spotting 4.6 µL of the reaction mixture onto a nitrocellulose membrane. Membranes were washed with 0.5% phosphoric acid (3x, 10 minutes each wash), air-dried, and the radioactivity was determined by phosphorimaging with a GE Typhoon FLA 9000 phosphor scanner. The scanned membranes were quantified with ImageQuant and data was analyzed using Prism Graphpad software (mean ± SEM, $n = 3$).

Chapter 2: Characterization of ATP-Binding Site – Regulatory Domain Allosteric Coupling in the Non-Receptor Tyrosine Kinase Abl using Conformation-Selective Inhibitors

I. Introduction:

The Abl kinases are a small group of non-receptor tyrosine kinases that share strong sequence and structural homology with SFKs, consisting of c-Abl (ABL1) and its paralogue Arg (ABL2) (Hanks, et al., 2003). Abl has been the focus of drug discovery efforts due to its pivotal role in Chronic Myelogenous Leukemia (CML), in which c-Abl becomes fused with the Breakpoint Cluster Region (BCR) through a chromosomal translocation in myeloid cells, generating constitutively active BCR-Abl (Raitano, et al., 1997; Daley, et al., 1990). This fusion protein's enhanced activity is a product of oligomerization via BCR, which enhances Abl activation loop autophosphorylation, and partially disrupts Abl's autoinhibitory mechanism (McWhirter, et al., 1993; Nagar, et al., 2003; Taylor and Keating, 2005).

The first successful kinase-targeted anti-cancer therapeutic, imatinib (Gleevec), is a Type II DFG-out inhibitor that potently and selectively inhibits the kinase activity of Abl, effectively curing CML (Buchdunger, et al., 1996; Druker, et al., 1996; Druker, et al., 2001). Due to the fact that SFK's do not readily bind imatinib, it was hypothesized that the ability to adopt the DFG-out inactive conformation is a unique property of Abl, which confers unique sensitivity to imatinib (Nagar, et al., 2003). This hypothesis has since been disproven by crystal structures of SFKs bound to imatinib in the DFG-out conformation, as well as the generation of DFG-out inhibitors that bind to Src and Abl with similar affinities. However, questions about how ATP-binding site conformation is coupled to Abl's structural regulation remain (Seeliger, et al., 2007; Seeliger, et al., 2009).

Specifically, how the conformation of the DFG-motif is coupled to the global conformation of Abl, and if this differs from SFKs despite substantial structural similarity between SFKs and Abl, is not well understood (Nagar, et al., 2007; Harrison, et al., 2003).

Here, a detailed discussion of Abl's structure, in relation to the SFKs, is provided in order to provide proper context. Like Src, the N-terminus of Abl consists of an N-terminal region (N-cap) that contains a glycine, which can be myristoylated. The N-cap is followed by SH3 and SH2 regulatory domains, which are connected via a SH2-catalytic domain linker to the catalytic domain (Nagar, et al, 2003, Pluk et al., 2002). A splice-variant–Abl1a–contains an N-terminal sequence with no myristoylation site but is otherwise identical in structure and regulation as Abl1b, which is myristoylated. Abl is twice as large as the SFKs and possesses a C-terminal segment, known as the last exon region, that is important for many biological functions. The last exon region contains sites for SH3 domain binding, nuclear localization (NLS) and nuclear export (NES) sequences, an actin binding domain, and a DNA binding domain (reviewed by Wang, 2014). Abl autoinhibition is analogous to Src's in that the intra-molecular engagement of the SH3 domain to the SH2-catalytic domain linker results in a decrease in catalytic activity (Nagar, et al., 2003; Pluk, et al., 2002). However, Abl does not have a C-terminal tail with a tyrosine residue that can be phosphorylated to serve as an intra-molecular ligand for its SH2 domain. Instead, Abl's SH2 domain docks against the C-lobe of the catalytic domain in the autoinhibited conformation. The SH2 domain-binding interface on the C-lobe is created upon binding of the N-cap myristate in a pocket located in the C-lobe. Myristate binding causes helix αI in the C-lobe to convert from one extended helix into two shorter helices (αI and αI') oriented roughly 90 degrees to each other, creating the SH2 domain-

binding site (Nagar, et al., 2003). This autoinhibited state is further stabilized by interactions between the rest of the N-cap and the SH2-SH3 domains (Pluk et al., 2002; Nagar, et al., 2006). Autoinhibition can also be achieved using small molecules, such as GNF-2, which bind the myristate pocket and allosterically inhibit the catalytic domain (Adrián, et al., 2006; Zhang, et al., 2010).

Figure 2-1

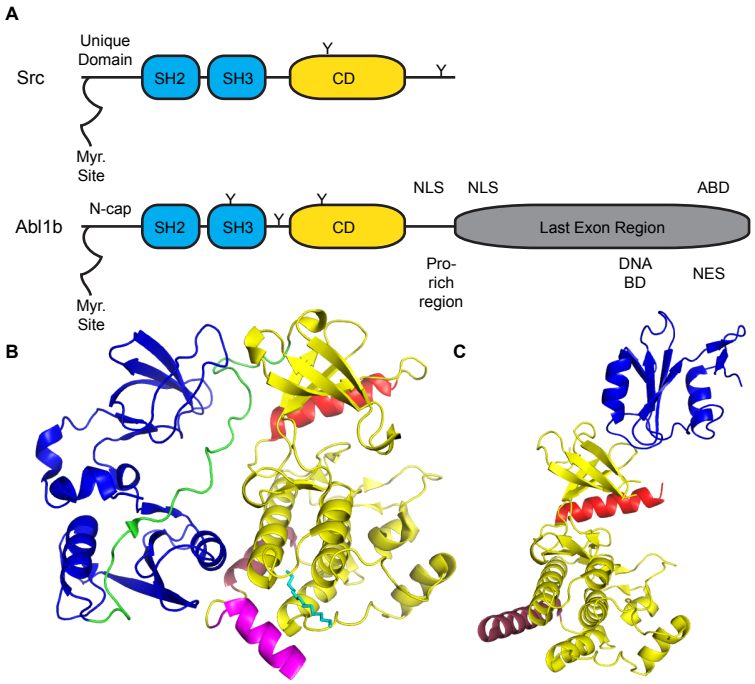

Figure 2- 1: An overview of c-Abl's structure

A. Linear representations of the structural features of Src and Abl. ABD (Actin-binding domain), DNABD (DNA-binding domain), NLS (nuclear localization sequence), NES (nuclear export sequence). **B**. Structure of autoinhibited Abl^{3D} (PDB: 2FO0). SH2 and SH3 domains shown in blue, SH2-catalytic domain linker shown in green, catalytic domain shown in yellow, αC helix shown in red, αI shown in light pink, αI' shown in bright pink, and myristate shown in cyan. **C**. Structure of Abl catalytic domain and SH2 domain (PDB: 4XEY) in an active conformation (same color scheme as in B).

When bound to the C-lobe, the SH2 domain is unable to bind phosphopeptide motifs. Binding of phosphopeptides to the SH2 domain results in displacement from the catalytic domain and an increase in catalytic activity (Nagar, et al., 2003; Hantschel, et

al., 2003; Lorenz, et al., 2015). In fact, in order for Abl to exhibit full catalytic activity the SH2 domain must dock on top of the N-lobe, near the αC helix (Nagar, et al., 2006; Filippakopoulos, et al, 2008; Grebien, et al., 2011). It has been shown that binding of the SH2 domain to the N-lobe positions the activation loop in a conformation that is more readily phosphorylatable than the kinase domain alone (Lamontanara, et al., 2014). Disrupting the SH2 domain–N-lobe interaction leads to a reduction of leukemogenesis in BCR-Abl expressing cells, highlighting the importance of this interaction for Abl's catalytic activity, as well as its therapeutic relevance (Grebien, et al., 2011). The non-receptor tyrosine kinase Fes is also activated by docking of the SH2 domain to the N-lobe, which positions helix αC in an active conformation, leading to the hypothesis that the same molecular mechanism is at play in Abl (Filippakopoulos, et al., 2008). This further suggests that Abl activation is coupled to αC helix conformation like in the SFKs. In contrast, it has been hypothesized that the SH2 domain's interaction with the C-lobe in Abl stabilizes the DFG-out conformation of the catalytic domain and that this characteristic differentiates autoinhibited Abl from autoinhibited Src, where the αC helix-out conformation is stabilized by the SH3 domain/SH2-catalytic domain linker interaction (Nagar, et al., 2003). However, this hypothesis is contradicted by the observation that imatinib shows higher affinity for the ATP-binding site of activated (SH3 and SH2 domain intra-molecular interactions disrupted) Abl versus autoinhibited (SH3 and SH2 domain intra-molecular interactions are engaged) Abl, suggesting that the ATP-binding site of activated Abl is more similar to imatinib's DFG-out binding mode than that of autoinhibited Abl (Hantschel, et al., 2003).

How exactly is ATP-binding site conformation, specifically the positions of the αC helix and the DFG motif, coupled to SH2 and SH3 domain accessibility in Abl? Several recent studies indicate that αC helix conformation plays an important role in Abl structural regulation (Dölker, et al., 2014; Levinson, et al., 2006). Additionally, an NMR structure of Abl bound to imatinib features more accessible SH3 and SH2 domains, the opposite of what one would expect if the DFG-out conformation defined autoinhibited Abl, and similar to what has been reported for SFKs bound to DFG-out inhibitors (Skora, et al., 2013; Leonard, et al., 2014; Register, et al., 2014). A systematic study using conformation-selective, ATP-competitive inhibitors and Abl regulatory state mutants has the potential to resolve open questions about the role of inactive ATP-binding site conformations in Abl. In this study, the affinities for αC helix-out-, DFG-out-, and active-preferring ligands were determined for Abl variants engineered to have accessible or intra-molecularly engaged SH3 domains–as well as the wild-type kinase. Comparisons between regulatory state mutants provides insight into the preferred active site conformation of each regulatory state. Furthermore, affinities of each inhibitor were measured for wild-type Abl bound to known allosteric activators and inhibitors in order to probe how these ligands affect ATP-binding site conformation. Finally, pull-down experiments utilizing SH2- and SH3 domain-binding peptides immobilized on beads were employed to directly measure the accessibility of Abl's SH2 and SH3 domains when the ATP-binding site is stabilized in a specific conformation by an inhibitor. Our results strongly suggest that the SH3 and SH2 domains of Abl are similarly coupled to ATP-binding site conformation in Abl as in the SFKs. Furthermore, these findings support the hypothesis that kinase inactive

conformations are conserved throughout the kinome as opposed to uniquely tailored for each kinase.

II. Results and Discussion:

A. Generation of Abl mutants with differential SH3 domain accessibility

In order to answer the question of how SH3 domain engagement affects ATP-binding site conformation in Abl, a series of Abl regulatory state mutants with intra-molecularly engaged or disrupted SH3 domain binding were generated using site-directed mutagenesis and expressed recombinantly in *E. coli* (**Figure 2-2A**). For ease of expression and purification, minimal three-domain Abl (Abl^{3D}) constructs consisting of the SH3, SH2, and catalytic domain were used for all experiments. The SH3disengaged construct ($Abl^{SH3diseng}$) was generated by mutating two Pro residues in the SH2-catalytic domain linker to Glu, making the linker a poor ligand for the SH3 domain and producing a more active construct compared to Abl^{3D} (Pluk et al., 2002). A fully active Abl construct (Abl^{Act}) was generated by phosphorylating the activation loop of $Abl^{SH3diseng}$ on Tyr412. An SH3engaged (Abl^{SH3eng}) construct was generated by mutating five residues in the SH2-catalytic domain linker to Pro, increasing its affinity for the SH3 domain and producing a less catalytically active construct compared to Abl^{3D} (Panjarian et al., 2013) (**Figure 2-2B**). Unfortunately, we were unable to generate Abl regulatory state mutants with intra-molecularly engaged or disrupted SH2 domain engagement, as it is not clear which residues in the C-lobe should be mutated to achieve this effect, and there are no examples of such constructs in the literature.

Figure 2-2

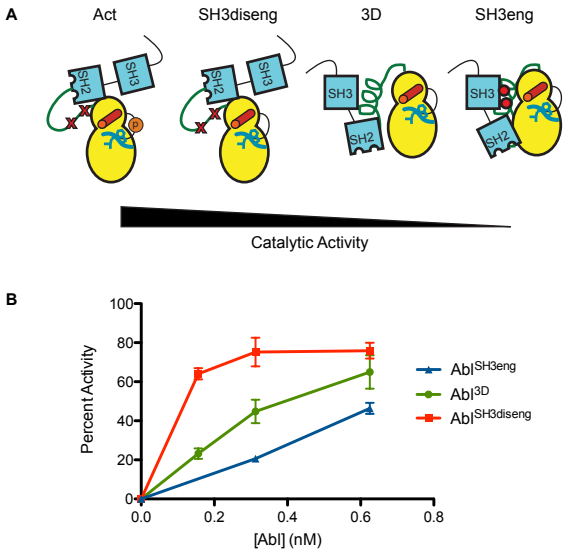

Figure 2- 2: Abl regulatory state mutants and their respective catalytic activities

A. Cartoon representations of each Abl regulatory state mutant. X's denote mutations that disrupt SH3 domain engagement, while dots denote mutations that enhance intra-molecular SH3 engagement. Abl^{Act}, SH3 domain disengaged and pTyr412; $Abl^{SH3diseng}$, SH3 domain disengaged; Abl^{3D}, no regulatory mutations; Abl^{SH3eng}, SH3 domain engaged. **B.** Relative catalytic activity of $Abl^{SH3diseng}$, Abl^{3D}, and Abl^{SH3eng} regulatory state mutants plotted as Percent Activity versus concentration (mean ± SEM, n=3). Plateau is the result of substrate depletion.

B. Activities of conformation-selective inhibitors against Abl regulatory state mutants

The same panel of conformation-selective inhibitors that was used in **Chapter 1** to investigate the relationship between SFK regulatory domain engagement and ATP-binding site conformation were tested against the regulatory state mutants shown in **Figure 2-2**. In addition, imatinib and AST-487—DFG-out stabilizing inhibitors—were added to the panel in order to more thoroughly investigate how Abl's DFG motif conformation affects coupling between the ATP-binding site and regulatory domains (**Figure 2-3A and B**). First, the K_is for activated Abl (Abl^{Act} and $Abl^{SH3diseng}$) for each inhibitor were measured and compared to the autoinhibited Abl^{SH3eng} construct (K_i values show in **Table 2-1**). By taking the ratio of K_i Abl^{Act}/K_i Abl^{SH3eng}, it can be determined

whether an inhibitor prefers the ATP-binding site of activated versus autoinhibited Abl. A preference for one construct over the other indicates that the equilibrium between active and autoinhibited favors the ATP-binding site conformation stabilized by the inhibitor. The magnitude of the preference provides a measure of the degree to which the equilibrium favors one conformation. Abl^{Act} and Abl^{SH3eng} were chosen for initial comparison because they represent the extremes of Abl activation and autoinhibition, and we expected to see the largest differences in inhibitor preference between these two constructs. Data in **Figure 2-3C** is plotted as the K_i Abl Abl^{SH3eng}/K_i Abl^{Act} for active-stabilizing inhibitors (**1**-**4**) and as K_i Abl^{Act} /K_i Abl^{SH3eng} for αC helix-out-preferring inhibitors (**5**-**7**) [the K_i ratios are arranged here, and for the rest of the chapter, with the denominator as the construct with the higher affinity in order to provide ratios that are positive in magnitude].

αC helix-out-stabilizing ligands **5**-**7** strongly prefer Abl^{SH3eng} over Abl^{Act} (**Figure 2-3C**, middle panel, and **Table 2-1**), suggesting that autoinhibited Abl favors the αC helix-out conformation. In contrast, active conformation-stabilizing ligands **2**-**4** modestly prefer Abl^{Act} (**Figure 2-3C**, left panel), suggesting that activated Abl favors an αC helix-in, active conformation. Ligand **1** shows no preference for one construct over the other, consistent with the fact that it does not make any contacts with the αC helix or DFG-motif. These data strongly suggest that Abl autoinhibition/activation is coupled to helix αC conformation in a manner similar to SFKs. DFG-out-stabilizing inhibitors also show a strong preference for Abl^{SH3eng}, which may be due to the fact that activation loop phosphorylation is believed to destabilize the DFG-out conformation.

Figure 2-3

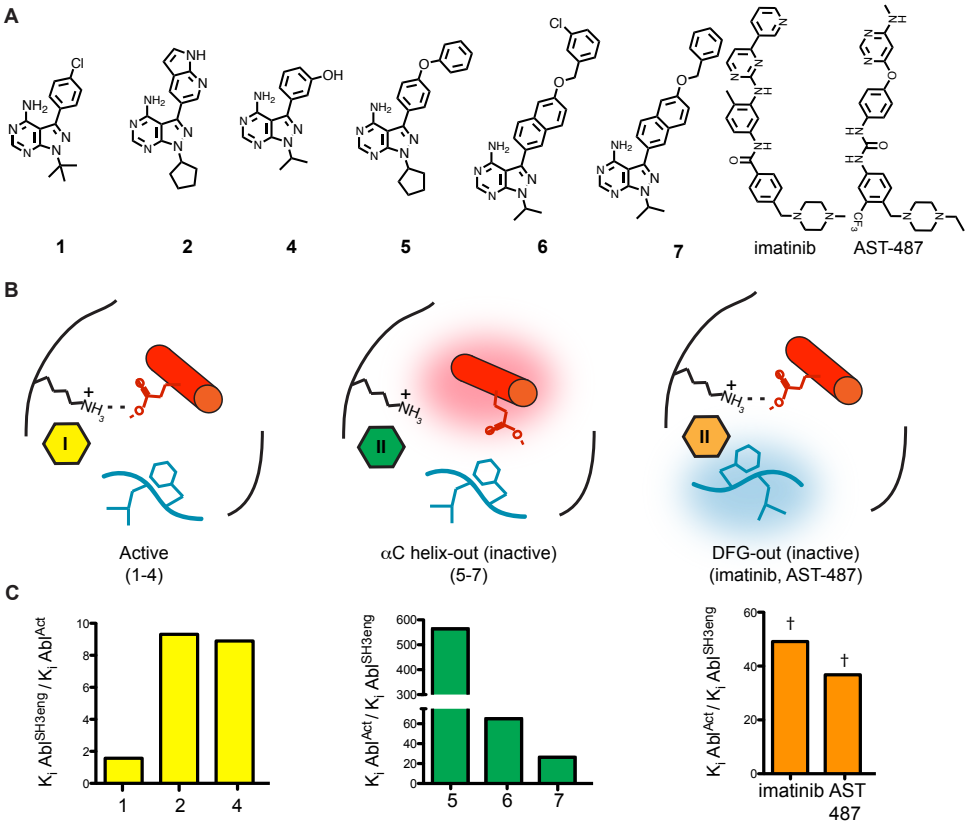

Figure 2- 3: Conformation-selective inhibitor structure, mode of binding, and preference for Abl^{Act} versus Abl^{SH3eng} regulatory state mutants

A. Structures of all conformation-selective inhibitors used in this analysis. **B**. Cartoon representations of the ATP-binding site stabilized by each class of inhibitor: Active-preferring "Type I" ligands (**1**-**4**; yellow hexagon), αC helix-out "Type II" inactive-preferring ligands (**5**-**7**; green hexagon), and DFG-out "Type II" inactive-preferring ligands (imatinib and AST-487; orange hexagon). The αC helix is colored red and the DFG-motif is colored blue. **C**. K_i ratio (Abl^{Act} t versus Abl^{SH3eng}) for each inhibitor, grouped by conformation preference (color-scheme same as described in B). For each, the denominator of the K_i ratio is the K_i for the construct with the highest affinity. Dagger indicates that absolute fold difference in K_i could not be determined because the affinity is at or below the Abl concentration used in the assay.

C. The effect of SH3 domain engagement and activation loop phosphorylation on conformation-selective inhibitor affinity

The same analysis can be used to probe the contribution of activation loop phosphorylation by comparing the K_is of Abl^{Act} for conformation-selective inhibitors relative to those determined for unphosphorylated Abl^{SH3diseng}, with the only difference

between the two constructs being activation loop phosphorylation state (**Figure 2-4A**; raw data **Table 2-1**). Plotting the K_i ratios for $Abl^{SH3diseng}/Abl^{SH3eng}$ on the same axis as $Abl^{Act}/Abl^{SH3diseng}$ allows for direct comparison of how much of each conformation-selective inhibitors regulatory state preference is the result of activation loop phosphorylation versus how much is the result of SH3 domain engagement (**Figure 2-4B**). For active-conformation stabilizing ligands **2**-**4**, the greatest difference in K_i ratio is observed between Abl^{Act} and $Abl^{SH3diseng}$, indicating that activation loop phosphorylation makes the largest contribution to the selectivity of these inhibitors—a result similar to Src in **Chapter 1**. In contrast, the greatest difference in K_i ratio for αC helix-out stabilizing ligands **6** and **7** is observed between $Abl^{SH3diseng}$ and Abl^{SH3eng}, suggesting that the majority of these ligands' preference can be attributed to SH3 domain engagement. Interestingly, this trend does not seem to hold for compound **5**, which shows a greater difference in K_i ratio between Abl^{Act} and $Abl^{SH3diseng}$ (~50-fold). However, a >500-fold difference in K_i is observed for **5** between Abl^{Act} and Abl^{SH3eng}, suggesting that SH3 domain engagement also contributes significantly to this ligand's ATP-binding site preference, although this is not as clearly reflected in the ratios shown in **Figure 2-4B** (green).

Table 2-1

Inhibitor	Abl^{Act} (0.5 nM)	$Abl^{SH3diseng}$ (0.1nM)	Abl^{SH3eng} (1 nM)
1	86	700	130
2	6.5	34	58
4	13	110	120
5	1600	27	2.8
6	10000	2500	160
7	3600	1100	130
imatnib	280	2.6*	5.7
AST-487	110	0.9*	3

Table 2- 1: K_i values for Abl regulatory state mutants shown in Figures 2-3 and 2-4

Enzyme concentrations are shown in parentheses. All SEMs are within 20% of the reported average (n=3). *Denotes that the measured K_i is approaching the enzyme concentration used in the assay.

As described above, activation loop phosphorylation accounts for a majority of the apparent preference of DFG-out-stabilizing ligands for Abl^{SH3eng} over Abl^{Act} (**Figure 2-4B,** right panel). DFG-out stabilizing inhibitors are difficult to study with activity assays because of their high potency for all Abl regulatory state mutants. This makes it difficult to measure their true and, thus, strong conclusions cannot be drawn about their regulatory state preference. However, a reduced K_i was observed for imatinib and AST-487 against Abl^{SH3eng} relative to $Abl^{SH3diseng}$ (**Figure 2-4B,** right panel). Although a true affinity could not be measured for $Abl^{SH3diseng}$, this indicates some degree of inhibitor preference for Abl in a more activated—though not activation loop phosphorylated—regulatory domain conformation than in an autoinhibited, regulatory domain conformation, supporting the notion that the DFG-out ATP-binding site conformation does not define autoinhibited Abl as previously believed.

Figure 2-4

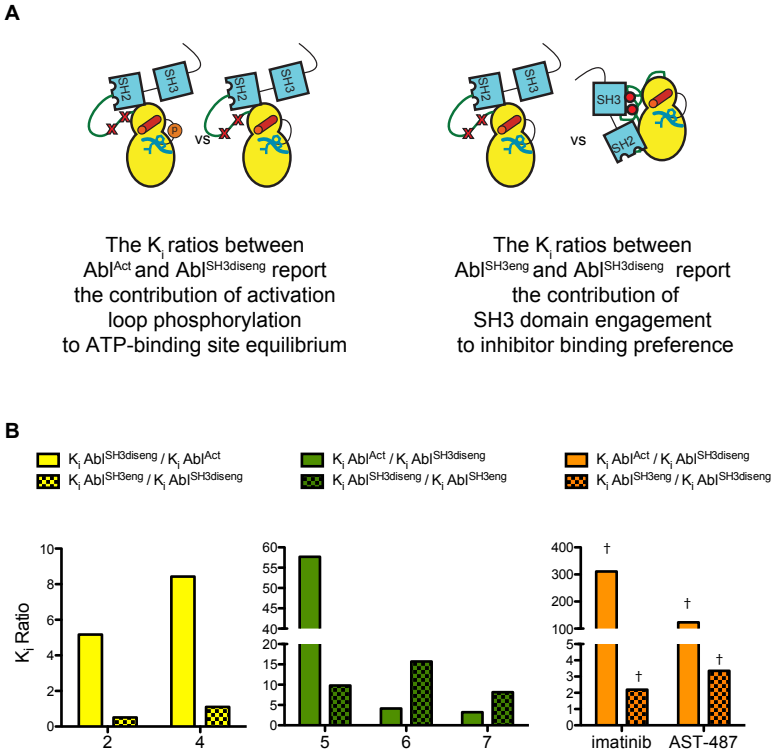

Figure 2- 4: Comparison of activation loop phosphorylation and SH3 domain engagement contribution to conformation-selective inhibitor preference

A. Cartoon and text describing the Abl constructs that were compared and what information this provides on coupling between regulatory domain engagement and ATP-binding site conformation. **B**. Bar graphs of K_i ratios comparing Abl^{Act} and $Abl^{SH3diseng}$ (solid bars) co-plotted with K_i ratios comparing $Abl^{SH3diseng}$ and Abl^{SH3eng} (checkered bars) for active-conformation preferring (yellow), αC helix-out preferring (green), and DFG-out preferring (orange) ligands.

D. The effect of SH2 domain-binding ligand and the allosteric inhibitor GNF-2 on conformation-selective inhibitor affinities

We further utilized conformation-selective inhibitors to detect changes in ATP-binding site conformation induced by a known allosteric activator—Abl phosphopeptide (AblPP), which binds to the phosphopeptide binding site on Abl's SH2 domain—and an allosteric inhibitor of Abl—GNF-2 (**Figure 2-5A**). First, we were curious as to whether the effects of AblPP binding and GNF-2 increased or decreased Abl^{3D}'s catalytic activity (**Figure 2-5B**). Increasing concentrations of GNF-2 reduced Abl's catalytic activity by

about 50% compared to Abl^{3D} in the absence of ligand, while incubation with AblPP increased Abl^{3D}'s activity only modestly (~10%). The fact that GNF-2 lead to only partial inhibition and AblPP led to only modest activation may be due to the fact that Abl^{3D} is missing its N-cap, which contributes to stabilization of fully activated and autoinhibited Abl.

Next, each inhibitor's K_i for Abl^{3D} was determined and compared to its affinity for Abl^{3D} bound to either AblPP or GNF-2 (see **Table 2-2** for K_i values). For both AblPP and GNF-2, saturating concentrations of ligand were used to ensure quantitative formation of the Abl^{3D}-ligand complex. The fold difference in K_i can be attributed to ATP-binding site conformational changes induced by AblPP or GNF-2 binding, assuming they do not directly affect ATP-competitive inhibitor binding, which is a reasonable assumption based on their respective sites of interaction. GNF-2 binding to the C-terminal lobe of Abl^{3D}'s catalytic domain lowers the affinities of inhibitors that stabilize an active ATP-binding site conformation. Ligands **1**-**4**, as well as the DFG-out ligand imatinib, show a greater than 10-fold decrease in affinity for the Abl^{3D}-GNF-2 complex compared to Abl^{3D} alone (**Figure 2-5C**). This result is consistent with the report that GNF-2 occupies the myristate binding pocket, causing Abl to adopt an autoinhibited conformation, presumably by enhancing the affinity of the C-lobe for the SH2 domain in a manner analogous to that observed upon myristate binding. Furthermore, the reduction in affinity observed for imatinib with GNF-2 supports the hypothesis that Abl regulatory domain engagement does not allosterically stabilize a DFG-out ATP-binding site conformation. Rather, these data support a model wherein SH2 domain engagement in Abl allosterically stabilizes an αC helix-out ATP-binding site conformation, most likely by increasing SH3 domain engagement with the

SH2-catalytic domain linker in a “snap-lock” mechanism, and that engagement of both the SH2 and SH3 domains is coupled to the conformation of the αC helix like in the SFKs.

Figure 2-5

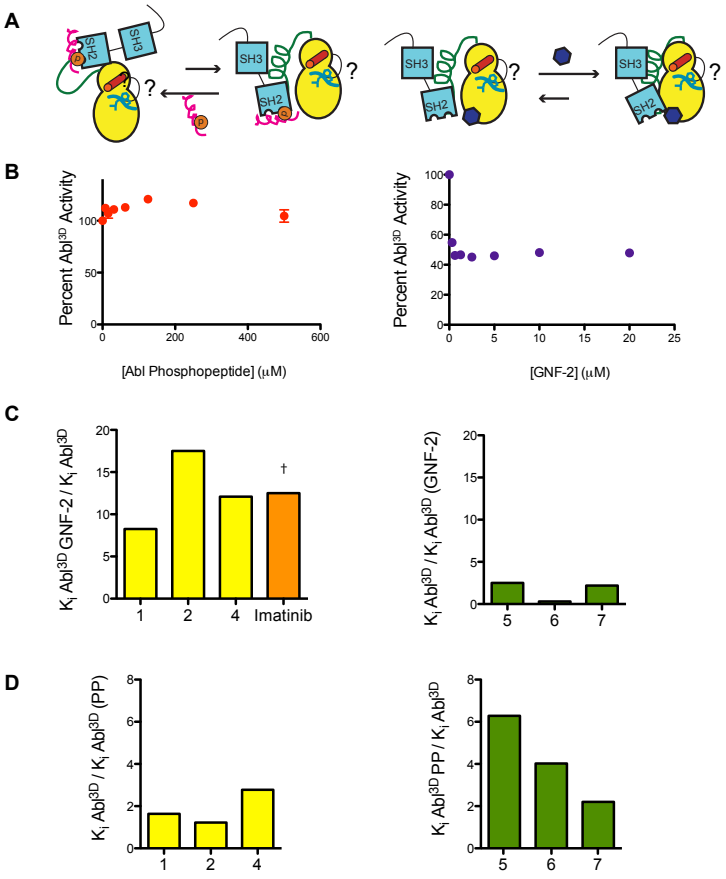

Figure 2- 5: GNF-2 and AblPP allosterically influence Abl's ATP-binding site conformation

A. Left: cartoon showing binding site of Abl phosphopeptide (PP; pink) as well as predicted effect on equilibrium. Right: cartoon showing binding site of GNF-2 (purple) and predicted effect on equilibrium. Question marks denote the unknown effects of AblPP and GNF-2 binding on ATP-binding site conformation. **B**. Percent Abl^{3D} activity relative to Abl^{3D} in the absence of ligand versus concentration Abl PP (left), GNF-2 (right). **C**. K_i ratio of active-preferring (yellow) and DFG-out-preferring (orange) ligands for the Abl^{3D}-GNF-2 complex versus Abl^{3D} alone. An analogous plot for αC helix-out preferring ligands is shown in the right panel in green. Dagger indicates that absolute fold difference in K_i could not be determined because affinity is at or below the Abl concentration used in the assay. **D**. K_i ratio of active-preferring (yellow) and αC helix-out-preferring (green) ligands for the Abl^{3D}-AblPP complex versus Abl^{3D} alone.

Table 2-2

Inhibitor	**Abl**^{3D} (0.3 nM)	**Abl**^{3D} +GNF-2 (3 nM)	**Abl**^{3D} +AblPP (0.8nM)
1	110	890	66
2	8.8	150	7.2
4	19	220	6.7
5	7	2.8	44
6	420	1400	1700
7	200	91	440
imatinib	2*	25	ND

Table 2- 2: K_i values for the ratios shown in Figure 2-5

Enzyme concentrations are shown in parenthesis. All SEMs are within 20% of the reported average (n=3). *Denotes that K_i is approaching the concentration of Abl used in the assay.

In contrast, binding of AblPP to the SH2 domain of Abl^{3D} reduces the affinities of inhibitors that stabilize the αC helix-out ATP-binding site conformation. Ligands **5-7** show about a 2- to 6-fold reduction in affinity for the Abl^{3D}-AblPP complex compared to Abl^{3D} alone (**Figure 2-5D**). This is consistent with studies reporting modestly increased Abl catalytic activity in the presence of SH2 domain-binding ligands, and suggests that occupying the phosphotyrosine binding site on this domain stabilizes an active ATP-binding site by disrupting autoinhibitory interactions with the C-lobe and/or stabilizing activating interactions with the N-lobe. Given this observation, we were curious whether we could observe an equal or greater reduction in the affinity of **5**-**7** upon binding of AblPP to the Abl^{SH3eng} regulatory state mutant (**Figure 2-6A**). Such a reduction would indicate that binding of phosphopeptide ligands to the SH2 domain is activating enough to overcome an enhanced SH3 domain – SH2-catalytic domain linker interaction. Assaying **5**-**7** against the AblPP-Abl^{SH3eng} complex and comparing the observed K_is to those for Abl^{SH3eng} alone does show a reduction in affinity approximately 2-fold greater than observed in the context of Abl^{3D} (**Figure 2-6B; Table 2-3**).

Taken together, these results demonstrate the utility of conformation-selective ligands for determining the molecular basis for allosteric activation/inactivation of kinase catalytic domains by both protein-protein interactions and small molecules. However, it is worth noting that there was virtually no change in preference observed for active-conformation stabilizing ligands for the Abl^{3D}-AblPP complex compared to Abl^{3D} alone, as one would predict for a model in which AblPP binding to the SH2 domain stabilizes an active ATP-binding site conformation (**Figure 2-5D,** yellow). Similarly, there was not a strong preference in αC helix-out stabilizing ligands for Abl^{3D}-GNF-2 compared to apo Abl^{3D}, as one would predict for a model in which GNF-2 binding allosterically stabilizes an autoinhibited ATP-binding site conformation (**Figure 2-5C,** green). These results may indicate a limitation in our ability to sense conformational changes with our current panel of ATP-competitive ligands. Another interpretation is that AblPP makes the αC helix-out inactive ATP-binding site conformation unfavorable without greatly affecting the ability of active-stabilizing ligands to bind. Analogously, GNF-2 binding may prevent active-preferring ligands from binding without greatly affecting the affinities of αC helix-out ligands.

Figure 2-6

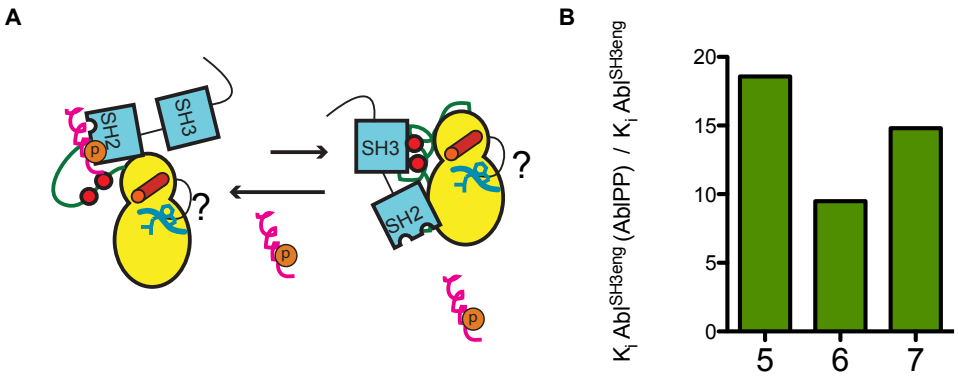

Figure 2- 6: AblPP binding to the Abl^{SH3eng} SH2 domain reduces the affinity of αC helix-out-stabilizing ligands for the ATP-binding site

A. Cartoon illustrating AblPP binding's effect on conformational equilibrium of Abl^{SH3eng}. Question marks denote the unknown effects of AblPP binding on ATP-binding site conformation. **B**. K_i ratio Abl^{SH3eng} +AblPP versus Abl^{SH3eng}.

Table 2-3

Inhibitor	Abl^{SH3eng} (1 nM)	Abl^{SH3eng} +AblPP
1	130	970
2	58	91
4	125	270
5	2.8	52
6	160	1500
7	130	2000

Table 2- 3: K_i values for the ratios shown in Figure 2-6

All SEMs are within 20% of the reported average (n=3).

E. Analysis of the effects of conformation-selective inhibitors on inter-molecular SH2 and SH3 domain accessibility

As discussed in the previous chapter about SFKs, coupling between the ATP-binding site and regulatory domains is *bidirectional*. Enhancing intra-molecular SH2 or SH3 domain engagement *via* site-directed mutagenesis shifts the ATP-binding site's conformational equilibrium towards an αC helix-out conformation, which can be

measured by an increase in affinity of αC helix-out inhibitors for the active site. Therefore, stabilizing Abl's ATP-binding site in an αC helix-out conformation with an inhibitor enhances SH3 and SH2 domain intra-molecular engagement, which can be measured directly with inter-molecular pull-down assays with immobilized SH3 and SH2 domain ligands. This method for studying the effects of ATP-binding site conformation on regulatory domain accessibility allows for study of all conformation-selective inhibitors, including DFG-out stabilizing ligands that are too potent to study using activity assays.

To complete this analysis, pull-down assays with immobilized SH3 domain-binding peptide and an SH2 domain-binding peptide were used, and comparisons of how each class of inhibitor allosterically influences SH2 and SH3 domain accessibility were made (**Figure 2-7A**). Abl^{3D} was pre-incubated with saturating concentrations of each inhibitor of interest before adding to beads displaying SH3 or SH2 domain-binding peptides. After washing, retained kinase was eluted by boiling with 1x SDS loading dye, separated by SDS-PAGE, and blotted with an anti-his6 antibody. Overall, the results from this experiment suggest that Abl is very similar to Src and Fyn2. Active- and DFG-out-stabilizing inhibitors increase SH3 and SH2 domain accessibility to inter-molecular ligands by ~2-fold and 3-fold, respectively, relative to DMSO, while αC helix-out-stabilizing inhibitors decrease regulatory domain accessibility by ~5-fold (**Figure 2-7A, 2-7B**). Fold changes in domain accessibility are clear but not as dramatic as those observed for Hck/Lyn. This supports the observation that Abl and Src have more structurally similar SH2-catalytic domain linkers than Hck and Src, providing further evidence that the SH2-catalyitc domain linker is the key determinant of allosteric coupling between the ATP-binding site and regulatory domains. Furthermore, these experiments show that the

conformation of the DFG-motif is coupled to regulatory domain engagement in Abl like it is in SFKs, refuting the claim that these highly structurally homologous kinases evolved fundamentally different mechanisms of autoinhibition.

Figure 2-7

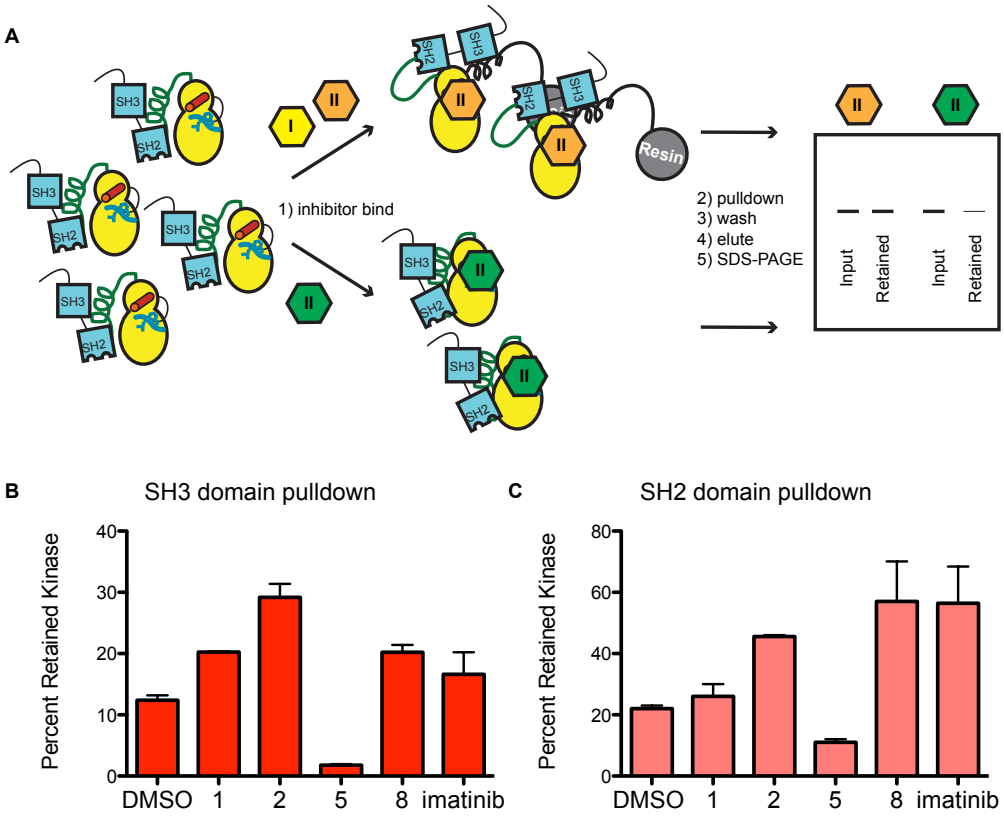

Figure 2- 7: Conformation-selective inhibitor effects on Abl SH3 and SH2 domain interactions with inter-molecular ligands

A. Cartoon illustrating the experimental scheme for SH3 pull-down assays of Inhibitor-bound Abl^{3D}. Complexation with active- or DFG-out-stabilizing inhibitors increases SH3 domain accessibility while αC helix-out-stabilizing inhibitors decrease SH3 domain accessibility, resulting in a difference in retained kinase when analyzed by SDS-PAGE (theoretical gel). **B**. Bar graph displaying results from SH3 pull-down experiments (mean ± SEM, n=3). **C**. Bar graph displaying results from SH2 pull down experiments (mean ± SEM, n=3).

III. Conclusion:

Conformation-selective inhibitors are useful tools for experimentally determining the molecular basis for allosteric activation of kinases, as well as for investigating how ATP-binding site conformation is coupled to the accessibility of distal domains for protein-protein interactions. Here, their utility has been demonstrated by thorough characterization of how the conformations of the DFG-motif and αC helix are coupled to SH3 and SH2 domain engagement in Abl, and how exogenous allosteric activators/inhibitors exert their effects on catalysis. Of particular note, conformation-selective inhibitors were employed to resolve a long-standing misconception about Abl's allosteric regulation derived from observations of the crystal structure of autoinhibited Abl bound to imatinib. While these experiments were done on minimal Abl^{3D} constructs expressed recombinantly in *E. Coli*, it is feasible to expand this strategy to explore how Abl's C-terminus is allosterically coupled to its ATP-binding site using full-length Abl and Abl C-terminal truncations expressed from eukaryotic cells. Such allosteric coupling has been reported but the molecular basis is not well understood (Preyer, et al., 2011; Woodring, et al. 2005).

Studying the mechanisms of allosteric regulation of kinases is key for fully understanding how multi-domain kinases participate in cell signaling events as well as the mechanism of action of ATP-competitive small molecule drugs. This work taken together with the previous study of SFKs provides a basis for future investigation of how modulating SH2 and SH3 domain availability for inter-molecular interactions changes SFK/Abl participation in signaling networks by modulating phosphorylation state, subcellular localization, scaffolding, etc—all of which are non-catalytic functions. This is

an exciting and underexplored avenue of cell signaling research that will hopefully one-day lead to new and improved therapeutic strategies targeting kinase non-catalytic function.

IV. Materials and Methods:

A. Abl regulatory state mutant design and protein expression

Quikchange mutagenesis was used to introduce all point mutations. The construct Abl^{3D} consists of residues 65 – 534 (Abl1b numbering) of full-length Abl. Point mutantations for each regulatory state mutant were introduced as follows: P242E/P249E ($Abl^{SH3diseng}$) and K241P/T243P/V245P/G246P/V247P (Abl^{SH3eng}). All constructs were expressed and purified as described previously (Seeliger, et al., 2005).

B. Preparation of activation loop phosphorylated $Abl^{SH3diseng}$ (Abl^{Act}; pTyr412)

$Abl^{SH3diseng}$ was autophosphorylated at Tyr412 by incubating $Abl^{SH3diseng}$ (15 μM) with ATP (500 μM) and 0.75nM Hck3D in activation buffer [50 mM HEPES (pH 7.5), 10 mM $MgCl_2$, 2.5 mM EGTA, 1 mM NA_3VO^4, and 100 mM NaCl]. The reaction mixture was incubated at 37 °C for 3 h. AL phosphorylation was detected via western blot using an anti-pY412 anitibody (Cell Signaling technologies, 247C7).

C. Enzymatic activity determination

Titrations of Abl regulatory state mutants (2-fold serial dilutions starting at 20 nM, seven data points) were assayed in buffer containing 75 mM HEPES (pH 7.5), 15 mM MgC_{l2}, 3.75 mM EGTA, 1 mM Na_3VO_4, 150 mM NaCl, 0.2 mg/mL BSA, [γ- 32P]ATP (0.2 μCi/well), and 130 μM Abl Peptide Substrate (APS; EAIYAAPFAKK). The final volume of

each assay well was 30 µL. The enzymatic reaction was conducted at room temperature for 2 h and then terminated by spotting 4.6 µL of the reaction mixture onto a phosphocellulose membrane. Membranes were washed with 0.5% phosphoric acid (three times, 10 min each wash) and dried, and the radioactivity was determined by phosphorimaging with a GE Typhoon FLA 9000 phosphor scanner. The scanned membranes were quantified with ImageQuant and converted to percent activity. Data were analyzed using GraphPad Prism (mean ± SEM; n = 3).

D. Activity assays for K_i determination

Inhibitors (initial concentration of 10 µM, 3-fold serial dilutions, 10 data points) were assayed in triplicate against all Abl constructs. Assay conditions were the same as those described for enzymatic activity assays. Concentrations of Abl constructs were determined to be in the linear range and are as follows: Abl^{3D}, 0.3 nM; Abl^{3D} + GNF-2, 3 nM; Abl^{3D} + AblPP (GNPVpYENV), 0.8 nM; Abl^{Act}, 0.5 nM; $Abl^{SH3diseng}$, 0.1 nM; Abl^{SH3eng}, 1 nM. For K_i's determined in the presence of AblPP, 125 µM AblPP was used. For K_i's determined in the presence of GNF-2, 20 µM GNF-2 was used. Blot radioactivity was determined by phosphorimaging with a GE Typhoon FLA 9000 phosphor scanner. The scanned membranes were quantified with ImageQuant and converted to percent inhibition. Data were analyzed using GraphPad Prism, and K_i values were determined using nonlinear regression analysis.

E. Pull-down Assays to determine regulatory domain engagement

Formation of the Kinase−Inhibitor Complex. The kinase of interest (100 nM) and mammalian lysate (0.2 mg/mL) were diluted in immobilization buffer [50 mM Tris, 100 mM NaCl, and 1 mM DTT (pH 7.5)]. A saturating amount of the inhibitor of interest (5 or 10

μM) was added to this kinase dilution. The mixture was allowed to incubate for 30 min before being loaded on the resin.

SH3 Pull-down. Forty microliters of a 50% slurry of SNAPCapture Pull-Down Resin (NEB) was placed in a microcentrifuge tube. The resin was washed (twice, 10 bed volumes) with immobilization buffer. A SNAP tag−polyproline peptide (APTYSPPPPP) fusion (10 μM) was loaded onto the resin at a final volume of 100 μL in buffer. The resin was rotated at room temperature for 90 min. After polyproline peptide immobiization, the resin was washed (twice, 10 bed volumes), and 100 μL of the kinase−inhibitor complex was loaded. The resin was allowed to shake at room temperature for 1 h. After incubation with the kinase−inhibitor complex, the flow-through was collected, and the resin was washed (three times, 10 bed volumes). To elute the retained kinase, 100 μL of 1× SDS loading buffer was added, and the beads were boiled at 90 °C for 10 min. All samples were separated via sodium dodecyl sulfate−polyacrylamide gel electrophoresis (SDS−PAGE) and visualized by Western blotting using a His6-specific antibody [at a 1:5000 dilution (abm, HIS.H8)]. The scanned blots were quantified with LI-COR Odyssey software to determine the percentage of kinase retained on the resin on the basis of the loaded and eluted fractions (mean ± SEM; n = 3).

SH2 Pull-down. Pull-downs were performed as described above using resin displaying an SH2-binding peptide (GNPVpYENV).

Chapter 3: A Chemical-Genetic Strategy for the Investigation of Kinase Non-Catalytic Function using Covalent Conformation-Selective Inhibitors

I. Introduction:

Drug discovery and crystallography efforts have led to the deposition of hundreds of structures of kinase catalytic domains (CDs) bound to hundreds of different ATP-competitive inhibitors in the PDB (Berman et al, 2000). As a result of this work, many investigators have noted that three structurally distinct, inhibitor-bound active site conformations are routinely adopted by many members of diverse kinase families (**Figure 3-1A**). The first, and most common, is Type I-stabilized, or "active," in which all active site residues are positioned to catalyze phosphate transfer and the catalytically important salt bridge between Glu310 and Lys298 remains intact. In contrast, Type II inhibitors stabilize one of two distinct catalytically incompetent, inactive conformations: αC helix-out, in which the αC-helix is rotated such that the Glu310/Lys298 salt bridge is disrupted; or DFG-out, in which the Phe residue on the activation loop's DFG motif is flipped 180° but the Glu310/Lys298 salt bridge remains intact (Muller et al, 2015; Palmieri and Rastelli, 2013) (**Figure 3-1A**).

Figure 3-1

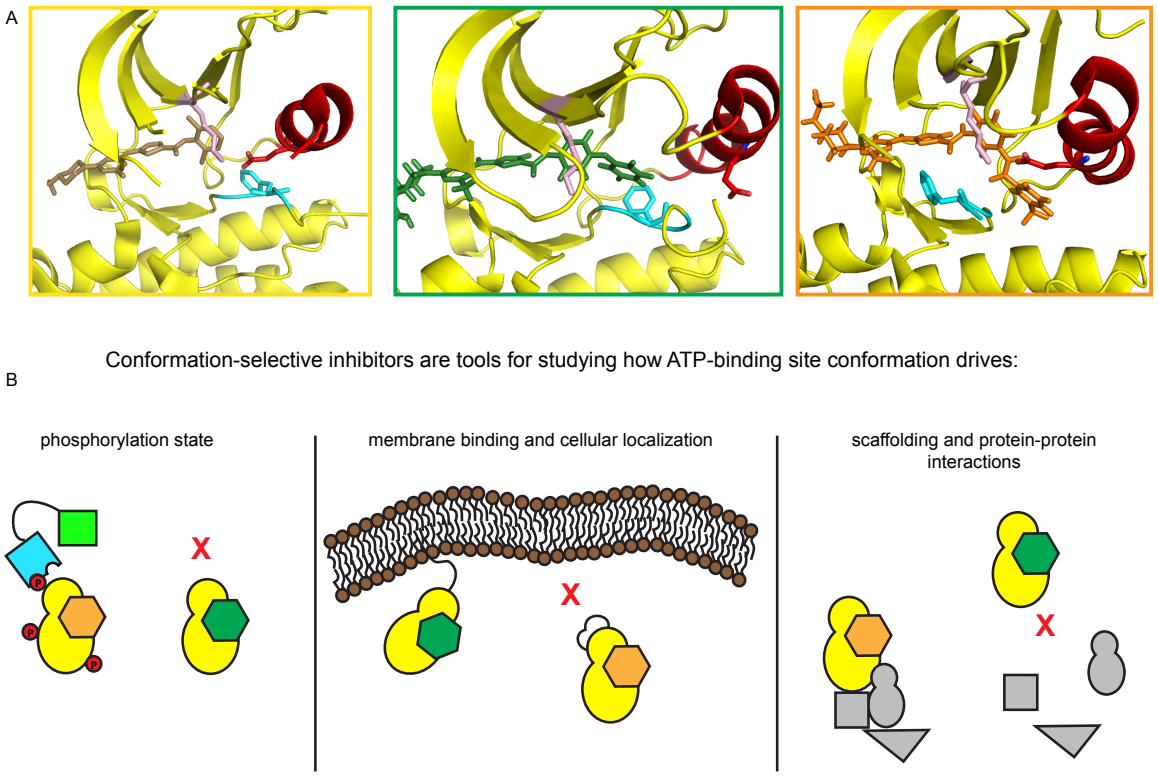

Figure 3- 1: Modes of conformation-selective inhibitor binding and their hypothesized effects on kinase non-catalytic function

A. Crystal structures of the Src catalytic domain bound to three conformation-selective analogues of the ATP-competitive inhibitor dasatinib. The panels are images of each distinct, inhibitor-stabilized ATP-binding site conformation. From left to right: active/Type I-stabilized (yellow box, PDB: 3G5D), αC helix-out-stabilized (green box, PDB: 4YBK), and DFG-out-stabilized (orange box, PDB: 4YBJ). In each ATP-binding site, the αC helix is shown in red, the DFG motif is colored cyan, and the catalytic Lys is colored pale pink. **B**. Cartoon illustrating hypothetical divergent effects on phosphorylation state, membrane localization, and protein-protein interactions by stabilizing a kinase in an active, αC helix-out, and DFG-out ATP-binding site conformation using conformation-selective inhibitors.

Thus, conformational plasticity in the ATP-binding site appears to be conserved throughout the kinome. The conformations of the αC helix and the DFG motif have been linked to the structural regulation of numerous kinases, including Src-family kinases (SFKs), Abl, EGFR, c-Kit, Cyclin-dependent kinases, RAF, and IRE1α. (Endicott et al., 2012; Kung et al., 2016; Huse and Kuriyan, 2002; Tong and Seeliger, 2014; Masterson,

et al. 2010; Jura et al, 2011; Eswaran and Knapp, 2010). Our lab and others in the field have reported divergent structural and biological effects from kinase binding to Type I/active-, αC helix-out-, and DFG-out-stabilizing inhibitors. For example, Erk2 enhances the activity of the phosphatase DUSP6 when bound to Type I- and αC helix-out-stabilizing inhibitors, but not when bound to a DFG-out-stabilizing inhibitor (Hari et al., 2013). Additionally, SFKs and Abl kinases exhibit *decreased* intra-molecular SH3 and SH2 regulatory domain engagement when bound to Type I- and DFG-out-stabilizing inhibitors but *increased* intra-molecular SH3 and SH2 domain engagement when bound to αC helix-out-stabilizing inhibitors (Krishnamurty et al, 2012, Leonard et al., 2014, Register et al., 2014). This difference in regulatory domain engagement affects the ability of the kinase Csk to phosphorylate an important regulatory site on an SFK's C-terminal tail (Tyr527). These examples and others have led many to hypothesize that ATP-binding site conformation allosterically controls global kinase conformation with significant effects on signaling by influencing phosphorylation state, cellular localization, and inter-molecular binding partners (**Figure 3-1B**). In support of this hypothesis, there are many examples in the literature of kinases playing important roles in signaling networks despite being rendered catalytically inactive, either with small molecules or *via* mutation of key catalytic residues (Chen et al., 2006; Galan-Moya et al., 2008). Inhibition by conformation-selective ligands presents an opportunity to manipulate kinase non-catalytic function by exploiting allosteric coupling with the ATP-binding site.

It has been challenging to study kinase non-catalytic function with ATP-competitive inhibitors due to a lack of selective Type I and Type II inhibitors for most kinases. The high degree of structural homology between kinase ATP-binding sites

makes selectively targeting a single kinase very difficult (Anastassiadis et al., 2011). Thus, developing unique conformation-selective inhibitors for multiple kinases of interest is not feasible. Methods such as the Shokat Lab's "bump-hole" approach, have solved the selectivity issue by mutating the gatekeeper residue in the ATP-binding site to small Gly or Ala residues, creating a "hole" to which "bumped" inhibitors engineered with bulky functionalities selectively bind (Bishop et al., 2000). However, mutating the gatekeeper residue has been shown to cripple many kinases and may alter sensitive allosteric networks between the ATP-binding site and distal regions of the kinase (Azam et al., 2008; Garske et al., 2011). Furthermore, no "bumped" Type II inhibitors have been developed to date.

In this study we report a general chemical-genetic strategy for studying the effects of stabilizing the ATP-binding site of a kinase of interest with Type I and Type II inhibitors on signaling events. By mutating a highly-conserved Val residue in the N-lobe of the kinase domain, a kinase can be engineered to be sensitive to a panel of cell-permeable, reversibly covalent, potent, and selective Type I and Type II inhibitors. In this work we demonstrate that each inhibitor stabilizes a Type I/active, αC helix-out, or DFG-out ATP-binding site conformation, is highly selective for the mutant kinase over the wild-type kinase, and engages few off-targets in cell lysate. We further demonstrate that kinases from diverse regions of the kinome can be sensitized to inhibition by these ligands, making this a readily generalizable strategy for studying non-catalytic function of any kinase of interest. Finally, we establish the utility of this strategy by exploring how ATP-binding site conformation divergently modulates Abl and SFK phosphorylation, localization, and protein-protein interactions in cells.

II. Results and Discussion:

A. Generation and characterization of potent and selective Type I and Type II inhibitors

Reversible-covalent inhibitors have shown increased specificity and selectivity for their targets by reducing the accumulation of irreversibly-labeled off targets in cells (Bradshaw et al., 2015). For this study, we were inspired by the Taunton Lab's development of electron-deficient olefin containing inhibitors designed to react with a non-catalytic Cys in the active site of the RSK2 C-terminal domain (CTD) (**Figure 3-2A**) (Serafimova et al., 2012; Miller et al, 2013). The active-site Cys exploited in the RSK2 CTD is not well-conserved—only 11 of 538 human kinases possess a Cys at this position—and sequence alignments with several other kinase active sites show that it aligns with a well-conserved Val residue in the N-lobe of most kinase domains (**Figure 3-2B**). Thus, site-directed mutagenesis was used to convert this Val residue to Cys in the kinases Src, Hck, Abl, Erk2, EphA2, and Pak1 in order to generate analogue-sensitive kinase mutants (Src^{AS}, Hck^{AS}, Abl^{AS}, $Erk2^{AS}$, $EphA2^{AS}$, and $Pak1^{AS}$). These kinases were selected for mutation because each has examples of important non-catalytic function in the literature that we predicted could be modulated with conformation-selective inhibitors.

In order to create a panel of reversible-covalent, conformation-selective inhibitors, known Type I-, αC helix-out-, and DFG-out-stabilizing pyrrolopyrimidine inhibitors were modified with cyanoacrylamide Michael acceptors in a position that presents the reactive β-carbon in close proximity to the mutant Cys when bound to the ATP-binding site. Activity assays were used to screen potential inhibitors for potency and selectivity for the analogue-sensitive (AS) kinase over the wild-type (WT), and molecules **1**-**4** were determined to be the most promising candidates (**Figure 3-2C**). Ligand **1** is an

electrophilic analogue of the well-known Type I-stabilizing inhibitor PP2 which contains a small aryl substituent a the C3 position and does not make significant contacts with the αC helix or DFG-motif (Krishnamurty et al., 2012; Miller et al. 2013). In contrast, ligand **2** contains an extended hydrophobic substituent at the C3 position, which has been shown to stabilize the ATP-binding of SFKs in an αC helix-out conformation (Krishnamurty et al., 2012; Levinson et al., 2008). Lastly, ligands **3** and **4** are predicted to stabilize an αC helix-in conformation by making electrostatic contacts with Glu310 and their amide linkages while occupying the DFG pocket—hallmarks of DFG-out-stabilizing ligands. Example IC_{50} curves for $Hck3D^{AS}$ (three-domain construct consisting of SH2, SH3, and catalytic domain; colored lines) and $Hck3D^{WT}$ (black lines) are shown below each ligand's structure in **Figure3-2C**. IC_{50} values measured at 1mM ATP for the analogue-sensitive versus wild-type kinases show a >1000-fold selectivity for $kinase^{AS}$ over the wild-type, with the exception of inhibitors **3** and **4** for $Erk2^{AS}$ which is not sensitive to inhibition by our DFG-out-stabilizing inhibitors and Pak1, whose wild-type construct needs to be assayed to make strong claims about selectivity (**Figure 3-2D**). True inhibitor affinities for the ATP-binding site of each analogue-sensitized kinase are reported as K_i values calculated using the Cheng-Prusoff equation for competitive inhibition and the determined K_m for ATP.

Figure 3-2

A

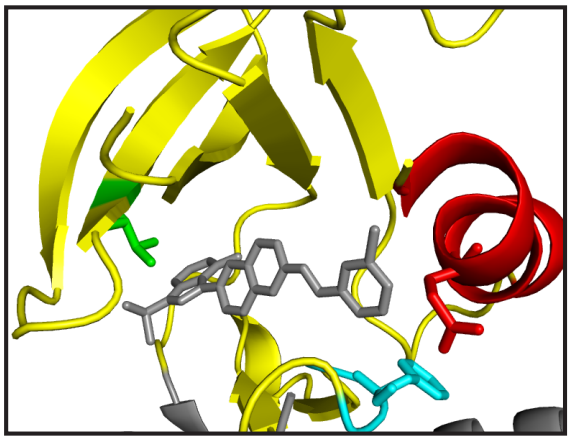

B

```
RSK2CTD FTDGYEVKEDIGVGSYSVCKRCIHKAT
Abl     ERTDITMKHKLGGGQYGEVYEGVWKKY
Hck     PRESLKLEKKLGAGQFGEVWMATYNKH
Src     PRESLRLEVKLGQGCFGEVWMGTWNGT
Erk2    VGPRYTNLSYIGEGAYGMVCSAYDNVN
Pak1    PKKKYTRFEKIGQGASGTVYTAMDVAT
```

C

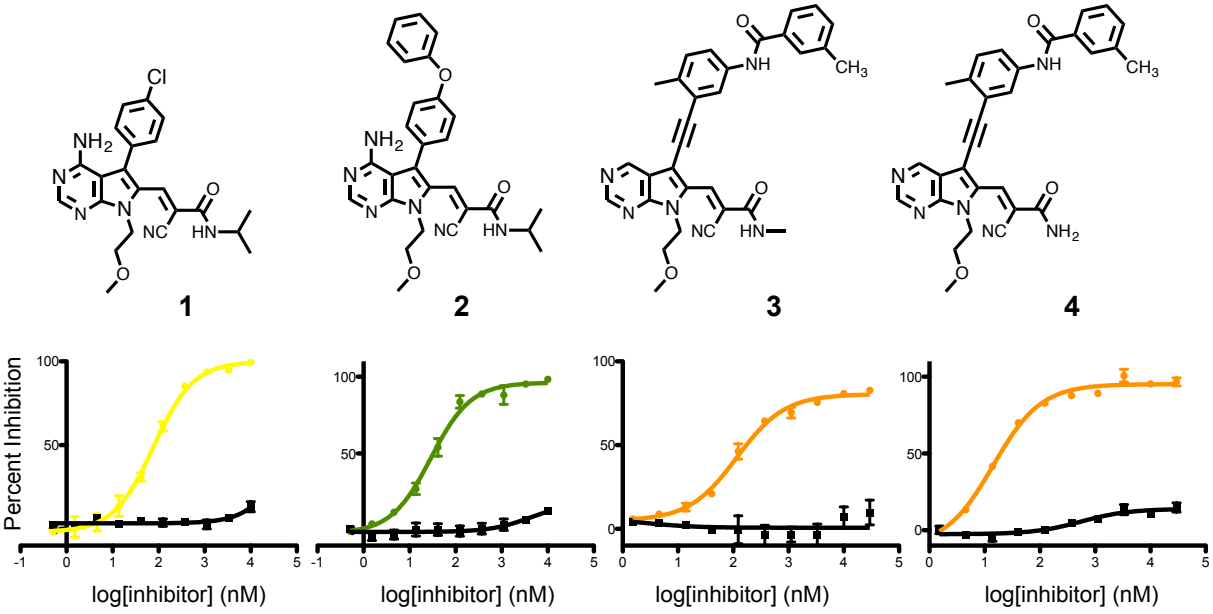

D

	AS		WT	AS		WT	AS		WT	AS		WT
	IC_{50}	K_i	IC_{50}	IC_{50}	K_i	IC_{50}	IC_{50}	K_i	IC_{50}	IC_{50}	K_i	IC_{50}
Abl	150±30	15 ± 6	>20000	200±40	22 ± 8	>20000	780±30	80 ± 15	>30000	26 ± 6	3 ± 1	>30000
Hck	77 ± 2	5.9±0.9	>20000	30 ± 6	2.3± 0.8	>20000	120±10	9 ± 2	>30000	14 ± 1†	NC	>30000
Src	26 ± 2	1.9±0.2	>30000	28 ± 3	2.1±0.2	>30000	44 ± 7	3.3±0.5	>30000	34 ± 3	2.5±0.2	>30000
Erk2*	ND	84 ± 6	>20000	6.3±0.7	3.4±0.2†	>20000	>30000	NC	>30000	ND	1200±120	ND
Pak1*	ND	ND	ND	ND	30	ND	ND	40	ND	ND	20	ND
EphA2*	18 ± 3	0.28±0.04	>30000	260±20	3.6±0.3	>30000	49 ± 4	0.71±0.05	1000±100	32 ± 2	0.43±0.03	840±50

Figure 3- 2: Hck, Abl, Src, Erk2, EphA2, and Pak1 can be sensitized to inhibition by covalent, conformation-selective inhibitors via non-catalytic active site Cys mutation

A. Crystal structure of the Src kinase domain ATP-binding site (PDB: 4DGG) bound to αC helix-out-stabilizing inhibitor RM 1-176 (grey). The αC helix is colored red and rotated such that Glu310 is no longer coordinated with Lys295 (αC helix-out, Type II). The DFG-motif on the activation loop (cyan) is in the "DFG-in" conformation. The Val residue to be mutated to Cys is shown in green. **B**. Sequence alignment of the kinases investigated in this study (Abl, Hck, Src, Erk2, EphA2, and Pak1) with the RSK2 C-terminal Domain (CTD). The RSK2 CTD Cys residue which can be targeted pharmacologically by reversible-covalent inhibitors is a conserved Val in most other kinases (green). **C**. Conformation-selective inhibitor structures and IC_{50} curves showing the potency of each inhibitor for the cysteine mutant Hck3D construct ($Hck3D^{AS}$) (colored) versus wild-type Hck3D (black). Yellow denotes that **1** stabilizes a Type I/active ATP-binding site, green denotes that **2** stabilizes a Type II/αC helix-out ATP-binding site, and orange denotes that **3** and **4** stabilize a Type II/DFG-out ATP-binding site conformation. This color scheme is maintained throughout the paper. **D**. Table displaying the IC_{50} and K_i values of **1**-**4** for each AS kinase construct tested and IC_{50} values for each WT kinase construct tested. All IC_{50} values were determined at 1mM ATP. K_i values were calculated via the Cheng-Prusoff equation assuming competitive inhibition. † Signifies that IC_{50} is too close to enzyme concentration used in the assay to be certain of true potency.

In order to determine how selectively our inhibitor panel binds analogue-sensitized kinase variants over endogenous kinases in cells, a SILAC proteomic experiment was performed (**Figure 3-3A**) (Golkowski et al., 2014). HEK293T cells expressing Hck^{AS} were grown in heavy and light media. Light or heavy labeled lysate was incubated with DMSO and oppositely labeled lysate was incubated with 50 μM **1**, **2**, **3**, or **4**, before being exposed to resin functionalized with a mixture of ATP-competitive inhibitors (KinoBeads) that has been demonstrated to interact with the majority of the kinome (up to 330 kinases) (Golkowski et al., 2014). After incubation, the unbound fraction was washed away, bound kinases were digested, and peptides were subjected to MS/MS analysis and quantified relative to the peptides identified in the DMSO-treated lysate. The majority of cellular kinases are robustly quantified in the DMSO-treated channel. However, kinases that are strongly inhibited by **1**-**4** do not interact with the immobilized inhibitors and are depleted in the drug-treated channel. A large portion of the kinome was quantified by this method (~220 kinases were quantified in total) and mapped by relative percent competition onto Kinome tree dendrograms (**Figure 3-3**). Each kinase profiled is labeled by name and the

size of circle corresponds to the percent competed by the ligand (large circle, strongly competed). The data is shown in **Figure 3-3 B-D**, and as predicted Hck^{AS} is most strongly competed by all inhibitors as shown by its quantification in the DMSO versus drug-treated channels.

Figure 3-3

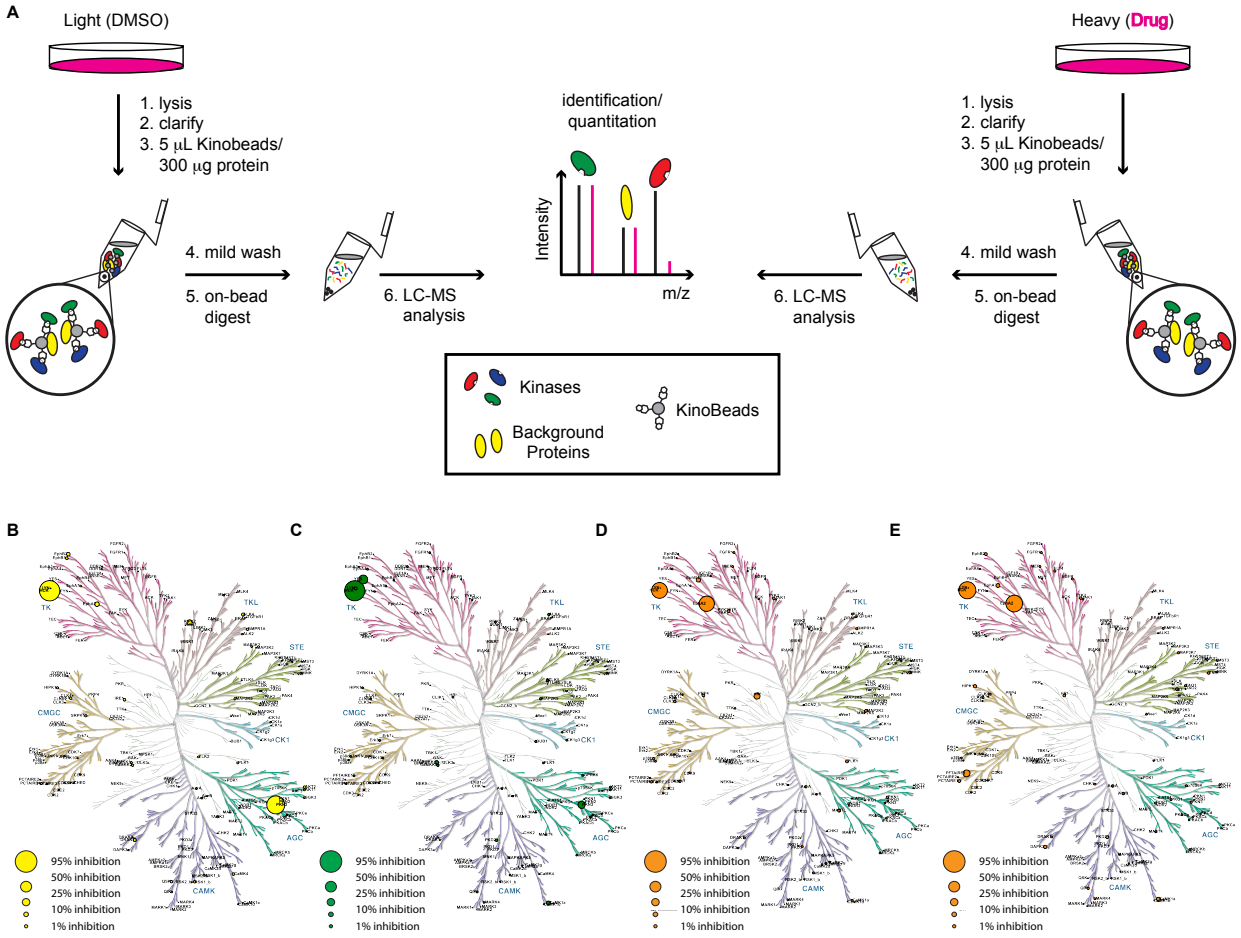

Figure 3- 3: Profiling against endogenous kinases in cell lysate demonstrates selectivity of 1-4

A. Experimental scheme describing the SILAC profiling experiment using KinoBeads. Kinases competed by free inhibitor (**1**, **2**, **3**, or **4**) are quantified at higher levels in the DMSO channel than the drug-treated channel (as seen with the red kinase in the theoretical spectrum). Kinases that are not inhibited show up as relatively equal in each channel. **B**. Results of profiling of ligand **1** mapped onto a kinase dendrogram. All profiled kinases are represented by circles and labeled by name. The size of the circle corresponds to relative percent competition (larger circle, more competed). **C**. Results for ligand **2** as described in B. **D**. Results for ligand **3** as described in B. **E**. Results for ligand **4** as described in B. Each profiling experiment was performed in triplicate.

The kinase PKN3 was also depleted in the drug-treated channel, most strikingly during profiling of ligand **1**. In order to assess whether PKN3 is inhibited by **1**-**4**, an activity assay using γP^{32}-ATP was performed with recombinant PKN3. Unfortunately, **1**-**4** are potent inhibitors of PKN3 (**Table 3-1**). However, the cause of this inhibition is not readily apparent as there is no crystal structure of the kinase available. We hypothesized that PKN3 contains an active-site Cys that is reactive with our reversible-covalent inhibitors, but sequence alignment suggests that this is not the case. We also assayed the RSK2 CTD, and showed that it too is potently inhibited by **1**-**4** (**Table 3-1**). This is not surprising considering the wild-type RSK2 CTD contains the same active site Cys as the analogue-sensitized kinases. While RSK2 was quantified in our profiling experiment it did not show up as being competed because full-length RSK2 contains two kinase domains, one of which is not analogue-sensitive. Though the CTD was inhibitor-bound, the N-terminal domain (NTD) was not and remained bound to the immobilized inhibitors in the presence of all compounds tested. EphA2 also appeared as an off-target in profiling with **3** and **4**. This is likely due to the high concentration (50 μM) used in profiling experiment. Activity assays performed at physiologically-relevant ATP concentrations, show that while $EphA2^{WT}$'s catalytic domain is inhibited by **3** and **4** there is a large window of selectivity between it and $EphA2^{AS}$, indicating that selectivity for AS kinase over EphA2 could be achieved by using lower inhibitor concentrations (**Figure 3-2D**). Despite the identification of these off targets, only two kinases (in addition to RSK2) among the hundreds of endogenous kinases identified from lysate bound potently to our inhibitors. This demonstrates that our covalent, conformation-selective molecules are highly selective for engineered analogue-sensitized kinase variants over endogenous kinases.

Table 3-1

Inhibitor	K_i RSK2 CTD	K_i PKN3
1	7 ± 2	10 ± 2
2	20 ± 3	110 ± 50
3	820 ± 180	520 ± 110
4	170 ± 30	26 ± 13

Table 3- 1: K_i values for 1-4 against RSK2 CTD and PKN3

All K_i values (nM) reported as mean ± SEM, n=3.

B. Biochemical characterization of kinases bound to conformation-selective inhibitors

In order to determine whether **1**-**4** stabilize Type I, αC helix-out, or DFG-out ATP-binding site conformations as predicted, pull-downs to assess SH3 domain accessibility of Src, Hck, and Abl were performed. Our lab has shown that stabilizing an SFK's ATP-binding site with a Type I or a DFG-out inhibitor decreases the SH3 domain's affinity for its intra-molecular binding partner: a poly-Pro helix contained within the linker sequence connecting the SH2 domain to the catalytic domain (SH2-catalytic domain linker) (Leonard et al., 2014). Conversely, stabilizing the ATP-binding site with an αC helix-out inhibitor increases the SH3 domain's intra-molecular affinity for the SH2-catalytic domain linker, making the SH3 domain less available for inter-molecular interactions. This occurs through *bi-directional*, allosteric communication between the αC helix and SH2-catalytic domain linker (Superti-Furga et al, 2000; Register et al, 2014). Stabilizing the αC helix in an inactive conformation, in which the Glu310/Lys298 salt bridge is disrupted (as in Type II, αC helix-out inhibition), aligns residues in the catalytic domain such that the linker is less optimal for binding the SH3 domain, whereas stabilizing the αC helix in an active conformation, in which the salt bridge is stabilized (as in Type I and Type II DFG-out

inhibition), aligns residues in the catalytic domain such that the linker is primed for SH3 domain binding. Incubating an inhibitor-bound SFK with resin displaying an SH3 domain-binding peptide provides a means of measuring the effects of ATP-binding site conformation on SH3 domain accessibility. If an inhibitor increases SH3 domain accessibility (Type I- or DFG-out stabilizing), more kinase is retained on the SH3 domain-binding resin. In contrast, if an inhibitor decreases SH3 domain accessibility (αC helix-out-stabilizing), less kinase is retained on the SH3 domain-binding resin (**Figure 3-4A**).

Figure 3-4

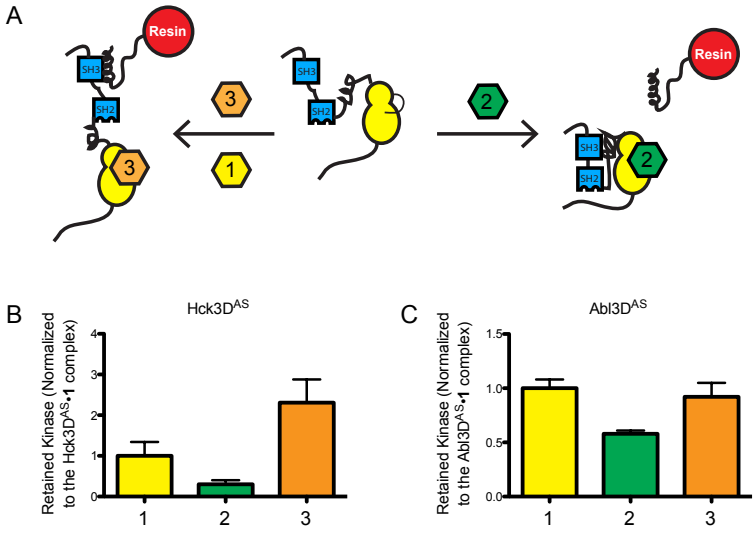

Figure 3- 4: 1-3 modulate Hck3D and Abl3D SH3 domain engagement by stabilizing their predicted ATP-binding site conformations

A. Experimental scheme for *in vitro* SH3 pull-down experiment. Type I- and DFG-out-stabilizing inhibitors (like inhibitors **1** and **3**) increase SH3 domain accessibility to an SH3 domain-binding peptide (left) compared to αC helix-out-stabilizing inhibitors (like inhibitor **2**), which decrease SH3 domain accessibility (right). **B**. Experimental results for Hck3D^{AS} retained on resin when bound to **1**, **2**, and **3**. All values are normalized to the Hck3D^{AS}•**1** complex and displayed as mean ± SEM, n=3. **C**. Experimental results for Abl3D^{AS} retained on resin when bound to **1**, **2**, and **3**. All values are normalized to the Abl3D^{AS}•**1** complex and displayed as mean ± SEM, n=3.

Pull-downs were performed on Hck3D^{AS} (three-domain construct containing the SH3, SH2, and catalytic domains, but lacking the N-terminal unique domain to facilitate

purification) recombinantly expressed and purified from *E. coli* as described previously (Seeliger et al., 2005). As expected, Hck3D^{AS}•**1** and Hck^{AS}•**3** display greater retained kinase than Hck3D^{AS}•2 by about 5-fold and 10-fold, respectively (**Figure 3-4B**). This experiment was also performed with Abl3D^{AS} expressed and purified from *E. coli*. Abl structural regulation is similar to SFKs in that SH3 domain binding to the SH2-catalytic domain linker also autoinhibits the catalytic domain by affecting αC helix conformation. Similar to what was observed for Src, twice as much Abl3D^{AS}•**1** and Abl3D^{AS}•**3** were retained on resin displaying an SH3 domain-binding peptide compared to Abl3D^{AS}•**2** (**Figure 3-4C**). This confirms the observation by NMR that stabilizing a DFG-out ATP-binding site conformation increases Abl's SH3 domain accessibility. It also suggests that despite differences in structural regulation, both SFK and Abl catalytic activity are regulated by the conformation of the αC helix, as discussed in **Chapter 2**.

Pull-downs were also performed on full-length, C-terminally Flag-tagged Src^{AS} and Hck^{AS} overexpressed in HEK293T cells (**Figure 3-5A**). Cells expressing Src^{AS} or Hck^{AS} were treated with inhibitors for 2 hrs prior to lysis, and lysates were pulled down with beads displaying an SH3 domain-binding peptide. Retained SFK^{AS} was visualized by western blot, probing for anti-Flag. The same trends as for recombinant Src3D and Hck3D were observed with more dramatic differences in retention between **1**, **2**, and **3** bound kinase. As observed previously, this inhibitor-dependent fold difference in SH3 domain availability is larger for Hck than for Src, and is consistent with Src's linker being less coupled to αC helix conformation than Hck's (**Figure 3-5B**) (Register et al., 2014). SH3 domain accessibility is also greater for SFK3D^{AS}•**3** than for SFK3D^{AS}•**1**, which is consistent with previous observations for DFG-out- versus Type I-stabilization of SFK

ATP-binding sites (**Figure 3-5C**) (Leonard et al., 2014). This may be due to the fact that many DFG-out-stabilizing ligands hydrogen bond with Glu310 on the αC helix, and thus more strongly stabilize an αC helix-in conformation than Type I-stabilizing inhibitors which lack this contact. No difference in retained kinase was observed for Hck^{WT} treated with **1**, **2**, or **3** (**Figure 3-5D**).

Figure 3-5

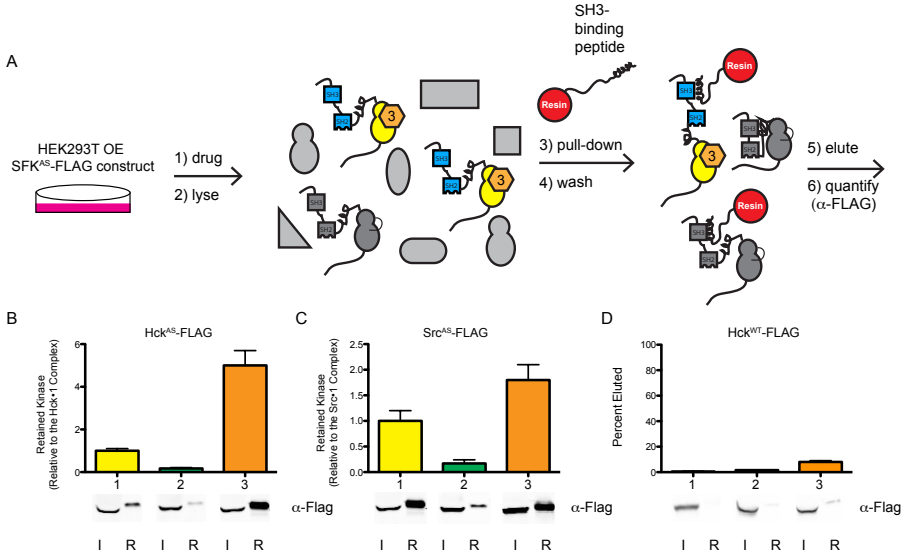

Figure 3- 5: 1-3 modulate full-length SFK SH3 domain engagement in cells

A. Experimental scheme for cellular SH3 pull-down experiment. HEK293T cells overexpressing (OE) Flag-tagged full-length SFK^{AS} construct are treated with **1**, **2**, or **3** for 2 hrs before lysis, pull-down with SH3 domain-binding peptide resin, and quantitation of retained $kinase^{AS}$ via anti-Flag western blot. **B**. Quantification of retained Hck^{AS} bound to **1**, **2**, and **3** represented as bar graphs with representative anti-Flag blots (I: input kinase; R: retained kinase). All data is normalized to the Hck^{AS}•**1** complex and displayed as mean ± SEM, n=3. **C**. Quantification of retained Src^{AS} bound to **1**, **2**, and **3** represented as bar graphs with representative anti-Flag blots (I: input kinase; R: retained kinase). All data is normalized to the Src^{AS}•**1** complex and displayed as mean ± SEM, n=3 **D**. Quantification of retained Hck^{WT} when incubated with **1**, **2**, or **3** represented as bar graphs. Data is represented as Percent Retained HckWT and displayed as mean ± SEM, n=3.

To further validate our conformation-selective inhibitors and investigate their effects on biologically-relevant phosphorylation events, an assay was designed and

performed to measure SFK C-terminal tail phosphorylation by Csk (**Figure 3-6A**). Csk regulates SFK activity by selectively phosphorylating the C-terminal tail of SFK's on Tyr527, thus increasing its affinity for the SH2 domain and promoting SFK autoinhibition (Okada et al., 1991; Levinson et al., 2008). Increasing regulatory domain accessibility by stabilizing the αC helix in an active conformation with Type I- or DFG-out- stabilizing ligands (**1** and **3**, respectively) should make the C-terminal tail—the intra-molecular binding partner for the SH2 domain of SFKs—more accessible for phosphorylation by Csk by decreasing SH2 domain intra-molecular engagement. In contrast, αC helix-out-stabilizing ligands (like **2**) should decrease pTyr527 by allosterically increasing SH2 domain engagement and making the SFK's C-terminal tail less accessible to phosphorylation by Csk. SFK^{AS} was incubated with Csk and a concentration of **2** or **3** at which all SFK^{AS} was inhibitor bound but Csk activity was uninhibited. Typically, ATP-competitive ligands that inhibit SFKs also inhibit Csk, due to high structural and sequence homology between the two kinases, but this hurdle is overcome by the use of SFK^{AS} and covalent conformation-selective inhibitors. Ligands **2** and **3** were chosen because we predicted based on the SH3 pull-down results presented above, that they would produce the greatest divergent effects on SH2-domain engagement. Tyr527 phosphorylation was measured by detection of γP^{32} retained on nitrocellulose after a fixed period of time. As expected, $Src3D^{AS}$•**3** and $Hck3D^{AS}$•**3** display 3-fold and 9-fold greater Tyr527 phosphorylation, respectively, than $Src3D^{AS}$•**2** and $Hck3D^{AS}$•**2** (**Figure 3-6B**). As observed for the SH3 pull-down and reported in **Chapter 1**, differences in pTyr527 reflect SH2-catalytic domain linker-dependent differences in coupling between the ATP-binding site and regulatory domains. This is further supported by the fact that inhibitor-driven

differences in pTyr527 are greater for Hck than for Src, which is characterized by tight allosteric coupling of SH3 domain engagement to ATP-binding site conformation relative to Src.

Figure 3-6

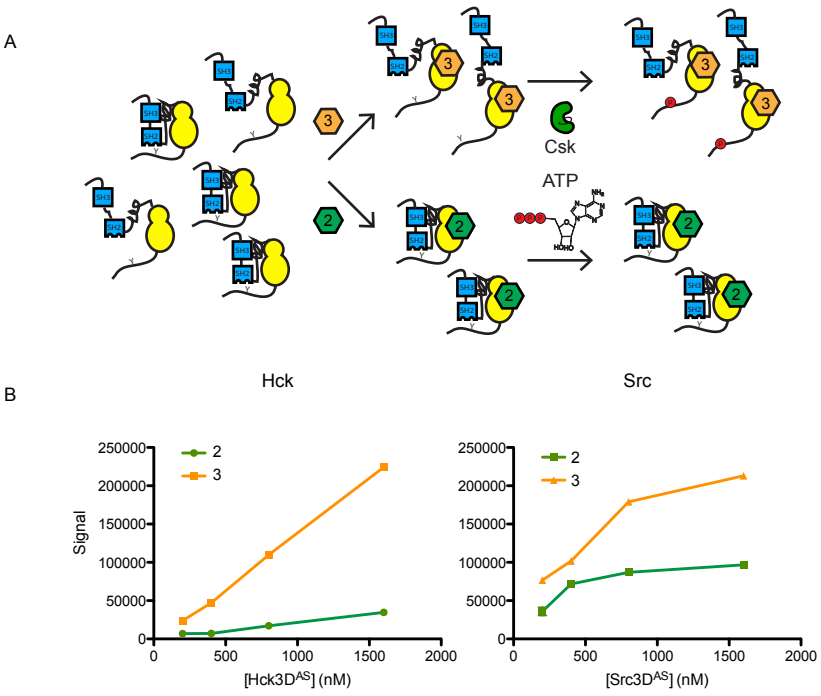

Figure 3- 6: Stabilization of DFG-out and αC helix-out ATP-binding site conformations with 3 and 2 divergently modulates SFK pTyr527 by Csk

A. Experimental scheme for SFK Y527 phosphorylation assay. SFK3D^{AS} was incubated with **2** or **3** for 1 hr before addition of Csk and γP^{32}-ATP. Accessibility of Tyr527 for phosphorylation by Csk is modulated by inhibitor-driven conformational changes. **B**. Results for Hck3D^{AS} and Src3D^{AS} bound to **2** (green) and **3** (orange) reported as mean ± SEM, n=3.

In order to be sure that observed differences in pTyr527 are the result of conformation-selective inhibitor binding, a variation on the assay described above was devised using analogue-*insensitive* Src3D and Hck3D constructs (**Figure 3-7A**). A kinase dead, K295M, mutation was installed in each kinase (SFK3D^{KM}) so that SFK autophosphorylation would not obscure the signal from Tyr527 phosphorylation. No

difference in tail phosphorylation was observed between Src3D^{KM} or Hck3D^{KM} when incubated with **2**, **3**, or DMSO (**Figure 3-7B**). This is consistent with ligands **2** and **3** having low affinity for the ATP-binding sites of non-analogue-sensitive SFKs. Furthermore, to demonstrate that observed differences in pTyr527 by Csk are the result of differential SH2-domain accessibility, another variation of the assay was designed using Src and Hck analogue-sensitive constructs consisting only of the catalytic domain and C-terminal tail (SFKCD^{AS}; **Figure 3-7C**). Neither SrcCD^{AS} nor HckCD^{AS} showed any inhibitor-specific differences in Tyr527 phosphorylation (**Figure 3-7D**), supporting the hypothesis that ATP-binding site conformational changes are driving differences in pTyr527 by allosterically modulating SH2 domain accessibility. Taken together, these results show that stabilizing a Type I, αC helix-out, or DFG-out ATP-binding site conformation can divergently affect kinase phosphorylation state. In order to probe the biological consequences of conformation-selective inhibition, cell experiments are necessary to connect ATP-binding site conformation to phenotype.

Figure 3-7

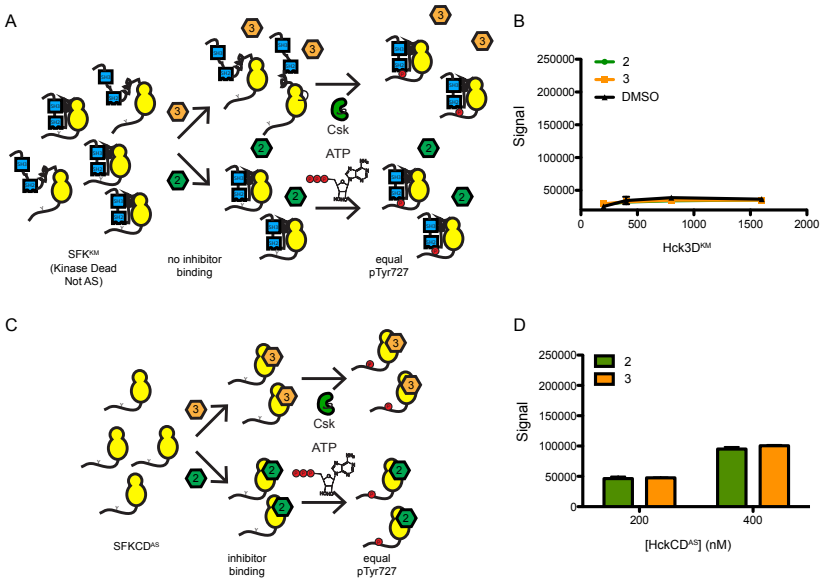

Figure 3- 7: Inhibitor-binding effects on pTyr527 require AS mutation and regulatory domains

A. Experimental scheme for SFK Tyr527 phosphorylation assay using a kinase dead, analogue-insensitive SFK construct. Hck3D^{KM} was incubated with **2** or **3** for 1 hr before addition of Csk and γP^{32}-ATP. Accessibility of Tyr527 for phosphorylation by Csk is not modulated by inhibitor-driven conformational changes because inhibitors do not bind to the active site of Hck3D^{KM}. **B**. Results for Hck3D^{KM} incubated with **2** (green), **3** (orange), and DMSO (black) reported as mean ± SEM, n=3. **C**. Experimental scheme for SFK Tyr527 phosphorylation assay using an SFKCD^{AS} construct. SFKCD^{AS} was incubated with **2** or **3** for 1 hr before addition of Csk and γP^{32}-ATP. Accessibility of Tyr527 for phosphorylation by Csk is not modulated by inhibitor-driven conformational changes because SFKCD^{AS} lacks SH3 and SH2 regulatory domains. **D**. Results for HckCD^{AS} bound to **2** (green) and **3** (orange) reported as mean ± SEM, n=3.

C. Stabilizing the Src^{AS} ATP-binding site in a DFG-out conformation increases Src co-localization with the plasma membrane, blebbing, and motility in fibroblasts

The SFK Src plays important roles in integrin signaling that have been investigated thoroughly over the past 25 years. Upon activation of integrin signaling Src localizes to the focal adhesion complex where it associates with Focal Adhesion Kinase (FAK) leading to phosphorylation of FAK at various sites (Rauch et al, 2011; Kaplan et al., 1994). Src's participation in this pathway is important for adhesion and motility in fibroblasts as Src-deficient fibroblasts exhibit defects in cell spreading. There is strong evidence in the literature that Src's participation in integrin signaling is largely non-catalytic, presumably through SH3 and SH2 domain scaffolding. For example, defects in cell spreading in Src-deficient fibroblasts can be reversed by reconstitution with kinase-dead Src (Kaplan et al., 1995). Additionally, activation of the Src-dependent adaptor protein p130^{CAS} in response to fibronectin does not require Src kinase activity, nor do many of the tyrosine phosphorylation events on FAK that occur upon overexpression of Src (Schlaepfer et al., 1997). In fact, phosphorylation of several sites requires Src's SH2 domain but not kinase activity (Brunton et al., 2005). Given this information, we were curious if we could affect Src's localization and association with focal adhesions by allosterically modulating

regulatory domain engagement through ATP-binding site conformation with our conformation-selective inhibitors.

To assess ATP-binding site conformation dependent effects on Src localization, fixed-cell confocal microscopy was performed on Src/Yes/Fyn (-/-) 3T3 cells (SYFs) transiently transfected with Src^{AS}-GFP (C-terminal GFP construct). Cells were treated with **2** or **3** for 15 min, before fixation and staining with wheat germ agglutinin conjugated to AlexaFluor 647, to visualize the plasma membrane, and DAPI, to visualize the nucleus. Incubation with 10 μM **3** resulted in an increase in Src^{AS} localization with the plasma membrane that was not observed when Src^{AS} was treated with **2** or DMSO (**Figure 3-8A**). Performing the identical experiment on SYF cells over expressing Src^{WT} showed no apparent difference in Src localization between treatments with **3** and DMSO. Additionally, introducing a G2A mutation to Src^{AS}—to prevent myristoylation of the N-terminus—reduced the amount of Src^{AS}•**3** co-localization with the plasma membrane to a similar level as observed for Src^{AS} and DMSO (**Figure 3-8B**). Myristoylation is critical for Src's association with the plasma membrane (David-Pfeuty et al., 1993), thus it makes sense that abolishing the myristoylation site on Src^{AS} would abolish ATP-binding site conformation-driven co-localization with the plasma membrane.

Interestingly, while performing these experiments, we also noticed an increase in membrane blebs—dynamic cytoskeleton-regulated membrane protrusions important for cell motility and invasiveness—in SYF cells reconstituted with Src^{AS}•**3**. Markedly fewer membrane blebs were observed for SYF cells reconstituted with Src^{AS} and treated with DMSO and for SYFs reconstituted with Src^{WT} treated with either **3** or DMSO (Fackler and Grosse, 2008) (**Figure 3-8B**; white arrows). Association of Src's N-terminus with the

plasma membrane has been shown to be associated with an increase in blebbing, providing further evidence that stabilizing the ATP-binding site of Src in a DFG-out conformation with ligand **3** is increasing Src's localization with the plasma membrane presumably by allosterically increasing SH3 and SH2 regulatory domain accessibility for inter-molecular interactions (Tournaviti et al., 2007). Currently, we are working on quantitatively measuring co-localization with the plasma membrane for Src^{AS}•**3** versus Src^{AS}•**2** and DMSO to account for any bias in our image analysis.

Figure 3-8

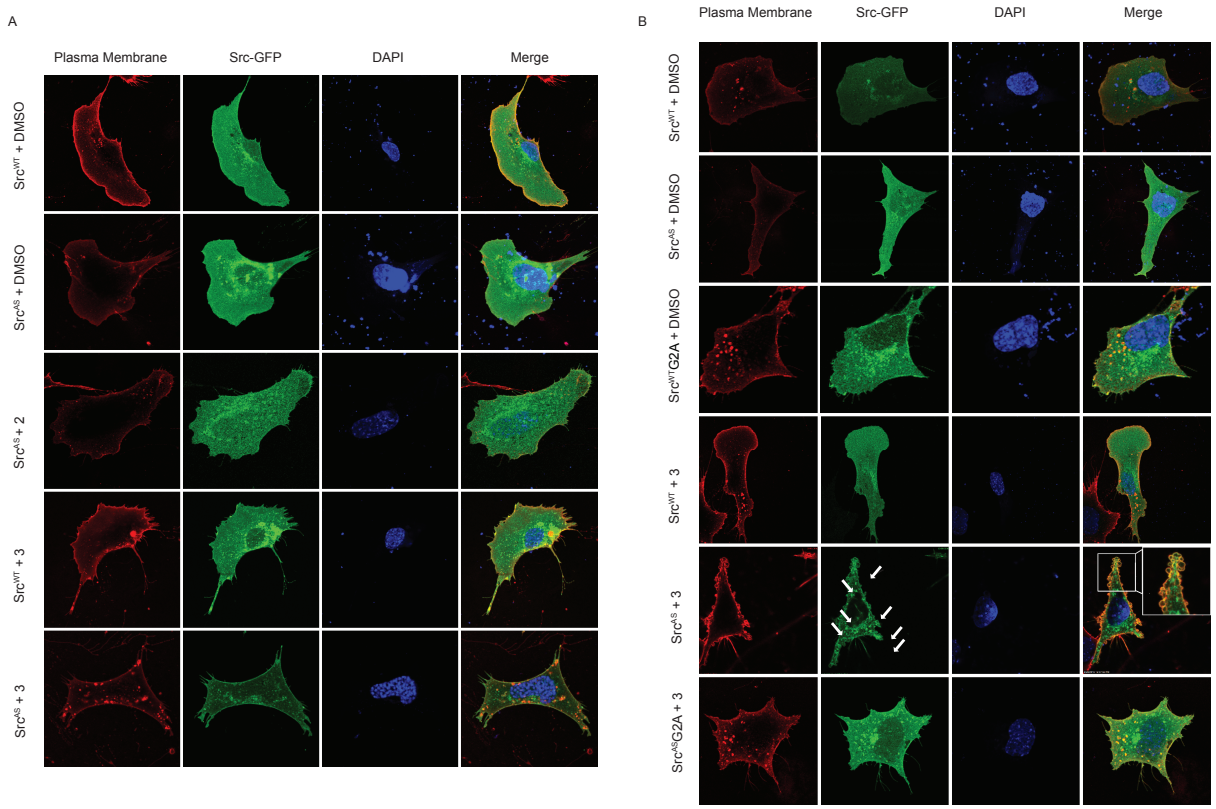

Figure 3- 8: Confocal microscopy shows ATP-binding site conformation-dependent changes in Src localization

A. Images of SYF cells overexpressing Src^{AS} or Src^{WT} C-terminal GFP fusion constructs obtained *via* confocal microscopy. Red (left-most panels) shows plasma membrane signal, green (middle-left panels) shows GFP (Src) signal, blue (middle-right panels) shows DAPI (nuclear) signal, and the right-most panels show merged images of all channels for a given condition. Cells were treated with 10 μM **3**, 3 μM **2**, or DMSO for 15 minutes before fixation and staining. **B**. Images of

SYF cells overexpressing Src^{AS}, Src^{AS}G2A, Src^{WT}, or Src^{WT}G2A C-terminal GFP fusion constructs obtained *via* confocal microscopy. Red (left-most panels) show plasma membrane signal, green (middle-left panels) show GFP (Src) signal, blue (middle-right panels) show DAPI (nuclear) signal, and the right-most panels show merged images of all channels for a given condition. Cells were treated with 10 μM **3** or DMSO for 15 minutes before fixation and staining. White arrows signify blebs.

Given the observation that Src but not Src catalytic activity is necessary to restore cell motility in fibroblasts, we were curious whether treatment with our conformation-selective inhibitors would modulate Src's ability to enhance cell motility. SYF cells transfected with Src^{AS} were plated on one side of a membrane in a media-filled chamber and treated with DMSO, **2**, or **3** for 48 hrs. Motile cells are able to migrate through the membrane to the other side, after which cells on top of the membrane are removed and motile cells are stained and quantified (**Figure 3-9A**). The data is normalized to cells treated with DMSO. Src^{AS}•**3** exhibited 4-fold more movement to the bottom plate compared to Src^{AS}•**2**, indicating that stabilizing a DFG-out ATP-binding site conformation increases Src's ability to enhance motility in fibroblasts, presumably through increased participation in integrin signaling at focal adhesion complexes (**Figure 3-9B**). This result provides further evidence that Src's important role in integrin signaling/cell-spreading is played largely through participation in protein-protein interactions via its SH3 and SH2 regulatory domains. Currently, we are performing SILAC co-immunoprecipitation (Co-IP) experiments to identify differences in proteins Co-IP'd with Src^{AS} between cells treated with **2** and **3**. Specifically, we hypothesize that members of focal adhesion complexes known to interact with Src, such as Nck, Grb2, FAK, and $p130^{CAS}$, will be enriched in Src^{AS}•**3** versus Src^{AS}•**2**.

Figure 3-9

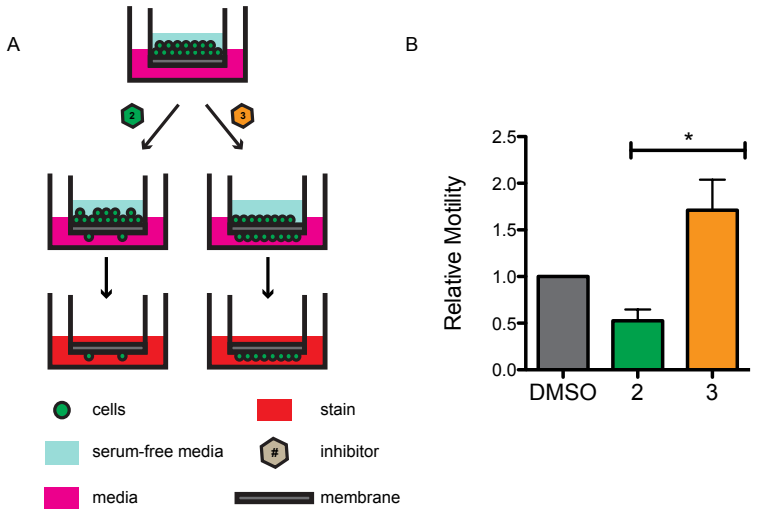

Figure 3- 9: Src's ATP-binding site conformation affects fibroblast motility

A. Experimental scheme for cell motility assay. SYF cells overexpressing Src^{AS} are plated in serum-free media on top of a membrane before 48-hr treatment with DMSO, 3 μM **2,** or 10 μM **3**, removal of top cells, and staining/quantification of motile cells. **B**. Bar graph showing quantification of motility relative to DMSO for each condition as mean ± SEM, n=3.

D. Type I- and DFG-out-stabilizing inhibitors allosterically increase c-Abl phosphorylation at Thr735 and interaction with 14-3-3 proteins

Given our previous biochemical investigation of the non-receptor tyrosine kinase c-Abl, we were hopeful that we could use conformation-selective inhibitors to modulate c-Abl non-catalytic function in cells. Thr735 on c-Abl has been shown to be an important determinant for c-Abl cellular localization (Mancini et al., 2009). Phosphorylation at Thr735 serves as a binding site for 14-3-3 proteins, obscuring a nuclear localization sequence (NLS) sequence on c-Abl's C-terminus, thus reducing shuttling of the kinase to the nucleus (Yoshida et al., 2005; Nihira et al., 2008). In order to assess whether conformation-selective inhibition of $c\text{-}Abl^{AS}$ with our panel of reversible-covalent Type I-, αC helix-out-, or DFG-out-stabilizing ligands affects c-Abl's phosphorylation at Thr735, HEK293T cells stably expressing C-terminally Flag-tagged $c\text{-}Abl^{AS}$ upon induction with

doxycycline, were treated with **1**, **2**, or **3** for 2 hrs before lysis (**Figure 3-10A**). Imatinib, a well-characterized, DFG-out-stabilizing inhibitor that is highly selective for Abl was also tested as a control. Lysates were separated by SDS-PAGE and immunoblotted for total c-Abl and pThr735 using an antibody specific for the phospho-site (Cell Signaling Technology). An ~5-fold increase in pThr signal was observed for **1**-treated cells and an ~3-fold increase in pThr was observed for cells treated with **3** or imatinib, providing further evidence that **3** is in fact stabilizing a DFG-out ATP-binding site conformation as predicted. In contrast, no increase in pThr signal was observed for **2**-treated cells. Each inhibitor reduced phosphorylation of the direct c-Abl substrate CrkL, indicating that the ATP-binding site of c-Abl^{AS} is fully bound at the concentrations used. A time-course experiment in which cells overexpressing c-Abl^{AS} were treated with **1**, **2**, or **3** for 0, 15, 30, 60, 120, or 180 min, showed that the increase in pThr signal observed upon treatment with **1** and **3** was quantifiable by 15 min, reached a maximum by 60 min, and was maintained until the last time point (180 min). No change in pThr was observed for any time point for cells treated with ligand **2** (**Figure 3-10C**).

Figure 3-10

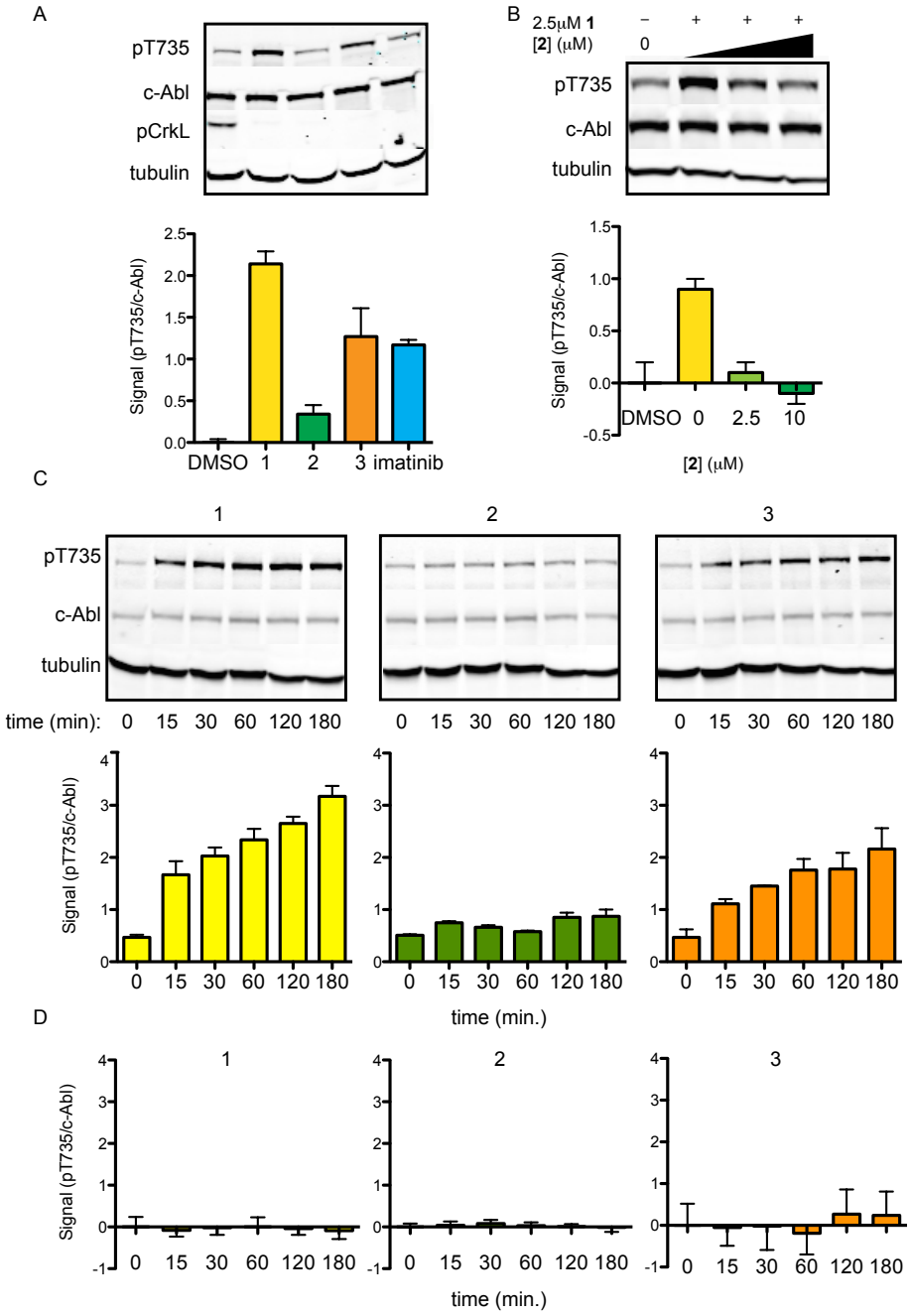

Figure 3- 10: c-Abl ATP-binding site conformation affects phosphorylation of Thr735 in 293T cells

A. Quantitation of pThr735/c-Abl signal for 2 hr DMSO, **1**, **2**, **3**, and imatinib-treated HEK293T cells overexpressing c-Abl^{AS}; mean ± SEM, n=3. Representative blots show pThr735, total c-Abl, pCrkL, and tubulin for each condition. **B**. Bar graph showing quantitation for pThr735/c-Abl signal for HEK293T cells overexpressing c-Abl^{AS} treated for 2 hrs with DMSO, 2.5 μM **1**, 2.5 μM **1** and 2.5 μM **2**, or 2.5 μM **1** and 10 μM **2**; mean ± SEM, n=3. Representative blots show pThr735, total

c-Abl, and tubulin levels for each condition. **C**. Bar graphs showing quantitation of pThr735/c-Abl signal for HEK293T cells overexpressing c-Abl^{AS} and treated with **1**, **2**, or **3** for the indicated times; mean ± SEM, n=3. Representative blots show pThr735, total c-Abl, and tubulin levels for each condition. **D**. Bar graphs showing quantitation of pThr735/c-Abl signal for HEK293T cells overexpressing c-Abl^{WT} treated for the indicated times with **1**, **2**, or **3**. Signal at time 0 is subtracted for clarity; mean ± SEM, n=3.

To address the possibility that our inhibitors were influencing phosphorylation of c-Abl on Thr735 through an off-target effect, HEK293T cells overexpressing c-Abl^{WT} were subjected to the time-course experiment described above with ligands **1**, **2**, and **3** (**Figure 3-10D**). c-Abl^{WT} did not exhibit inhibitor-dependent changes in pThr735 signal at any time point for any of the inhibitors, demonstrating that modulation of pThr735 is occurring through inhibitor binding to the ATP-binding site of c-Abl^{AS}. Additionally, because no increase in pThr735 was observed for cells treated with ligand **2** compared to DMSO, a competition experiment was designed to determine whether or not **2** is cell-permeable. HEK293T cells overexpressing c-Abl^{AS} were treated with 2.5 μM **1** and 0, 2.5, or 10 μM **2** for 2 hrs before being lysed and blotted for pThr735 (**Figure 3-10B**). The increase in pThr signal at 2.5 μM caused by **1** was dose-dependently reduced by the addition of **2**, demonstrating that **2** is cell permeable and able to compete with **1** for the ATP-binding site of c-Abl^{AS}.

It has been reported that the kinase responsible for phosphorylating c-Abl at Thr735 if Mps1/TTK1 (Nihira et al., 2008). Therefore, we were curious to see if conformation-selective inhibitor driven changes in c-Abl pThr735 would be observed in the presence of a potent Mps1/TTK1 inhibitor. A similar increase in pThr735 signal was observed upon treatment with **1** in the presence of Mps1/TTK1 inhibitor as in the absence of inhibitor, suggesting that this Mps1/TTK1 is not the only kinase responsible for phosphorylation of Abl at this site (data not shown).

pThr735 is a known binding site for 14-3-3 proteins that sequester c-Abl in the cytoplasm, preventing it from entering the nucleus where it drives apoptosis in response to oxidative and genotoxic stress (Yoshida et al., 2005). We hypothesized that Thr735 is more available when c-Abl is bound to Type I- and DFG-out-stabilizing inhibitors, and therefor binding of c-Abl^{AS} to ligands **1** and **3** would result in increased interaction with 14-3-3 proteins compared to c-Abl^{AS} bound to **2** or treated with DMSO. To test this hypothesis, HEK293T cells overexpressing Flag-tagged c-Abl^{AS} were plated on 10cm^2 plates, treated with **1**, **2**, or **3** for 2 hrs before being lysed and immunoprecipitated (IP'd) with anti-Flag magnetic beads (Sigma). The beads were washed twice with lysis buffer before c-Abl and any Co-IP'd proteins were eluted with 3x Flag peptide, mixed with loading dye, separated by SDS-PAGE, and blotted for total c-Abl, pThr735, and 14-3-3 ε. As predicted, c-Abl^{AS}•**1** displayed more Co-IP of 14-3-3 ε than c-Abl^{AS}•**2** and DMSO (**Figure 3-11A**). c-Abl^{AS}•**3** also appears to increase 14-3-3 Co-IP (shown in blot, but not quantified). A proteomic SILAC experiment was also performed in which c-Abl^{AS}-overexpressing HEK293T cells were grown in heavy or light labeled media and treated with **1** or **2** for 2 hrs, before lysis, anti-Flag IP, elution, trypsin digestion, and MS/MS analysis (**Figure 3-11B**). While not many Co-IP'd proteins were identified in total, more 14-3-3 proteins were quantified in **1**-treated samples versus **2**-treated samples, corroborating the results of blots described above (**Figure 3-11C**).

Figure 3-11

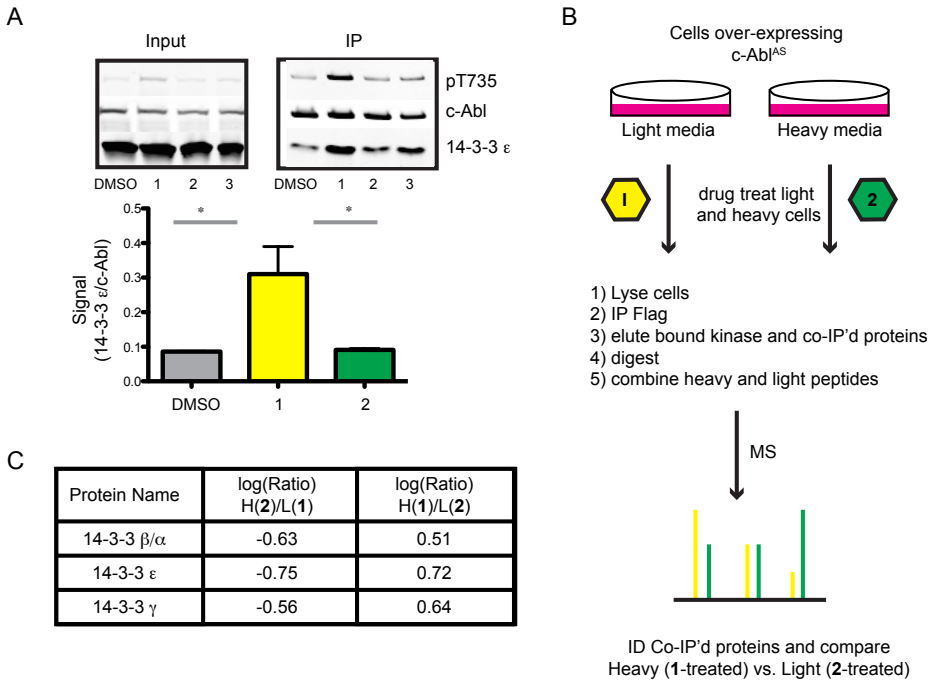

C

Protein Name	log(Ratio) H(**2**)/L(**1**)	log(Ratio) H(**1**)/L(**2**)
14-3-3 β/α	-0.63	0.51
14-3-3 ε	-0.75	0.72
14-3-3 γ	-0.56	0.64

Figure 3- 11: ATP-binding site conformation-dependent changes in pThr735 affect c-Abl's interaction with 14-3-3 proteins

A. Bar graph showing quantitation of Co-IP'd 14-3-3 ε signal relative to c-Abl signal IP'd from HEK293T cells overexpressing c-Abl^{AS} and treated with DMSO, **1**, **2**, or **3** 2 hrs prior to lysis; mean ± SEM, n=3. * signifies that p value is < 0.05. **B**. Cartoon illustrating SILAC Co-IP experiment. **C**. Quantification of 14-3-3 proteins Co-IP'd with **1** versus **2** and showed as $\log_2$(Heavy/Light). Labels were switched for each replicate leading to a change in sign between each experiment. More 14-3-3s were pulled down when cells were treated with **1** than with **2**.

Furthermore, oxidative stress has been shown to affect c-Abl phosphorylation at Thr735 (Nihira et al., 2008; Yoshida et al., 2005). In HeLa cells, treatment with H_2O_2 produced a marked increase in pThr735 from 20-60 min, after which phosphorylation at this site returned to untreated levels. Transfecting HeLa cells with c-Abl^{AS} and treating with DMSO, **1**, **2**, or **4** produced analogous changes in pThr735 as observed in HEK293T cells (**Figure 3-12A,** left 4 bars). To address the question of whether we could enhance or dampen the effects of H_2O_2 on pThr735 of c-Abl^{AS} with our conformation-selective

inhibitors, HeLa cells were transfected with c-Abl^{AS} and pre-treated for 1 hr with DMSO, **1**, **2**, or **4** before being exposed to 1mM H_2O_2 for 20 mins (**Figure 3-12A**, right 4 bars). After IP with anti-Flag resin, wash, and elution with 3x Flag peptide, a 4-fold increase in pThr735 was observed for DMSO + H_2O_2 compared to DMSO alone. This increase was 2-fold greater for treatments with **1** and **4** in combination with H_2O_2. Interestingly, treatment with **2** and H_2O_2 produced a similar increase in pThr735 as observed with DMSO and H_2O_2. This may indicate that c-Abl^{AS}•**2** is less sensitive to phosphorylation at Thr735 than c-Abl^{AS}•**1** and c-Abl^{AS}•**4**, but is not protected completely. Another possibility is that H_2O_2 increases pThr735 levels equally for all conditions and inhibitor-dependent differences are the result of drug treatment prior to oxidative stress. This would suggest that under unstressed conditions, c-Abl's ATP-binding site conformation influences phosphorylation at Thr735, while ATP-binding site conformation does not affect phosphorylation at this site under oxidative stress conditions.

We were curious whether c-Abl's interaction with 14-3-3 proteins could be modulated in HeLa cells as observed in HEK293T cells. Blotting for 14-3-3 proteins with a pan 14-3-3 antibody (Santa Cruz) showed more 14-3-3 Co-IP'd with c-Abl^{AS}•**1** and c-Abl^{AS}•**4** than c-Abl^{AS}•**2** and DMSO, similar to results in HEK293T cells (**Figure 3-12A**, representative blot). Interestingly, Co-IP of 14-3-3 seemed to increase for all conditions when H_2O_2 was added.

To confirm that **1**, **2**, and **4** exert their effects on pThr735 through conformation-selective inhibition of c-Abl, several control experiments were performed. No change in pThr735 was observed with any inhibitor for any of the conditions tested when HeLa cells were transfected with c-Abl^{WT} instead of c-Abl^{AS} (**Figure 3-12B**). Additionally, a

competition experiment identical to the one described for HEK293T cells showed that treatment with **2** reduced pThr735 back to basal levels in the presence of **1**, confirming that **2** is cell permeable and prevents pThr735 increase by binding to the ATP-binding site of c-Abl^{AS} (**Figure 3-12C**). Consistent with this, pCrkL levels were reduced by half upon treatment with **2**. Catalytically-active endogenous c-Abl^{WT} is the likely reason why pCrkL is not abolished despite complete c-Abl^{AS} inhibition.

Figure 3-12

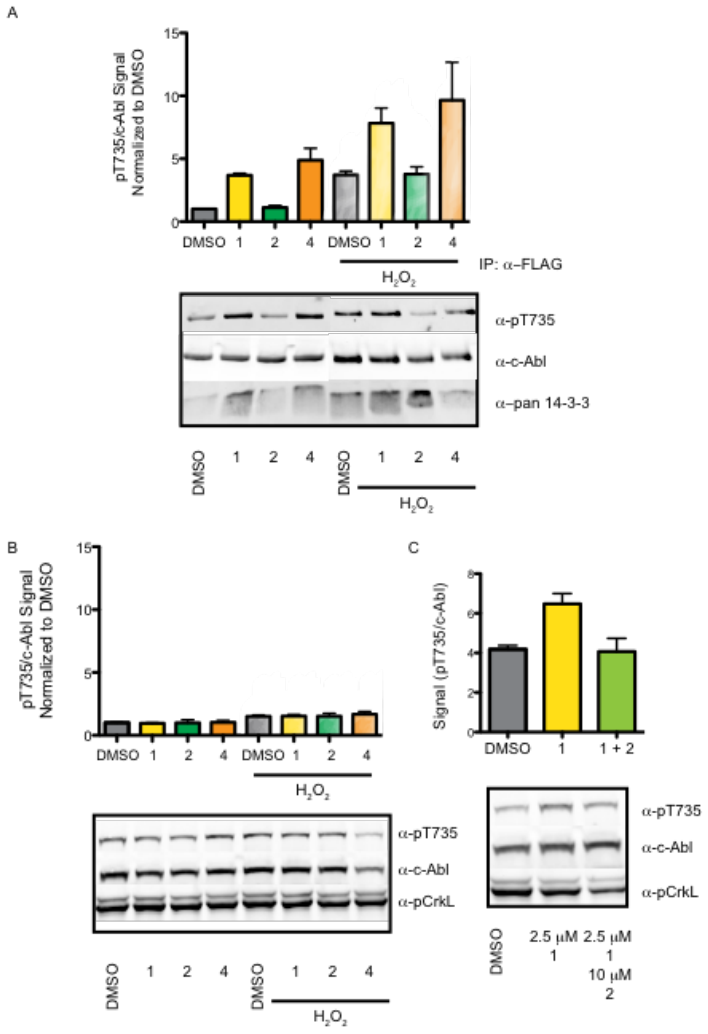

Figure 3- 12: ATP-binding site conformation-dependent changes in pThr735 are observed in unstressed HeLa cells and HeLa cells under oxidative stress

A. Bar graph showing quantitation of pThr735/c-Abl signal for DMSO, **1**, **2**, and **4** treated HeLa cells overexpressing c-Abl^{AS} with and without H_2O_2 after Flag IP; mean ± SEM, n=3. Representative blots show pThr735, total c-Abl, and pan 14-3-3 levels for each condition. **B**. Bar graph showing quantitation of pThr735/c-Abl signal for DMSO, **1**, **2**, and **4** treated HeLa cells overexpressing c-Abl^{WT} with and without H_2O_2; mean ± stdev, n=2. Representative blots show pThr735, total c-Abl, and pCrkL levels for each condition. C. Bar graph showing quantitation for pThr735/c-Abl signal for HeLa cells overexpressing c-Abl^{AS} treated with DMSO, 2.5 μM **1**, or 2.5 μM **1** and 10 μM **2**; mean ± stdev, n=2. Representative blots show pThr735, total c-Abl, and pCrkL levels for each condition.

III. Conclusion:

In this work we have described a novel chemical-genetic strategy for investigating the effects of ATP-binding site conformation on a kinase of interest. A panel of covalent inhibitors (**1**-**4**) were generated and shown to stabilize either Type I/active, αC helix-out, or DFG-out ATP-binding site conformations thorough biochemical characterization of their allosteric effects on SFK and c-Abl regulatory domain engagement. Crystal structures (data not shown) have also recently been solved of SrcCD^{AS} bound to **1**, **2**, and **3.** These structures confirm that **1**-**3** stabilize the predicted Type I, αC helix-out, or DFG-out ATP-binding site conformations. The fact that Erk2, Pak1, and EphA2 in addition to the non-receptor tyrosine kinases Src, Hck, and Abl can be sensitized to inhibition by ligands **1**-**4** with only a handful of off-targets and without greatly affecting their wild-type catalytic properties, suggests that this strategy can be used to study non-catalytic functions of kinases from potentially any family of the kinome.

Covalent conformation-selective inhibitors in combination with the analogue-sensitizing mutation have the potential to help scientific investigators generate a more complete and nuanced understanding of how kinases function in cell signaling networks by allowing for the dissection of catalytic roles from non-catalytic roles. Such investigations may reveal new drug targets as well as new strategies for perturbing cell

signaling networks. To this end, we have used our panel of ligands to modulate Src's participation in integrin signaling by affecting its co-localization with the plasma membrane and association with focal adhesion complexes. Stabilizing a DFG-out ATP-binding site conformation in Src increases cell motility, membrane localization, and blebbing in fibroblasts. This result indicates that much of Src's function in integrin signaling can be attributed to SH3 and SH2 regulatory domain accessibility, and that increased regulatory domain accessibility affects myristoylation of Src's N-terminus through an unknown mechanism. More experiments are necessary to characterize how ATP-binding site conformation modulates Src protein-protein interactions. This will allow for more conclusions to be drawn about the mechanism of Src's non-catalytic enhancement of blebbing and motility in fibroblasts. The fact that stabilizing Src's ATP binding-site in a DFG-out conformation increases fibroblast motility demonstrates the importance of understanding how ATP-binding site conformation affects signaling. For example, a drug that stabilizes a DFG-out ATP-binding site conformation in Src or another target could increase tumor cell motility—the opposite of the desired outcome.

Additionally, we have shown that Type I- and DFG-out-stabilized c-Abl shows increased phosphorylation at Thr735, a site known to be important for c-Abl's cellular localization. Increasing pThr735 results in greater Co-IP of 14-3-3 proteins responsible for sequestering c-Abl in the cytoplasm. Furthermore, the observed increase in pThr735 enhances pThr beyond levels observed in oxidative stress. More work is needed to understand how Thr735 phosphorylation affects the cellular localization of c-Abl and what effects manipulating phosphorylation levels at this site may have on c-Abl's ability to drive apoptosis in response to DNA damage and oxidative stress. Additionally, it is not clear

how ATP-binding site conformation is coupled to phosphorylation of Thr735 as the allosteric relationship between c-Abl's ATP-binding site and the last exon region is not well-understood.

The chemical-genetic tools described in this paper will enable drug-developers searching for therapeutic candidates through targeted kinase inhibition to assess how an inhibitor's ATP-binding site conformation preference affects signal propagation in any cell type—hopefully avoiding scenarios like the paradoxical activation of CRAF by Type I- and DFG-out-stabilized BRAF (Poulikakos et al., 2010; Hatzicassiliou et al., 2010; Zhang et al., 2015). The increasing ease and accessibility of gene-editing technology presents the exciting opportunity to introduce the analogue-sensitizing mutation into any endogenous kinase of interest in any cell type and screen for phenotypic differences connected to ATP-binding site conformation. This has the potential to be expanded to patient-specific cancers as personalized medicine becomes increasingly available.

IV. Materials and Methods

A. Cloning and protein expression

Analogue-sensitizing mutations were engineered using site-directed mutagenesis. To pick mutation site, the catalytic domain sequences of Hck, Src, Abl, EphA2, Erk2, and PAK1 were aligned with the RSK2 CTD and Val residue corresponding to Cys436 in the RSK2 CTD (numbering varies for each kinase).

Src3D, Hck3D, and Abl3D constructs were expressed and purified as described previously (Seeliger et al., 2005; Register et al., 2014; Leonard et al., 2014). His-tagged

Erk2, EphA2 catalytic domain, and Pak1 catalytic domain constructs were grown to OD 1.2 in 2 L flasks of LB in a shaking incubator at 37°C. The temperature was dropped to 18°C for 1 hr before induction with 0.2 mM IPTG. Overexpression proceeded overnight at 18°C before cells were harvested by centrifugation, lysed by sonication in lysis buffer (50mM HEPES, 150 mM NaCl, 20 mM Imidazol, 10 mM PMSF, 0.1% Triton-X 100 pH 8.0), and cleared for 40 min at 10000xg. Cleared lysates were incubated to 500 μL Ni-NTA resin for 1 hr, after which the lysate was discarded and beads were washed with 20 mL lysis buffer before bound protein was eluted with lysis buffer containing 300 mM imidazole. Eluted protein was analyzed for purity by SDS-PAGE and dialyzed overnight in 1 L dialysis buffer (50mM Tris, 150 mM NaCl, 1 mM DTT, 5% glycerol pH 8.0) at 4°C.

c-Abl1b was purchased from Addgene (plasmid #31284) and cloned into pcDNA5/FRT/TO (Invitrogen, product number V6520-20) using Gibson Assembly (NEB, product number E2611L). Overlap extension PCR was used to install GSGT-Flag sequence (GSGTDYKDDDDK) to the C-terminus of c-Abl immediately before the Stop codon to generate C-terminally Flag-tagged c-Abl constructs. Full-length Src and Hck were cloned into pcDNA5/FRT/TO and Flag-tagged using the same method. The Src C-terminal GFP fusion was generated by Gibson Assembly of PCR amplified Src (no tag) and GFP with PCR-linearized pcDNA5/FRT/TO.

B. Cell culture, stable cell line generation, and transient transfection conditions

Flp-In T-REx 293T (Invitrogen, product number R78007), SYF 3T3s, and HeLa cells were maintained in DMEM (Gibco, product number 11065092) supplemented with 10% FBS

(Gibco, product numberA3160602). Dox-inducible stable 293Ts were generated using the Flp-In T-REx system as described in product documentation, and maintained with 50 μg/mL hygromycin and 15 μg/mL blasticidin after selection. All transient transfections were done using Turbofectin8.0 (OriGene) at a ratio of 3:1 μL Turbofectin: μg DNA (HeLa cells) or 4:1 (SYF cells) prepared in serum-free DMEM 12-24 hrs after plating of cells. Transfections were allowed to proceed 24-48 hrs before experiments were performed.

C. SILAC cell culture

Flp-In T-REx 293T cells were grown in custom -Lys/-Arg DMEM (Caisson Labs, North Logan, UT) supplemented with 10% dFBS (Sigma, St Louis, MO), 200 μg/ml proline and SILAC amino acids (0.2 mM Lys0/Arg0 for light label, 0.2 mM Lys8/Arg10 for heavy label; Cambridge Isotope Labs, Andover, MA). Cells were grown for at least 5 cell doublings in SILAC medium and harvested when reaching 90% confluency and after induction with 0.5 mg/mL doxycycline (dox.) to induce Hck^{AS} or c-Abl^{AS} overexpression (24 hr overexpression).

D. Activity assays to determine IC_{50}s for 1-4 against $Kinase^{AS}$ and $Kinase^{WT}$

All assays were performed in assay buffer (75 mM HEPES pH 7.5, 150 mM NaCl, 15 mM $MgCl_2$, 3.75 mM EGTA, 1 mM Na_2VO_3, and 1 mM DTT). Abl3D, Hck3D, and Src3D AS and WT constructs were assayed using a self-reporting, fluorometric assay utilizing Pyrene-Dap containing peptide substrates (Wang et al., 2006; Abl pyrene peptide sequence: Ac-AEAIYAA(dap-pyrene)-LA- NH2 and SFK pyrene peptide sequence: Ac-EEEITGE(dap-pyrene)-EA-NH_2). Titrations of inhibitors (3-fold serial dilutions starting at

30 μM, eight data points) were assayed in a black 384-well plate (Corning, product number 3573) in assay buffer containing 30 nM Abl3D^{WT}, 38 nM Abl3D^{AS}, 7.5 nM Hck3D^{WT}, 7.5 nM Hck3D^{AS}, 8 nM Src3D^{AS}, or 10 nM Src3D^{WT} and 1 mM ATP the final volume per well for each assay was 30 μL and the final DMSO concentration was 4%. Enzymatic reaction was initiated with Abl/SFK pyrene substrate after 1-hr incubation at room temperature of Abl3D, inhibitor, and ATP. The reaction proceeded for 2 hrs after which the plate was read on a Perkin Elmer EnVision fluorimeter (Ex 340, Em 405). Data was exported to excel, quantified as percent Abl inhibition, and plotted using Prism Graphpad software.

ppErk2^{AS} (1.5 nM), ppErk2WT (3 nM), EphA2^{WT} (2.5 nM), EphA2^{AS} (7 nM), Pak1^{WT} (x nM), and Pak1^{AS} (x nM) were assayed at a substrate-limiting ATP concentration using γ32-ATP (final concentration 0.0067 μCi per well). The Erk2^{AS} construct contained DFG-out-inhibitor sensitizing mutations (Hari et al., 2014), and the EphA2 and Pak1 constructs tested consisted only of the kinase catalytic domains. The final volume of each assay well was 30 μL. Myelin Basic Protein (MBP, final concentration 0.1 mg/mL) was used as a substrate for Erk2 and Pak1 assays, while 4:1 Glu:Tyr peptide substrate (Sigma, P0275; final concentration 0.1 mg/mL) was used for EphA2. The enzymatic reactions were initiated by the addition of γ32-ATP, run at room temperature for 2 hrs, and terminated by spotting 4.6 μL of the reaction mixture onto a phosphocellulose membrane. Membranes were washed with 0.5% phosphoric acid (3x, 10 minutes each wash), dried, and the radioactivity was determined by phosphorimaging with a GE Typhoon FLA 9000 phosphor

scanner. The scanned membranes were quantified with ImageQuant. Data was analyzed using Prism Graphpad software.

E. Inhibitor selectivity profiling

Kinase affinity and sample enrichment: For kinase enrichment, 20 µl of a 50% kinobead slurry in 20% aqueous ethanol was pipetted into a 1.5 ml microtube and washed twice with 200 µl of mod. RIPA buffer (50 mM tris, 150 mM NaCl, 1% NP-40, 0.25% Na-deoxycholate, 1 mM EDTA and 10 mM NaF, pH = 7.8 with 1x Halt^{TM} Protease Inhibitor Cocktail (100x, Thermo Scientific, Rockford, IL)). In parallel 600 µg of cell extract in mod. RIPA buffer (ca. 4 mg/ml protein concentration) from either light or heavy labeled cells was pipetted into a 1.5 ml micro tube for each pulldown. The inhibitor in DMSO (competitor, 100x) or pure DMSO (control) was added to the corresponding SILAC lysate (1% DMSO final conc.) and the tubes were agitated for 20 min at 4°C on a rotator. For the SILAC label swap experiment the addition of competitor to e.g. the light lysate was switched to heavy lysate, and addition of the DMSO ctrl to the heavy lysate was switched to light lysate. After the 20 min incubation the pretreated lysate was pipetted individually to the tubes containing kinobead affinity resin and the slurry was agitated on a rotator for 3 hrs at 4°C. The supernatant was removed and the beads were washed twice with 200 µl of ice cold mod. RIPA buffer. Then the beads were re-suspended in 200 µl of ice cold TBS (50 mM Tris, 150 mM NaCl, pH = 7.8), the SILAC samples (beads) were combined pairwise (competition and ctrl experiments) and the supernatant was removed. The beads were washed twice more with TBS and then re-suspended in 100 µl of 8 M aq. urea containing 5 mM *tris*-(2-carboxyethyl)phosphine (TCEP) and 10 mM 2-chloroacetamide

(CAM). The bead slurry was agitated for 30 min at 37°C and 1400 rpm on a thermomixer. For digestion, the slurry was diluted two-fold with 100 mM aqueous triethylammonium bicarbonate solution (TEAB, urea concentration ≤4 M), the pH was adjusted to 9 with 1 N NaOH and 1 µg of LysC was added. The slurry was shaken for 2 hrs at 1400 rpm and 37°C. Then the slurry was further diluted 2-fold with 100 mM TEAB (urea concentration ≤2 M) and 1 µg of trypsin per 5 µl of affinity resin was added. Samples were digested overnight on a thermo shaker at 37°C, diluted two-fold with 5% aqueous acetonitrile (ACN) containing 0.1% TFA and acidified with formic acid (1% final). Peptides were extracted using StageTips (Rappsilber et al., 2007) and then analyzed in single nanoLC-MS/MS runs.

LC-MS/MS and data analysis*:* Peptides were separated on a Thermo-Dionex RSLCNano UHPLC instrument (Sunnyvale, CA) with 10 cm long fused silica capillary columns made in-house with a laser puller (Sutter, Novato CA) and packed with 3 µm 120 Å reversed phase C18 beads (Dr. Maisch, Ammerbuch, DE). The LC gradient was 90 min long with 10-35% B at 200 nL/min. LC solvent A was 0.1% acetic acid and LC solvent B was 0.1% acetic acid, 99.9% ACN. MS data was collected with a Thermo Orbitrap Elite spectrometer. Data-dependent analysis was applied using Top15 selection with CID fragmentation. Raw files were analyzed by MaxQuant/Andromeda (Cox et al., 2011) version 1.5.2.8 using protein, peptide and site FDRs of 0.01 and a score minimum of 40 for modified peptides, 0 for unmodified peptides; delta score minimum of 17 for modified peptides, 0 for unmodified peptides. MS/MS spectra were searched against the UniProt human and mouse databases (updated July 22nd, 2015). MaxQuant search parameters: Variable modifications included Oxidation (M). Carbamidomethyl (C) was a fixed

modification. Max. labeled amino acids was 3, max. missed cleavages was 2, enzyme was Trypsin/P, max charge was 7, multiplicity was either 1, 2 or 3, SILAC labels were Arg0/Lys0 (light), Arg6/Lys4 (medium), Arg10/Lys8 (heavy). The MaxQuant Re-Quantification feature was enabled. The initial search tolerance for FTMS scans was 20 ppm and 0.5 Da for ITMS MS/MS scans. Data was further processed using the Perseus software package (version 1.5.2.6), the R environment, Origin Pro 8.0 and Microsoft Excel.

F. Pull-down assays to measure SH3 domain engagement

In vitro SH3 pull-down: **Formation of the kinase–inhibitor complex**. The kinase of interest (100 nM) and mammalian lysate (0.2 mg/ml) were diluted in immobilization buffer (50 mM Tris, 100 mM NaCl and 1 mM DTT, pH 7.5). A saturating amount of the inhibitor of interest (5 μM or 10 μM) was added to this kinase dilution. The mixture was allowed to incubate for 30 min before loading on the resin.

SH3 Pull-down*.* Forty microliters of a 50% slurry of SNAP-Capture Pull-Down Resin (NEB) was placed in a microcentrifuge tube. The resin was washed (twice, ten-bed volumes) with immobilization buffer. A SNAP tag–polyproline peptide fusion (VSLARRPLPPLP) (10 μM) was loaded onto the resin at a final volume of 100 μl in buffer. The resin was rotated at room temperature for 90 min. After polyproline peptide immobilization, the resin was washed (twice, ten-bed volumes), and 100 μl of the kinase–inhibitor complex was loaded. The resin was allowed to shake at room temperature for 1 hr. After incubation with the kinase–inhibitor complex, the flow through was collected, and the resin was washed (three times, ten-bed volumes). To elute the retained kinase, 100

μl of 1× SDS loading buffer was added, and the beads were boiled at 90 °C for 10 min. All samples were separated by SDS-PAGE and visualized by western blotting using a His6-specific antibody (at a 1:5,000 dilution (abm, HIS.H8)). The scanned blots were quantified with LI-COR Odyssey software to determine the percentage of kinase retained on the resin on the basis of the loaded and eluted fractions (mean ± SEM, *n* = 3).

Cellular SH3 pull-down: Flp-In T-REx 293T cells engineered to overexpress Src^{AS}, Hck^{AS}, or Hck^{WT} upon induction with doxycycline (dox) were plated on 6-well plates and grown to 90% confluency before induction of protein expression with 0.5 μg/mL dox. After 18 hr dox-induction cells were treated with 10 μM **1**, **2**, or **3** (0.5% DMSO final) for 2 hrs before removal of media, 1x PBS wash, and lysis in 100 μL Mod. RIPA buffer (50 mM tris, 150 mM NaCl, 1% Igepal-630, 1 mM EDTA, 1x Pierce Protease Inhibitor Tablet (Pierce, product number 88266), and 1x Pierce Phosphatase Inhibitor tablet (Pierce, product number 88665), pH = 7.8) containing 10 μM of **1**, **2**, or **3** for 20 min on ice before clarification by centrifugation 17,000xg at 4°C. Cleared lysates were then added to SH3 domain-binding resin (prepared as described above), and incubated at room temperature for 1 hr, before beads were extracted and washed twice with Mod. RIPA buffer (containing 10 μM **1**, **2**, or **3**). After wash, retained kinase was eluted by addition of 50 μL 1x SDS loading dye and boiled for 10 min. Eluents were then separated by SDS-PAGE and visualized by wester blotting with anti-FLAG antibody (1:2000 dilution; M2, Sigma). Percent retained kinase was calculated by dividing retained signal, by input signal quantified using LiCor Odyssey software.

G. pTyr527 by Csk

Titrations of Hck and Src constructs starting at 1600 nM (2-fold serial dilutions, 4 data points) were incubated with 10 μM **2** or **3** in assay buffer (75 mM HEPES pH 7.5, 150 mM NaCl, 0.25 mg/mL BSA, 1mM Na_3VO_4, 1 mM DTT, 15 mM $MgCl_2$, and 3.75 mM EGTA). Following 1 hr incubation at room temperature, 50 nM Csk was added and phosphorylation was initiated by the addition of γ32P ATP (0.2 μCi/well). The final volume of each assay well was 30 μL. The enzymatic reaction was run at room temperature for 1 hr and then terminated by spotting 4.6 μL of the reaction mixture onto a nitrocellulose membrane. Membranes were washed with 0.5% phosphoric acid (3x, 10 minutes each wash), air-dried, and the radioactivity was determined by phosphorimaging with a GE Typhoon FLA 9000 phosphor scanner. The scanned membranes were quantified with ImageQuant and data was analyzed using Prism Graphpad software (mean ± SEM, *n* = 3).

H. Confocal microscopy to track SFK localization

24 hrs before transfection $4x10^4$ SYF cells, were plated onto 18mm glass cover slips (Fisher, 12-546) in a standard 12-well plate. After transfection with the appropriate Src construct (see section B for details) cells were allowed to recover for 24 hrs before treatment with 10 μM **3**, 3 μM **2**, or DMSO (0.5% DMSO final for all conditions). Cells were incubated with drug for 15 min before media was removed and cells were washed once with PBS. After the PBS wash was removed, cells were fixed in 4% paraformaldehyde prepared to 1x PBS (16% paraformaldehyde, Electron Microscopy Sciences 15710) for 10 min. Paraformaldahyde was then removed and the cells were washed twice with PBS before simultaneous staining with Nucblue (2 drops per mL;

Fisher, NC0302873) and Wheat Germ Agglutinin AlexaFluor-647 conjugate (1.5 μL/well of 1 mg/mL stock solution; Thermo, W32466) prepared in PBS (250 μL total volume per well). After staining, slides were mounted onto glass cover slips using Fluoromount G (Southern Biotechnology, 0100-01) and sealed. Images were generated using a Leica SP8X Confocal Microscope and appropriate wavelengths to visualize GFP, DAPI, and AF647.

I. Cell motility assay

Experiments were performed using the Cytoselect 24-well Cell Invasion Assay (Basement Membrane, fluorometric format, product number CBA-111). The invasion chamber plate was allowed to warm to room temperature for ten minutes before rehydration of basement membrane layer by addition of 300 μL warm, serum-free media to inner compartment. After 1 hr, the rehydration medium was removed and replaced with 300 μL of cell suspension ($1x10^6$ SYF cells transfected 24 hours previously with Src^{AS} in serum-free media) while 500 μL DMEM +10% FBS was placed in the lower well of the invasion chamber. 3 μM **2**, 10 μM **3**, or DMSO (0.5% final DMSO for all conditions) was added to the cell suspension before the plate was incubated at 37°C in a 5% CO_2 atmosphere. After 48 hrs, media was removed from the insert, and insert was transferred to a clean well containing 225 μL cell detachment solution and incubated for 30 min at 37°C. Cells were then dislodged from the underside of the membrane and the insert was discarded. 75 mL 4x Lysis buffer/CyQuant GR solution was then added to each well containing cells in detachment solution and incubated for 20 min at room temperature, after which 200 μL

of the mixture was transferred to a 96-well plate and read for fluorescence using a plate reader at 480nm/520nM (EnVision Perkin Elmer, 485nM/538nM filter).

J. pThr735 phosphorylation assay

$3x10^5$ cells were plated on a standard 12-well plate 24 hours before transfection of c-Abl constructs (HeLa cells) or dox induction of c-Abl constructs (293T cells). After 24 (293T) or 48 hrs (HeLa) expression, cells were treated with 10 mM **1**, **2**, **3**, or **4** or DMSO (final DMSO concentration was %0.5 for all conditions) for the indicated time. For competition experiments solutions of inhibitor mixtures were prepared in DMSO such that the final inhibitor concentration desired would be achieved in a final DMSO concentration of 0.5%. After inhibitor incubation, media was removed and cells were lysed as quickly as possible in 75 μL 1x SDS loading dye by scraping and transferred to PCR tubes. Lysates were boiled for 15 min at 98°C in a thermocycler before separation by SDS-PAGE and visualization by western blotting with anti-pThr735 (1:3000 dilution; Cell Signaling #2864), anti-c-Abl (1:1000 dilution; Santa Cruz 8E9), anti-tubulin (1:5000 dilution; Cell Signaling #3873), and pCrkL (1:2000 dilution; Cell Signaling #3181 for 293T experiments or 1:1000; Santa Cruz C-20 for HeLa experiments). Signal was quantified using LiCor Odysses software and data was analyzed and graphed using Microsoft Excel and Graphpad software.

K. Co-IP of c-Abl interactors

For IPs from 293Ts, $1x10^6$ cells were plated on standard $10cm^2$ plates and allowed to recover for 12-24 hrs prior to induction of $c\text{-}Abl^{AS}$ with dox. For IPs from HeLa cells, $6x10^5$

cells were plated on standard 6-well plates and allowed to recover for 12-24 hrs prior to transfection with c-Abl^{AS} or c-Abl^{WT}. Following 48 hrs c-Abl overexpression, cells were treated with 10 μM **1**, **2**, **4**, or DMSO (0.5% final DMSO for all conditions) for 2 hrs (293T) or 1 hr (HeLa). For HeLa experiments under oxidative stress, transfected cells were pre-incubated with 10 μM **1**, **2**, **4**, or DMSO for 1 hr before treatment with H_2O_2 to a final concentration of 1 mM (prepared from 30% H2O2 in PBS) for 20 min. After drug treatments, media was removed and cells were washed once with PBS before lysis by cell scraping in 1x Mod. RIPA buffer (50 mM Tris, 150 mM NaCl, 1% Igepal-630, 1 mM EDTA, 1x Pierce Protease Inhibitor Tablet (Pierce, product number 88266), and 1x Pierce Phosphatase Inhibitor Tablet (Pierce, product number 88665), pH = 7.8). 300 μL Mod. RIPA was used for 10cm^2 plate lyses and 100 μL Mod RIPA was used for 6-well plate lyses. After lysis and transfer to 1.5 mL Eppendorf tubes, cells were kept on ice for 10 min before clearing by centrifugation at 17,000xg for 20 min at 4°C. A small fraction of the cleared lysate was removed and mixed with 3x SDS loading dye for later SDS-PAGE analysis, and 10 μL anti-FLAG magnetic beads were added to each tube of remaining lysate (Sigma, M8823). Tubes were rotated for 1hr at 4°C, before beads were isolated and washed twice with Mod. RIPA buffer. IP'd c-Abl and Co-IP'd proteins were eluted by incubation with 1 mg/mL 3x Flag peptide prepared in TBS (APExBIO #A6001) for 15 min at room temperature, after which the eluted fraction was separated from the beads and mixed with 3x SDS loading dye. Samples (input and eluted) for each condition were separated by SDS-PAGE and visualized by western blot using anti-pThr735 (1:3000 dilution; Cell Signaling #2864), anti-c-Abl (1:1000 dilution; Santa Cruz 8E9), anti-14-3-3e (1:3000 dilution; Cell Signaling #9635), or anti-pan14-3-3 (1:1000 dilution; Santa Cruz sc-

629). Signal was quantified using LiCor Odysses software and data was analyzed and graphed using Microsoft Excel and Graphpad software.

L. SILAC Co-IP of c-Abl interactors

Prior to lysis, SILAC labeled 293T cells overexpressing c-Abl^{AS} were treated with 10 μM **2** or **3** for 2 hrs. Lysis and IP were carried out exactly as described in section I until the wash step post-IP. On the first wash, beads from opposite channels and drug treatments were combined and treated as one sample for the remainder of the work up—for example: beads from Heavy, **2**-treated cells combined with beads from Light, **1**-reated cells, and vice versa for the label swapped replicate experiment. Beads were washed one more time with 10 bead volumes cold Mod. RIPA before elution with 50 μL 1x LDS for 30 min at 55°C. The eluent was then removed from the beads and applied to a buffer-equilibrated detergent removal column spin column (ThermoFisher, product number 87777). TEAB was used for all steps of the buffer replacement. After detergent removal, 100 µl of 8 M aqueous urea containing 5 mM *tris*-(2-carboxyethyl)phosphine (TCEP) and 10 mM 2-chloroacetamide (CAM) was added to each sample. The bead slurry was agitated for 30 min at 37°C and 1400 rpm on a thermomixer. For digestion, the slurry was diluted two-fold with 100 mM aqueous TEAB (urea concentration ≤4 M), the pH was adjusted to 9 with 1 N NaOH and 1 µg of LysC was added. The slurry was shaken for 2 hrs at 1400 rpm and 37°C. Then the slurry was further diluted 2-fold with 100 mM TEAB (urea concentration ≤2 M) and 1 µg of trypsin was added. Samples were digested overnight on a thermo shaker at 37°C, diluted two-fold with 5% aqueous acetonitrile (ACN) containing

0.1% TFA and acidified with formic acid (1% final). Peptides were extracted using StageTips (Rappsilber et al., 2007) and then analyzed in single nanoLC-MS/MS runs.

References

Adams, J.A., McGlone, M.L., Gibson, R., and Taylor, S.S. (1995). Phosphorylation modulates catalytic function and regulation in the cAMP-dependent protein kinase. Biochemistry *34*, 2447-2454.

Adrian, F.J., Ding, Q., Sim, T., Velentza, A., Sloan, C., Zhang, G., Hur, W., Ding, S., Manley, P., Mestan, J., Fabbro, D., and Gray, N.S. (2006). Allosteric inhibitors of Bcr-abl-dependent cell proliferation. *Nat. Chem. Biol*. 2, 95-102.

Alvarado, J. J., Betts, L., Moroco, J. A., Smithgall, T. E. and Yeh, J. I. (2010) Crystal structure of the Src-family kinase Hck SH3-SH2 linker regulatory region supports an SH3-dominant activation mechanism. J. Biol. Chem. *285*, 35455–35461.

Anastassiadis, T. Deacon, S.W., Devarahan, K., Ma, H., and Peterson, J.R. (2011). Comprehensive assay of kinase catalytic activity reveals features of kinase inhibitor selectivity. Nat. Biotech. *29*, 1039-1045.

Azam, M., Seeliger, M.A., Gray, N.S., Kuriyan, J., and Daley, G.Q. (2008). Activation of tyrosine kinases by mutation of the gatekeeper threonine. Nat Struct. Mol. Biol. *15*, 1109-1118.

Berman, H.M., et al. (2000). The protein data bank. Nucleic Acids Res. *28*, 235-242.

Bishop, A.C., Ubersax, J.A., Petsch, D.T., Matheos, D.P., Gray, N.S., Blethrow, J., Shimizu, E., Tsien, J.Z., Schultz, P.G., Rose, M.D., et al. (2000). A chemical switch for inhibitor-sensitive alleles of any protein kinase. Nature, *407* 395-401.

Boggon, T. J. and Eck, M. J. (2004) Structure and regulation of Src-Family kinases. Oncogene *23*, 7018-7927.

Bradshaw, J.M., McFarland, J.M., Paavilainen, V.O., Biscong A., Tam, D., Phan, V.T., Romanov, S., Finkle, D., Shu, J., Patel, V., et al. (2015) Prolonged and tunable residence time using reversible covalent inhibitors. Nat. Chem. Biol. *11*, 525-531.

Brignatz, C., Paronetto, M. P., Opi, S., Cappellari, M., Audebert, S., Feuillet, V., Bismuth, G., Roche, S., Arold, S. T., Sette, C. and Collette, Y. (2009) Alternative splicing modulates autoinhibition and SH3 accessibility in the Src kinase Fyn. Mol. Cell. Biol. *29*, 6438–6448.

Brunton, V.G., Avizienyte, E., Fincham, V.J., Serrels, B., Metcalf, C.A., Sawyer, T.K., and Frame, M.C. (2005). Identification of Src-specific phosphorylation site on focal adhesion kinase: dissection of the role of Src SH2 and catalytic functions and their consequences for tumor cell behavior. Cancer Res. *65*, 1335-1342.

Buchdunger, E., Zimmerman, J., Mett, H., Meyer, T., Muller, M. Druker, B.J., and Lydon, N.B. (1996). Inhibition of the Abl protein-tyrosine kinase *in vitro* and *in vivo* by a 2-phenylaminopyrimidine derivative. Caner Res. *56*, 100-104.

Chen, X., Zhang, J., Lee, J., Lin, P.S., Ford, J.M., Zheng, N., and Zhou, P. (2006). A kinase-independent function of c-Abl in promoting proteolytic destruction of damaged DNA binding proteins. Mol. Cell *22*, 489-499.

Cox, A.D., and Der, C.J. (2010). The Raf inhibitor paradox: unexpected consequences of targeted drugs. Cancer Cell *17*, 221-223.

Cox, J., Neuhauser, N., Michalski, A., Scheltema, R. A., Olsen, J. V., and Mann, M. (2011). Andromeda: a peptide search engine integrated into the MaxQuant environment. J Proteome Res *10*, 1794-805.

Daley, G.Q., Van Etten, R.A., and Baltimore, D. (1990). Induction of chronic myelogenous leukemia in mice by the P210bcr/abl gene of the Philadelphia chromosome. Science 247, 824-830.

David-Pfeuty, T., Bagrodia, S., and Shalloway, D. (1993). Differential localization patterns of myristoylated and nonmyristoylated c-Src proteins in interphase and mitotic c-Src overexpressor cells. J. Cell Sci. *105*, 613-628.

Delgarno, D. C., Botfiled, M. C. and Rickles, R. J. (1997) SH3 domains and drug design: ligands, structure, and biological function. Peptide Science *43*, 383-400.

Dolker, N., Gorna, M.W., Sutto, L., Torralba, S., Superti-Furga, G., and Gervasio, F.L. (2014). PLoS Comput. Biol. *10*, e1003863.

Douangamath, A., Filipp, F. V., Klein, A. T .J., Barnett, P. Zou, P., Voorn-Brouwer, T., Vega, M. C., Mayans, O. M., Sattler, M., Distel, B. and Wilmanns, M. (2002) Topography for independent binding of a-helical and PPII-helical ligands to a peroxisomal SH3 domain. Mol. Cell *10*, 1007-1017.

Druker, B.J., Tamura, S., Buchdunger, E., Ohno, S., Segal, G.M., Fanning, S., Zimmerman, J., and Lydon, N. (1996). Effects of a selective inhibitor of the Abl tyrosine kinase on growth of Bcr-Abl positive cells. Nat. Med. *2*, 561-566.

Druker, B.J., Talpaz, M., Resta, D.J., Peng, B., Buchdunger, E., Ford, J.M., Lydon, N.B., Kantarjian, H., Capdeville, R., Ohno-Jones, S., and Sawyers, C.L. (2001). Efficacy and

safety of a specific inhibitor of the BC-ABL tyrosine kinase in Chronic Myelogenous Leukemia. N Eng. J. Med. *344*, 1031-1037.

Endicott, J.A., Noble, M.E.M., and Johnson, L.N. (2012). The structural basis for control of eukaryotic protein kinases. Ann. Rev. Biochem. *81*, 587-613.

Engen, J. R., Wales, T. E., Hochrein, J. M., Meyn, M. A., Banu Ozkan, S., Bahar, I. and Smithgall, T.E. (2008). Structure and dynamic regulation of Src-family kinases. Cell. Mol. Life Sci. *65*, 3058–3073.

Erpel, T., Superti-Furga, G. and Courtneige, S. (1995) Mutational analysis of the Src SH3 domain: the same residues of the ligand binding surface are important for intra- and inter-molecular interactions. EMBO J. *14*, 963-975.

Eswaran, J., and Knapp, S. (2010). Insights into protein kinase regulation and inhibition by large scale structural comparison. Biochim. Biophys. Acta *1804*, 429-432.

Fackler, O.T., and Grosse, R. (2008). Cell motility through plasma membrane blebbing. J. Cell Biol. *181*, 879-884.

Falanga, Y. T., Chaimowitz, N. S., Charles, N., Finkelman, F. D., Pullen, N. A., Barbour, S., Dholaria, K., Faber, T., Kolawole, M., Huang, B., Odom, S., Rivera, J., Carlyon, J., Conrad, D. H., Spiegel, S., Oskeritzian, C. A., and Ryan, J. J. (2012) Lyn but not Fyn kinase controls IgG-mediated systemic anaphylaxis. J. Immunol. *188*, 4360-4368.

Filippakopoulos, P., Kofler, M., Hantschel, O., Gish, G.D., Grebien, F., Salah, E., Neudecker, P., Kay, L.E., Turk, B.E., Superti-Furga, G., Pawson, T., and Knapp, S. (2008). Cell *132*, 793-803.

Galan-Moya, E.M., Hernandez-Losa, J., Aceves, C.L., de la Cruz-Morcillo, M.A., Ramirez-Castillejo, C., Callejas-Valera, J.L., Arriaga, A., Aranburo, A.F., Ramon y Cajal, S., Silvio Gutkind, J., and Sanchez-Prieto, R. (2008). c-Abl activations p38 MAPK independently of its tyrosine kinase activity: implications in cisplatin-based therapy. Int. J. Cancer *122*, 189-297.

Garske, A.L., Peters, U., Cortesi, A.T., Perez, J.L., and Shokat, K.M. (2011). Chemical genetic strategy for targeting protein kinases based on covalent complimentarity. Proc. Natl. Acad. Sci. USA *108*, 15046-15052.

Golkowski, M., Brigham, J.L., Perera, G.K., Romano, G.E., Maly, D.J., and Ong, S.E. (2014). Rapid profiling of protein kinase inhibitors by quantitative proteomics. Medchemcomm. *5*, 363-369.

Gonfloni, S., Williams, J. C., Hattula, K., Weijland, A., Wierenga, R. K. and Superti-Furga, G. (1997) The role of the linker between the SH2 domain and catalytic domain in the regulation and function of Src. EMBO J. *16*, 7261–7271.

Grebian, F., Hantschel, O., Wojcik, J., Kaupe, I., Kovacic, B., Wyrzucki, A.M., Gish, G.D., Cemy-Reiterer, S., Koide, A., Beug, H., Pawson, T., Valent, P., Koide, S., and Superti-Furga, G. (2003). Targeting the Sh2-kinase interface in Bcr-Abl inhibits leukemogenesis. Cell *147*, 306-319.

Hah, J., Sharma, V., Li, H. and Lawrence, D. S. (2006) Acquisition of "Group A" – selective kinase inhibitor via a global targeting strategy. J. Am. Chem. Soc. *128*, 5996-5997

Hanks, S.K. (2003). Genomic analysis of the eukaryotic protein kinase superfamily: a perspective. Genome Biol. *4*, 111.

Hantschel, O., Nagar, B., Guettier, S., Kretzschmar, J., Dorey, K., Kuriyan, J., and Superti-Furga, G. (2003). A myristoyl/phosphotyrosine switch regulates c-Abl. Cell *112*, 845-857.

Hari, S.B., Merritt, E.A., and Maly, D.J. (2014). Conformation-selective ATP-competitive inhibitors control regulatory interactions and noncatalytic functions of mitogen-activated protein kinases. Chem. Biol. *21*, 628-635.

Harrison, S.C. (2003). Variation on a Src-like theme. Cell 112, 737-740.

Hatzivassiliou, G., Song, K., Yen, I., Branduber, B.J., Anderson, D.J., Alvarado, R., Ludlam, M.J.C., Stokoe, D., Gloor, S.L., Vigers, G., et al. (2010). RAF inhibitors prime wild-type RAF to activate the MAPK pathway and enhance growth. Nature *464*, 431-435.

Heidorn, S.J., Milagre, C., Whittaker, S., Nourry, A., Niculescu-Duvas, I., Dhomen, N., Hussein, J., Reis-Filho, J.S., Springer, C.J., Pritchard, C., et al. (2010). Kinase-dead BRAF and oncogenic RAS cooperate to drive tumor progression through CRAF. Cell *140*, 209-221.

Hirai, H. and Varmus, H. E. (1990) SH2 mutants of c-Src that are host dependent for transformation are trans-dominant inhibitors of mouse cell transformation by activated c-Src. Genes Dev. *4*, 2342-2352.

Hoffman, G., Schweimer, K., Kiessling, A., Hofinger, E., Bauer, F., Hoffman, S., Roch, P., Campbell, I. D., Werner, J. M. and Sticht, H. (2005) Binding, domain orientation, and dynamics of the Lck SH3-SH2 domain pair and comparison with other Src-family kinases. Biochemistry *44*, 13043-13050.

Honegger, A.M., Dull, T.J., Felder, S., Van Obberghen, E., Bellot, F., Szapary, D., Schmidt, A., Ullrich, A., and Schlessinger, J. (1987). Point mutation at the ATP binding site of EGF receptor abolishes protein-tyrosine kinase activity and alters cellular routing. Cell *51*, 199-209.

Hu, J., Stites, E.C., Yu, H., Germino, E.A., Meharena, H.S., Stork, P.J.S., Kornev, A.P., Taylor, S.S., and Shaw, A.S. (2013). Allosteric activation of functionally asymmetric RAF kinase dimers. Cell *154*, 1036-1046.

Huang, H., Zhao, R., Dickson, B.M., Skeel, R.D., and Post, C.B. (2012). αC helix as a switch in the conformational transition of Src/CDK-like kinase domains. J. Phys. Chem. B *116*, 4465-4475.

Huse, M. and Kuriyan, J. (2002) The conformational plasticity of protein kinases. Cell *109*, 275–282.

Jura, N. et al. (2011). Catalytic control in the EGF receptor and its connection to general kinase regulatory mechanisms. Mol. Cell *42*, 9-22.

Kaplan, K.B., Bibbins, K.B., Swedlow, J.R., Arnaud, M., Morgan, D.O., and Varmus, H.E. (1994). Association of the amino-terminal half of c-Src with focal adhesions alters their properties and is regulated by phosphorylation of tyrosine 527. EMBO J. *13*, 4745-4756.

Kaplan, KB., Swedlow, J.R., Morgan, D.O., and Varmus, H.E. (1995). c-Src enchances the spreading of src-/- fibroblasts on fibronectin by a kinase-independent mechanism. Genes and Development *9*, 1505-1517.

Kashishian, A., MacAuley, A. and Cooper, J.A. (1990) Properties of tripartite chimeras between Src and Lck. Oncogene *5*, 1463-70.

Kay, B. K., Williamson, M. P and Sudol, M. (2000) The importance of being proline: the interaction of proline-rich motifs in signaling proteins with their cognate domains. FASEB J. *14*, 231-241.

Kim, L. C., Song, L. and Haura, E. B. (2009) Src kinases as therapeutic targets for cancer. Nat. Rev. Clin. Oncol. *6*, 587-595.

Knighton, D.R., Zheng, J., Eyck, L.F.T., Ashford, V.A., Xuong, N. Taylor, S.S., and Sowadski, J.M. (1991). Crystal structure of the catalytic subunit of cyclic adenosine monophosphate-dependent protein kinase. Science 253, 407-413.

Krishnamurty, R., Brigham, J. L., Leonard, S. E., Ranjitkar, P., Larson, E. T., Dale, E. J., Merritt, E. A. and Maly, D. J. (2012) Active site profiling reveals coupling between domains in Src-family kinases. Nat. Chem. Biol. *9*, 43–50.

Kung, J.E., and Jura., N. (2016). Structural basis for the non-catalytic functions of protein kinases. Structure *24*, 7-24.

LaFevre-Bernt, M., Sicheri, F., Pico, A,, Porter, M., Kuriyan, J. and Millwer, W. T. (1998) Intra-molecular regulatory interactions in the Src-family kinase Hck probed by mutagenesis of a conserved tryptophan residue. J. Biol. Chem. *273*, 32129–32134.

Lamontanara, A., Georgeon, S., Tria, G., Svergun., D.I., and Hantschel, O. (2014). The SH2 domain of Abl kinases regulates kinase autophosphorylation by controlling activation loop accessibility. Nature Comm. *5*, 5470.

Lavoie, H., Thevakumaran, N., Gavory, G., Li, J.J., Padeganeh, A., Guiral, S., Duchaine, J., Mao, D.Y.L., Bouvier, M., Sicheri, F., and Therrien, M. (2013). Inhibitors that stabilize a closed RAF kinase domain conformation induce dimerization. Nat. Chem. Biol. *9*, 428-439.

Leonard, S.E., Register, A.C., Krishnamurty, R., Brighty, G.J., and Maly, D.J. (2014). Divergent modulation of Src-family kinase regulatory interactions with ATP-competitive inhibitors. ACS Chem. Biol. *9*, 1894-1905.

Lerner, E. C., Trible, R. P., Schiavone, A. P., Hockrein, J. M. and Engen, J. R. (2005) Activation of the Src-family kinase Hck without SH3-linker release. J. Biol. Chem. *280*, 40832-40837.

Levinson, N.M., Kuchment, O., Shen, K., Young, M.A., Koldobskiy, M., Karplus, M., Cole, P.A., and Kuriyan, J. (2006). A Src-like inactive conformation in the Abl tyrosine kinase domain. PLoS Biol. *4*, e144.

Levinson, N. M., Seeliger, M. A. and Kuriyan, J. (2008) Structural basis for the recognition of c-Src by its inactivator Csk. Cell *134*, 124-134.

Lim, W.A. (1996) Reading between the lines: SH3 recognition of an intact protein. Structure *4*, 657-659.

Lorenz, S., Deng, P., Hantschel, O., Superti-Furga, G., and Kuriyan, J. (2015). Crystal structure of an SH2-kinase construct of c-Abl and effect of the SH2 domain on kinase activity. Biochemical J. *468*, 283-291.

MacAuley, A. and Cooper, J.A. (1988) The carboxy-terminal sequence of p56lck can regulate p60C-src. Mol. Cell. Biol. *8*, 3560.

Mancini, M., Veljkovic, N., Corradi, V., Zuffa, E., Corrado, P., Pagnotta, E., Martinelli, G., Barbieri, E., and Santucci, M.A. (2009). 14-3-3 ligand prevents nuclear import of c-Abl protein in chronic myeloid leukemia. Traffic *10*, 637-647.

Masterson, L.R., Cheng, C., Yu, T., Tonelli, M., Kornev, A., Taylor, S.S., and Veglia, G. (2010). Dynamics connect substrate recognition to catalysis in protein kinase A. Nat. Chem. Biol. *6*, 821-828.

McWhirter, J.R. and Wang, J.Y.J. (1993). An actin-binding function contributes to transformation by the Bcr-Abl oncoprotein of Philadelphia chromosome-positive human leukemias. EMBO J. *12*, 1533-1546.

Meyer, B. J. (2001). SH3 domains: complexity in moderation. J. Cell Sci. *114*, 1253- 1263.

Miller, W. T. (2003) Determinants of substrate recognition in nonreceptor tyrosine kinases. Acc. Chem. Res*. 36,* 393-400.

Miller, R.M., Paavilainen, V.O., Krishnan, S., Serafimova, I.M., and Taunton, J. (2013). Electrophilic fragment-based design of reversible covalent kinase inhibitors. J. Am. Chem. Soc. *135*, 5298-5301.

Moarefi, I., LaFevre-Bernt, M., Sicheri, F., Huse, M., Lee, C. H., Kuriyan, J. and Miller, W.T. (1997) Activation of the Src-family tyrosine kinase Hck by SH3 domain displacement. Nature *385*, 650–653 (1997).

Mol, C.D., Dougan, D.R., Schneider, T.R., Skene, R.J., Kraus, M.L., Scheibe, D.N., Snell, G. P., Zou, H., Sang, B., and Wilson, K.P. (2004). Structural basis for the autoinhibition and STI-571 inhibition of c-Kit tyrosine kinase. J. Biol. Chem. *279*, 31655-31663.

Muller, S., Chaikuad, A., Gray, N.S., and Knapp, S. (2015). The ins and outs of selective kinase inhibitor development. Nat. Chem. Biol. *11*, 818-821.

Nagar, B., Hantschel, O., Young, M.A., Scheffzek, K., Veach, D., Bornmann, W., Clarkson, B., Superti-Furga, G., and Kuriyan, J. (2003). Structural basis for the autoinhibition of c-Abl tyrosine kinase. Cell *112*, 859-871.

Nagar, B., Hantschel, O., Seeliger, M., Davies, J.M., Weis, W.I., Superti-Furga, G., and Kuriyan, J. (2006). Organization of the SH3-SH2 unit in active and inactive forms of the c-Abl tyrosine kinase. Mol. Cell *21*, 787-798.

Nagar, B. (2007). c-Abl tyrosine kinase and inhibition by the cancer drung imatinib (Gleevec/STI-571). J. Nutr. *137*, 1518S-1523S.

Nihira, K., Taira, N., Miki, Y., and Yoshida, K. (2008). TTK/Mps1 controls nuclear targeting of c-Abl by 14-3-3-coupled phosphorylation in response to oxidative stress. Oncogene 27, 7285-7295.

Nguyen, J. T., Porter, M., Amoui, M., Miller, W.T., Zuckermann, R. N. and Lim, W. A. (2000) Improving SH3 domain ligand selectivity using a non-natural scaffold. Chem. Biol. *7*, 463-473.

Nolen, B., Taylor, S.S., and Ghosh, G. (2004). Regulation of protein kinases: controlling activity through activation segment conformation. Mol. Cell *15*, 661-675.

Ohashi, K., Nagata, K., Maekawa, M., Ishizaki, T., Narumiya, S., and Mizuno, K. (2000). Rho-associated kinase ROCK activates Lim-kinase 1 by phosphorylation at threonine 508 within the activation loop. J. Biol. Chem. *275*, 3577-3582.

Okada, M., Nada, S., Yananashi, Y., Yamamoto, T. and Nakagawa, H. (1991) Csk: a protein-tyrosine kinase involved in regulation of Src-family kinases. J. Biol. Chem. *266*, 24249-24252.

Okutaro, T., Asue, Y., Irofumi, H., Ishizumi, N., Hinichi, S., Izawa, A., Adashi, T., Amamoto, Y., Ensuke, K., Iyake, M., Hieko, C. Izoguchi, M., Hoji, S., Uji, Y., Ikuchi, K. and Akatsu, T. (1997) A critical role of Lyn and Fyn for B cell responses to CD38 ligation and interleukin 5. Proc. Natl. Acad. Sci. *94*, 10307-10312.

Osusky, M., Taylor, S. J. and Shalloway, D. (1995) Autophosphorylation of purified c-Src at its primary negative regulation site. J. Biol. Chem. *270*, 25729-25732.

Palacios, E. H. and Weiss, A. (2004) Function of the Src-family kinases, Lck and Fyn, in T-cell development and activation. Oncogene *23*, 7990-8000.

Palmieri, L., and Rastelli, G. (2013). αC helix displacement as a general approach for allosteric modulation of protein kinases. Drug Disc. 18, 407-414.

Panjarian, S., Iacob, R., Chen, S., Wales, T.E., Engen, J.R., and Smithgall, T.E. (2013). Enhanced SH3/linker interaction overcomes Abl kinase activation by gatekeeper and myristic acid binding pocket mutations and increases sensitivity to small molecule inhibitors. J. Biol. Chem. *288*, 6116-6129.

Pargellis, C., Tong, L., Churchill, L., Cirillo, P.F., Gilmore, T., Graham, A.G., Grob, P.M., Hickey, E.R., Moss, N., Pav, S., and Regan, J. (2002). Inhibition of p38 MAP kinase by utilizing a novel allosteric binding site. Nat. Struct. Biol. *9*, 268-272.

Parravicini, V., Gadina, M., Kavarova, M., Odom, S., Gonzalex-Espinosa, C., Furumoto, Y., Saitoh, S., Samelson, L. E., O'Shea, J. J. and Rivera, J. (2002) Fyn kinase initiates complementary signals required for IgE-dependent mast cell degranulation. Nat. Immunol. *3*, 741-748.

Pluk, H., Dorey, K., and Superti-Furga, G. (2002). Autoinhibition of c-Abl. Cell *108*, 247-259.

Porter M., Schindler T., Kuriyan J. and Miller W. T. (2000) Reciprocal regulation of Hck activity by phosphorylation of Tyr(527) and Tyr(416). Effect of introducing a high affinity intra-molecular SH2 ligand. J. Biol. Chem. *275*, 2721–2726.

Preyer, M., Vigneri, P., and Wang, J.Y.J. (2011). Interplay between kinase domain autophosphorylationg and F-actin binding domain in regulating imatinib sensitivity and nuclear import of BCR-Abl. PLoS One *6*, e17020.

Raitano., A.B., Whang, Y.E., and Sawyers, C.L. (1997). Signal transduction by wild-type and leukemogenic Abl proteins. Biochim. Biophys. Acta. *1333*, F201-16.

Rappsilber, J., Mann, M., and Ishihama, Y. (2007). Protocol for micro-purification, enrichment, pre-fractionation and storage of peptides for proteomics using StageTips. Nat Protocols *2*, 1896-906.

Rauch, J., Volinsky, N., Romano, D., and Kolch, W. (2011). The secret life of kinases: functions beyond catalysis. Cell Commun. Signal. *9*, 1-28.

Register, A.C., Leonard, S.E., and Maly, D.J. (2014). SH2-CD linker heterogeneity affects allosteric coupling across the SFK family. Biochemistry *53*, 6910-6923.

Resh, M.D. (1998) Fyn, a Src-family tyrosine kinase. Int. J. Biochem. Cell Biol. *30*, 1159-1162.

Roberts, P.J., and Der, C.J. (2007). Targeting the Raf-MEK-ERK mitogen-activated protein kinase cascade for the treatment of cancer. Oncogene *26*, 3291-3310.

Roskoski, R. (2016). Pharm. Res. Classification of small molecule protein kinase inhibitors based upon the structures of their drug-enzyme complexes.103, 26-48.

Schlaepfer D., Broome, M., and Hunter, T. (1997). Fibronectin-stimulated signaling from a focal adhesion kinase c-Src complex: involvement of the Grb2, p130cas, and Nck adaptor proteins. Mol Cell. Biol. *17*, 1702.

Seeliger, M. A., Young, M., Henderson, M. N., Pellicena, P., King, D. S., Falick, A. M. and Kuriyan, J. (2005) High yield bacterial expression of active c-Abl and c-Src tyrosine kinases. Protein Sci*. 14*, 3135-3139

Seeliger, M.A., Nagar, B., Frank, F., Cao, X., Henderson, M.N., and Kuriyan, J. (2007). c-Src binds to the cancer drug imatinib with an inactive Abl/c-Kit conformation and a distributed thermodynamic penalty. Structure 15, 299-311.

Seeliger, M.A., Ranjitkar, P., Kasap, C., Shan, Y., Shaw, D.E., Shah, N.P., Kuriyan, J., and Maly, D.J. (2009). Equally potent inhibition of c-Src and Abl by compounds that recognize inactive kinase conformations. Cancer Res. *69*, 2384-2392.

Seger, R., and Krebs, E.G. (1995). The MAPK signaling cascade. FASEB J. *9*, 726-735.

Serafimova, I.M., Pufall, M.A., Krishnan, S., Duda, K., Cohen, M.S., Maglathlin, R.L., McFarland, J.M., Miller, R.A., Frodin, M., and Taunton, J. (2012). Reversible targeting of noncatalytic cysteines with chemically tuned electrophiles. Nat. Chem. Bio. *8*, 471-476.

Shan, Y., Arkhipov, A., Kim, E.T., Pan, A.C., and Shaw, D.E. (2013). Transitions to catalytically inactive conformations in EGFR kinase. Proc. Natl. Acad. Sci. *110*, 7270-7275.

Sicheri, F. and Kuriyan, J. (1997) Structures of Src-family tyrosine kinases. Curr. Opin. Struct. Biol. *7*, 777–785.

Sicheri, F., Moarefi, I. and Kuriyan, J. (1997) Crystal structure of the Src-Family tyrosine kinase Hck. Nature *385*, 602–609.

Skamnaki, V.T., et al. (1999). Catalytic mechanism of phosphorylase kinase probed by mutation studies. Biochemistry *38*, 14718-14730.

Skora, L., Mestan, J., Fabbro, D., Jahnke, W., and Grzesiek, S. (2013). NMR reveals the allosteric opening and closing of Abelson tyrosine kinase by ATP-site and myristoyl pocket inhibitors. Proc. Natl. Accad. Sci. *110*, 4437-4445.

Smart, J. E., Oppermann, H., Czernilofsky, A.P., Purchio, A.F, Erikson, R.L and J.M. Bishop, J. M. (1981) Characterization of sites for tyrosine phosphorylation in the transforming protein of Rous sarcoma virus (pp60v-src) and its normal cellular homologue (pp60c-src). Proc. Natl. Acad. Sci. U. S. A. *78*, 6013–6017.

Sondhi, D., Xu, W., Songyang, Z., Eck, M.J. and Cole, P.A. (1998) Peptide and protein phosphorylation by protein tyrosine kinase Csk: Insights into specificity and mechanism. Biochemistry *37*, 165-172.

Superti-Furga, G., Fumagalli, S., Koegl, M., Courtneidge, G. and Draetta, G. (1993) Csk inhibition of c-Src activity requires both the SH2 and SH3 domains of Src. EMBO J. *12*, 2625-2634.

Superti-Furga, G., Gonfloni, S., Frischknecht, F. and Way, M. (1999) Leucine 255 of Src couples intra-molecular interactions to inhibition of catalysis. Nat. Struct. Biol. *6*, 760–764

Superti-Furga, G., Gonfloni, S., Weijland, A. and Kretzschmar, J. (2000) Crosstalk between the catalytic and regulatory domains allows bidirectional regulation of Src. Nat. Struct. Biol. *7*, 281–286.

Taylor, C.M. and Keating, A.E. (2005). Orientation and oligomerization specificity of the Bcr coiled-coil oligomerization domain. Biochemistry *44*, 16246-16256.

Thevakumaran, N., Lavoie, H., Critton, D.A., Tebben, A., Marinier, A., Sicheri, F., and Therrien, M. (2015). Nat Struct. Mol. Biol. 22, 37-43.

Thomas, S. M. and Brugge, J. S. (1997) Cellular functions regulated by Src-Family kinases. Annu. Rev. Cell Dev. Biol. *13*, 513–609.

Tong, M., and Seeliger, M.A. (2014). Targeting conformational plasticity of protein kinases. ACS Chem. Biol. *10*, 190-200.

Tournaviti, S., Hannemann, S., Terjung, S., Kitzing, T.M., Stegmayer, C., Ritzerfeld, J., Walther, P., Grosse, R., Nickel, W., and Fackler, O.T. (2007). SH4-domain-induced plasma membrane dynamization promotes bleb-associated cell motility. J. Cell Sci. 120, 3820-3829.

Trible, R. P., Emert-Sedlak, L. and Smithgall, T. E. (2006) HIV-1 Nef selectively activates Src-family kinases Hck, Lyn, and c-Src through direct SH3 domain interaction. J. Biol. Chem. *281*, 27029-27038.

Wang, J.Y.J. (2014). The capable ABL: what is its biological function? Mol. Cell Biol. *34*, 1188-1197.

Wang, Y., Lin, X., Gu, X. Parang, K. and Sun, G. (2006) Conformational basis for SH2-Tyr(p)527 binding in Src inactivation. J. Biol. Chem. *281*, 23776 – 23784.
Wang, Q., Cahill, S.M., Blemenstein, M., and Lawrence, D.S. (2006). Self-reporting fluorescent substrates of protein tyrosine kinases. *128*, 1808-1809.

Wang, L., Perera, G.B.K., Hari, S.B., Bhhatarai, B., Backes, B.J., Seeliger, M.A., Schurer, S.C., Oakes, S.A., Papa, F.R., and Maly, D.J. (2012). Divergent allosteric control of the IRE1a endoribonuclease using kinase inhibitors. Nat. Chem. Biol. *8*, 982-989.
Williams, J. C., Wierenga, R. K. and Saraste, M. (1998) Insights into Src kinase functions: structural comparisons. Trends Biochem. Sci. *23*, 179-184.

Woodring, P.J., Hunter, T., and Wang J.Y.J. (2005). Mitotic phosphorylation rescues Abl from F-actin-mediated inhibition. J. Biol. Chem. *280*, 10318-10325.

Xu, W., Doshi, A., Lei, M., Eck, M. J. and Harrison, S. C. (1999) Crystal Structures of c-Src Reveal Features of Its Autoinhibitory Mechanism. Mol. Cell *3*, 629–638.

Xu, Y., Huntington, N. D., Harder, K. W., Nandurkar, H., Hibbs, M. L. and Tarlinton, D. M. (2012) Phosphatidylinositol-3 kinase activity in B cells is negatively regulated by Lyn tyrosine kinase. Immunol. Cell Biol. *90*, 903-911.

Yadav, S. S. and Miller. W. T. (2007) Cooperative activation of Src-family kinases by SH3 and SH2 ligands. Cancer Letters *257*, 116-123.

Yoshida, K., Yamaguchi, T., Natsume, T., Kufe, D., and Miki, Y. (2005). JNK phosphorylation of 14-3-3 proteins regulates nuclear targeting of c-Abl in the apoptotic response to DNA damage. Nat. Cell Biol. *7*, 278-285.

Young, M. A., Gonfloni, S., Superti-Furga, G. and Roux, B. (2001) Dynamic coupling between the SH2 and SH3 domains of c-Src and Hck underlies their inactivation by C-terminal tyrosine phosphorylation. Cell *105*, 115-126.

Zeqiraj, E., Filippi, B.M., Deak, M., and Van Aalten, D.M.F. (2009). Structure of the LKB1-STRAD-MO25 complex reveals an allosteric mechanism of kinase activation. Science *326*, 1707-1711.

Zhang, C., Spevak, W. Zhang, Y., Burton, E.A., Habets, G., Zhang, J., Lin, J., Ewing, T., Matusow, B., Tsang, G., Marimuthu, A., Cho, H., Wu, G., Wang, W., Fong, D., Nguyen, H., Shi, S., Womack, P., Nespi, M., Shellooe, R., Carias, H., Powell, B., Light, E., Sanftner, L., et al. (2015). RAF inhibitors that evade paradoxical MAPK pathway activation. Nature *526*, 582-586.

Zhang, J., Adrian, F.J., Jahnke, W., Cowan-Jacob, S.W., Li, A.G., Iacob, R.E., Sim, T., Powers, J., Dierks, C., Sun, F., Guo, G., Ding, Q., Okram, B., Choi, Y., Wojciechowski, A., Deng, X., Liu, G., Fendrich, G., Strauss, A., Vajpai, N., Grzesiek, S., Tuntland, T., Liu, Y., Bursulaya, B., Azam, M., Manley, P.W., Engen, J.R., Daley, G.Q., Warmuth, M., and Gray, N.S. (2010). Targeting Bcr-Abl by combining allosteric with ATP-binding-site inhibitors. Nature *463*, 501-506.